Estimating the root-zone storage capacity to predict discharges in the river Moselle

Bachelor Thesis – Final Report

A. ten Berge

Image: (Heuver, 2018)

Author: Amy ten Berge
Supervisor: Laurène Bouaziz
UT-Supervisor: Jaap Kwadijk

Date: 30/06/2021

UNIVERSITY OF TWENTE.

Deltares

Preface

In front of you is the final report of my bachelor thesis '*Estimating the root-zone storage capacity to predict discharges in the river Moselle*', which I carried out in the *Oppervlaktewater hydrologie* department of Deltares. With this research, I conclude my bachelor study Civil Engineering at the University of Twente. In this thesis, the differences between two methods for estimating the root-zone storage capacity in the wflow_sbm model are evaluated by comparing the predictive power of the model. I hope the outcome will contribute towards further understanding of estimating parameters that are hard to measure and will eventually lead towards more reliable hydrological predictions.

Looking back at the past twelve weeks, I can say that I have learned a lot regarding hydrological model prediction and parameter estimation. Next to that, even though doing this research individually was sometimes challenging, I have experienced that my skills on setting up and conducting a research developed substantially.

I would like to thank my external supervisor at Deltares, Laurène Bouaziz, for all her help and support throughout the entire graduation period. She was always willing to answer my questions or give me critical, but helpful feedback. As the internal supervisor from the University of Twente, I would like to thank Jaap Kwadijk for his guidance as well. His experience in the research field helped me to improve my report. In addition to my two supervisors, I would like to thank Deltares for the opportunity for conducting my bachelor assignment in their organization. Despite I did this research from home due to COVID-19, I still got insight in the working environment of Deltares and felt warmly welcomed.

Hopefully, you will enjoy reading my thesis as much as I did writing it.

Amy ten Berge

Enschede, June 30, 2021

Summary

This study evaluates the differences between two methods to estimate the root-zone storage capacity in the hydrological wflow_sbm model of the Moselle, in order to obtain more reliable hydrological predictions. The first method for estimating the root-zone storage capacity is currently used in the wflow_sbm model and relies on look-up tables that relate rooting depth to land-use. As this approach is rather uncertain and static, a more dynamic method was used to estimate the root-zone storage capacity. This second method is the water balance approach, in which climate data is used, and has as main assumption that vegetation adapts its root-zone storage capacity to overcome dry periods. The differences between the two methods were evaluated by comparing the predictive power of both versions of the wflow_sbm model.

The sensitivity of the wflow_sbm model of the Moselle to a change in root-zone storage capacity was assessed by creating different scenarios for the rooting depth. The root-zone storage capacity has substantial influence on both annual and event time scale, as a higher root-zone storage capacity leads to an increase in evaporation and thus a decrease in discharge.

In the estimation of the root-zone storage capacity using the water-balance approach, four different return periods were used. For a return period of 10 years, this resulted in an average root-zone storage capacity of 171 mm. The root-zone storage capacity was translated to a rooting depth in order to implement the new estimations in the wflow_sbm model, using estimates of the saturated and residual water contents. The resulting average rooting depth for a return period of 10 years (635mm) was 99.7% higher than the current average rooting depth in the wflow_sbm model of the Moselle.

The predictive power of both versions of the wflow_sbm model was compared using different metrics at different locations. The annual average run-off coefficient at Cochem simulated with the version in which the water balance approach was used, deviated 1.4% from the observed run-off coefficient, while this deviation was 11.7% for the current version of the model. This makes the water balance approach for estimating the root-zone storage capacity recommended for application in water management planning.

For application in operational water management, the water balance approach is recommended as well, as the height of peaks in wet periods of wet years were simulated closer to the observations when using the root-zone storage capacity values derived with the water balance approach, even without any further calibration of the model.

Table of Contents

1. Introduction

1.1 Problem Context

Extreme discharges in rivers can lead to a variety of problems. Low discharges can lead to problems with freshwater supply, water quality and river navigation (Pushpalatha, Perrin, Moine, Mathevet, & Andréassian, 2011). On the other side, extreme high discharges can lead, and already have led, to problems as well. For example, the floods of the Meuse in 1993 in large parts of Limburg, the Netherlands led to 114 million euros of economic damage (Wind, Nierop, Blois, & Kok, 1999). To prevent or minimize these water-related problems in the future, it is crucial to be able to predict the discharges as accurately as possible. Forecasting flows on the short term and also understanding long-term flow indicators thus have societal and scientific value (Demirel, Booij, & Hoekstra, 2015).

Deltares is an important party in doing research on river hydraulics. Deltares is an independent institute for applied research (Deltares, sd). Currently, one of the research topics of the *Catchment Hydrology* department of Deltares focuses on the development of a hydrological model of the river Moselle (Section 2.3). To predict the discharges in the river Moselle, the wflow_sbm model is used. My research will focus on the improvement of the wflow_sbm model of the Moselle.

The discharges in the river Moselle are expected to become more extreme, due to climate change and increasing human activity in the Moselle basin. Climate change in the Moselle basin is already observed by higher average temperatures, more high-temperature extremes and increased precipitation in northern Europe in the past years (IPCC, 2014, pp. 1275-1279). According to the IPCC climate projection, hydrological droughts may become more severe (Wong, Stein, Torill, Ingjerd, & Hege, 2011) and precipitation extremes will occur more often. The climate change is projected to affect the hydrology in river basins (IPCC, 2014). Increases in extreme river discharges were observed in Germany (Petrow, Zimmer, & Merz, 2009) and it is expected to have even more frequent extreme discharges in the future. Next to that, river discharges are affected by human activity (Hrachowitz, et al., 2020). The regulation of the discharges by locks, urbanisation and cultivation will lead in general to more extreme, mainly low, discharges (Hurkmans, et al., 2009).

Climate change in the Moselle basin influences the vegetation (Savenije & Hrachowitz , 2017). For example, to respond to water stress in dry periods, vegetation systems may adapt their root systems (Merz, Parajka, & Blöschl, 2011) to be able to access more water for evaporation. This affects the discharge in the river Moselle. On the longer term, human activity may lead to land-use changes and therefore the type of vegetation changes as well. It is important to incorporate these changing vegetation conditions in hydrological models, to simulate the discharges in the Moselle as accurately as possible (Merz, Parajka, & Blöschl, 2011). However, the optimal way of how to incorporate these changing conditions in hydrological models has not been found yet.

1.2 Research Gap

The root-zone storage capacity is a parameter that describes the amount of water in the unsaturated soil that is available to the roots of vegetation for transpiration (Boer-Euser, McMillan, Hrachowitz, Winsemius, & Savenije, 2016). The root-zone storage capacity is currently estimated by relating rooting depth to land-use, which is done by using look-up tables. These values are determined using literature which is partly based on field experiments (Vittal & Subbiah, 1984). This parameter is in the current model of the Moselle as a constant, not variable in time: Climate change is not included in the estimation of the root-zone storage capacity.

However, for incorporating changes in vegetation response and/or land use change, it is preferred to have a more dynamic representation of the root-zone storage capacity. Since 2005, much progress on model parameter estimation under changing conditions has been made (Peel & Blöschl, 2011). An example of a more dynamic way of estimating the root-zone storage capacity is the water balance approach. When using the water balance approach, the root-zone storage capacity is estimated using climate data (Nijzink, et al., 2016) (Hrachowitz, et al., 2020). The assumption on which this approach is based is that vegetation adapts its root-zone storage capacity to overcome dry periods (Nijzink, et al., 2016). Currently, it is not known how this approach for estimating the root-zone storage capacity in the Moselle basin relates to the current look-up table approach.

1.3 Research Aim

In this research, the water balance approach to estimate the root-zone storage capacity will be implemented in the wflow_sbm model. Then, this adapted version of the model will be compared with the existing wflow_sbm model, that uses look-up tables relating the rooting depth to land-use. To evaluate the differences between both methods, the predictive power in simulating the observed flow of both versions of the model will be compared.

The objective of this research will be 2-fold:

- "To evaluate the differences between two methods to estimate the root-zone storage capacity in the hydrological wflow_sbm model of the Moselle by comparing the predictive power of both versions of the model" and
- "to recommend one of the methods for application in operational water management and water management planning".

The first method here refers to the use of look-up tables that relate rooting depth to land-use and the second method refers to the estimation of the root-zone storage capacity using a water balance approach.

1.4 Research Questions

To achieve the research objective, one main question needs to be answered:

"Which of the two methods for estimating the root-zone storage capacity yields the best predictive power of the hydrological wflow_sbm model of the Moselle?"

To answer this main question, I formulated four sub-questions. By answering these four sub-questions, I will be able to answer the main question as well.

First of all, it is important to know how sensitive the discharge of the Moselle is to a change in root-zone storage capacity. The expectation is that changing the root-zone storage capacity leads to substantial differences in simulated discharge. If this is not the case, I will further investigate the role of the root-zone storage capacity in the model before continuing to next sub-questions. The first sub-question will therefore be:

1. How sensitive is the simulated discharge of the Moselle to changes in root-zone storage capacity?

The first method for estimating the root-zone storage capacity, relying on look-up tables to relate rooting depth to land use, is currently used in the wflow_sbm model. The other method, relying on estimating the root-zone storage capacity from water balance data, was not applied for the Moselle basin yet. Therefore, I will answer the second sub-question:

2. How large is the root-zone storage capacity for catchments within the Moselle basin according to the water balance approach and how much does it differ from the current estimation based on look-up tables related to land-use?

After having applied the water balance approach for estimating the root-zone storage capacity for the Moselle basin, I can implement the results of this method in the wflow_sbm model:

3. How can the method for estimating the root-zone storage capacity from water balance data best be implemented in the hydrological wflow_sbm model of the Moselle?

When both versions of the model are ready, the actual comparison between both methods can be made. This will lead to the answer to sub-question 4:

4. What are the differences in predictive power of both versions of the hydrological wflow_sbm model of the Moselle?

1.5 Report Outline

This chapter has introduced the research by explaining the research gap and research aim. In the next chapter, background information about the wflow_sbm model and information about the data of this study and Moselle basin is provided. Chapter 3 provides information on the methodology that is used to answer the four sub research-questions. In this chapter, the approach for checking the sensitivity of the root-zone storage capacity in the wflow_sbm model is explained, as well as the water balance approach and how the results of this approach can be implemented in the wflow_sbm model. Furthermore, the methodology that is used for analysing the differences between the both versions of the model is provided. The results of these methods can be found in Chapter 4. Successively in chapter 5, these results are discussed by comparing the results with results from other studies and describing limitations of the research. The conclusions and recommendations for further research are given in Chapter 6.

2. Study area, used models and data

2.1 Study area

The study area for this research is the Moselle basin, covering an area of approximately 27262 km^2 (Demirel, Booij, & Hoekstra, 2015). The basin is located in France, Luxembourg, Belgium and Germany (Figure 1).

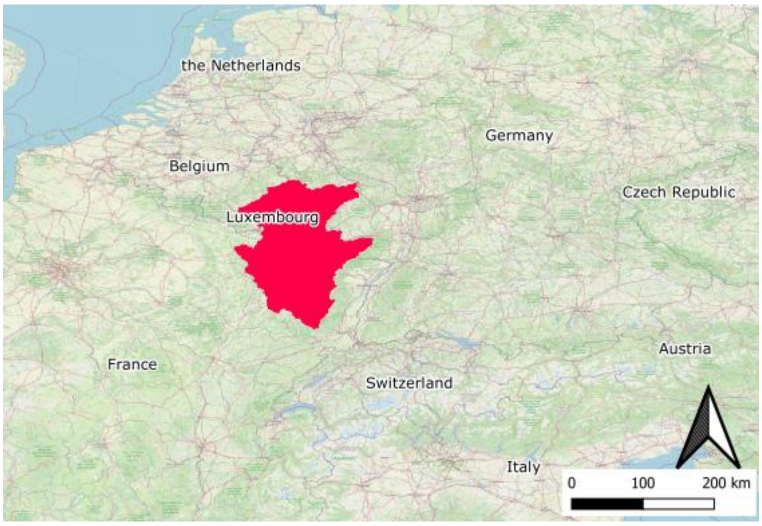

Figure 1: Location of the Moselle basin in Europe

The Moselle has its source in the Vosges Massif (Uehlinger, Wantzen, Leuven, & Arndt, 2009), at an elevation of 1283m, and flows to Koblenz, elevated at 71m, where it joins the river Rhine (Vriend, Havinga, Visser, & Wang, 2006) (Figure 2). The mean elevation in the Moselle catchment is 342m. The Moselle is an important tributary of the Rhine and has a length of approximately 550km. The main tributaries of the Moselle itself are the Saar, the Sauer and the Meurthe (Behrmann-Godel & Eckmann, 2003). Especially the German part of the flow of the Moselle is regulated by locks. This makes navigation one of the important functions of the Moselle (Demirel, Booij, & Hoekstra, 2015).

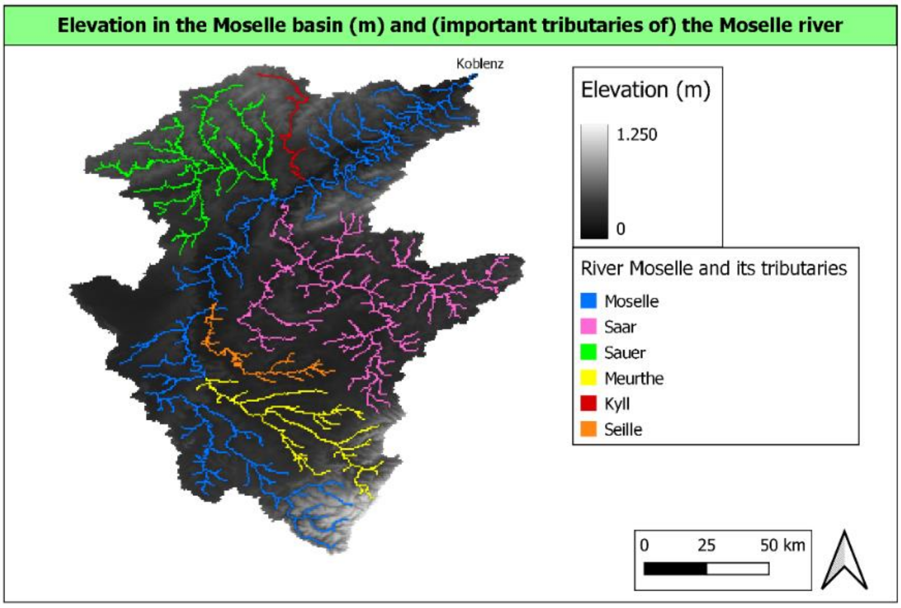

Figure 2: The elevation in the Moselle basin (m) and the most important tributaries of the Moselle

The dominating land-use type in the Moselle basin is cropland (31%). Next to that, pastures (21%), broadleaved forest (21%), coniferous forest (11%) and urban areas (9%) are common land-use types (Figure 3, (European Environment Agency, 2018)). In the two most south-eastern sub-catchments, coniferous forest is the dominant land-use type (54%).

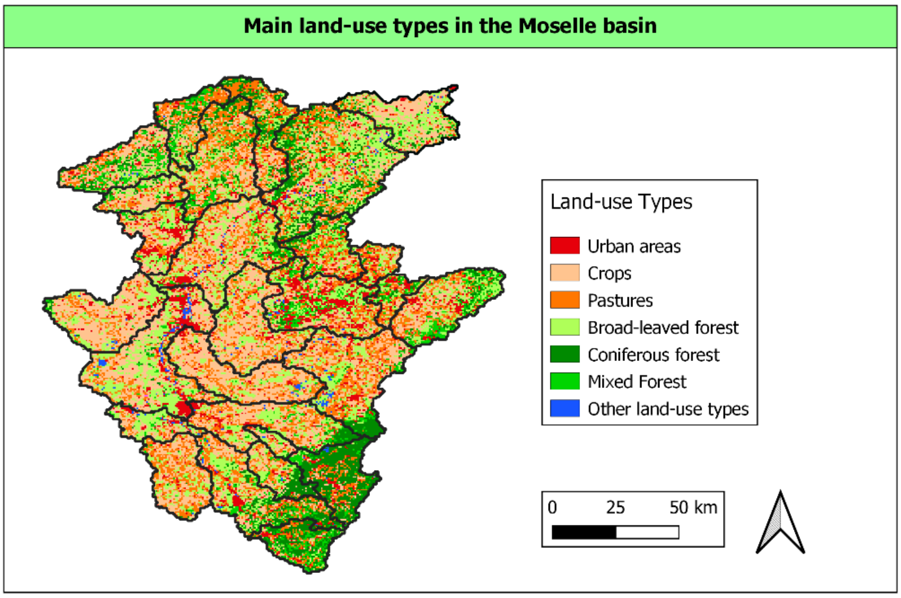

Figure 3: Main land-use types in the Moselle basin (CORINA Land Cover (European Environment Agency, 2018))

The Moselle river is a rain-fed river. Due to the canalization of the river, the steep slope in especially the northern and southern part of the basin and cultivation in the catchments, the response times in the Moselle river are relatively short. Due to the seasonality in potential evaporation (Figure 4), there is a seasonality in the discharges in the Moselle river (Demirel, Booij, & Hoekstra, 2013). The observed discharges at Cochem, the most downstream location for which observed discharge data is available, fluctuate between 40 m^3/s in dry summers and 3496 m^3/s during peak periods. The average discharge in the Moselle basin is 308 m^3/s (≈ 358 mm/year). The average annual precipitation is 923 mm/year, with the highest values between October and February (Figure 4). The average potential evaporation in the Moselle basin is 681 mm/year, with a maximum of 109 mm/month in the month July.

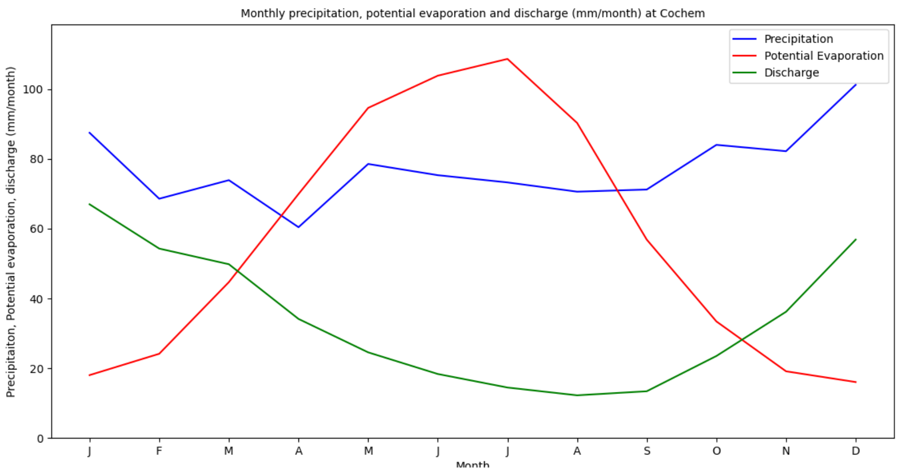

Figure 4: Average precipitation, potential evaporation and discharge per month, at Cochem

2.2 Hydrological processes in the Moselle basin

In the Moselle basin, different hydrological processes are playing a role. Precipitation is the most important factor in determining the discharge (Booij, 2019). The precipitation can be either snow or rain, depending on the temperature. Rainfall and snow melt drain as surface water or infiltrate into the soil. Whether it is drained as surface water or infiltrates into the soil, depends on the soil moisture conditions: Where the soil is completely saturated or the surface is paved, precipitation is discharged immediately. If the soil is not completely saturated yet, the precipitation infiltrates into the soil.

A part of the precipitation does not reach the surface but is intercepted by the canopy. This part evaporates before entering the soil. Water in the soil can evaporate directly, or through the leaf system of vegetation, which is called evaporation transpiration.

Below the unsaturated zone, there is a saturated zone, also called ground water, in which all soil pores are filled with water. Water is transferred from the unsaturated zone to the saturated zone. The opposite process is occurring as well: capillary rise is the process of water going from the saturated zone to the unsaturated zone. This occurs in case there is a difference in potential energy between the saturated and unsaturated zone and is caused by surface tension (Castillo, Castelli, & Entekhabi, 2015)

The water in the saturated zone is slowly discharged to the river. At the same time, water that has not infiltrated in the soil is directly discharged to the river as well. The total river discharge therefore consists of groundwater flow and overland flow.

2.3 Wflow_sbm model

To model these hydrological processes in the Moselle, the hydrological wflow_sbm model is used. This model is developed by Deltares (Schellekens, 2013). The wflow_sbm model is based on the topog_sbm model (Vertessy & Elsenbeer, 1999). A considerable difference between these two models is that the topog_sbm model is designed to simulate fast run-off processes in small catchments, while the wflow_sbm model has a wider application (Deltares Github, 2021).

The wflow_sbm model is based on physical characteristics of a catchment. It is a fully distributed hydrological model where the catchment characteristics are represented by grid cells (with a resolution of approximately 1 km x 1 km) (Schellekens, wflow Documentation, 2020) . The wflow_sbm model includes vertical water movements (such as infiltration and capillary rise) by having different vertical layers for each cell.

The wflow_sbm model simulates the hydrological states and fluxes over time. The output is gridded. This means that for any point in the model, for example the discharge is simulated. For the input of the model, a distinction is made between static and dynamic input data. The static input data consists of physical catchment characteristics, including different kind of maps, for example an elevation map and a map indicating land-use. The dynamic input data changes over time and includes precipitation, potential evapotranspiration and temperature data.

In the wflow_sbm model, different processes and fluxes are included, which are schematically represented in Figure 5.

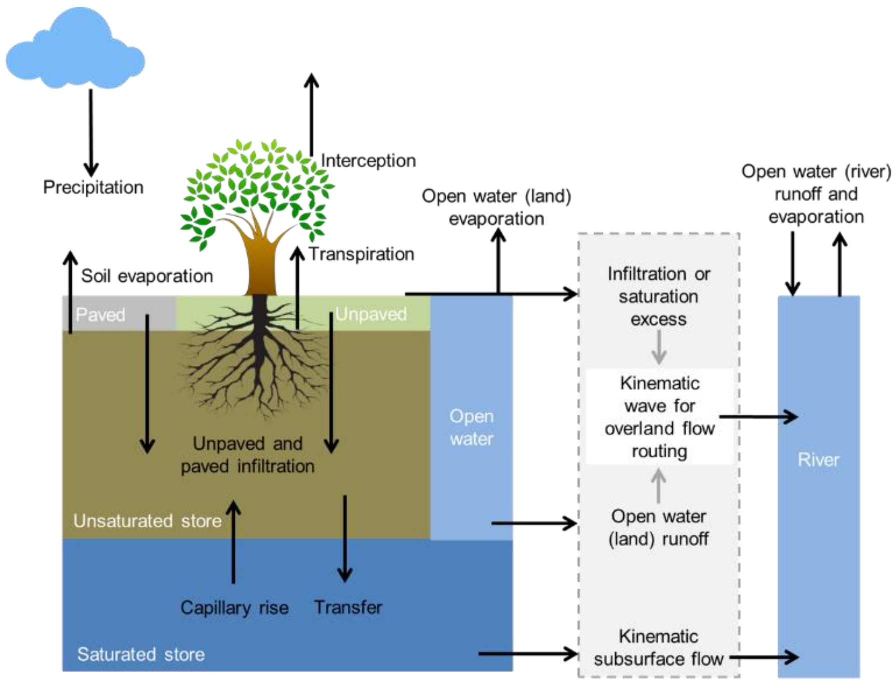

Figure 5: Overview of the different processes and fluxes in wflow_sbm model (Schellekens, 2013)

All processes that were described in section 2.1 are included in the wflow_sbm model (Schellekens, wflow Documentation, 2020). Precipitation is separated between snow and rainfall. The proportion of snow is determined using temperature measurements. When the air temperature is below a certain threshold, precipitation occurs as snowfall. Otherwise, the precipitation is in the form of rainfall. To estimate rainfall interception by vegetation, the analytical Gash model is used (Schellekens, wflow_funcs Module, 2020B).

In case the soil is saturated, the precipitation that is not intercepted is discharged to the overland runoff component. When the soil is not completely saturated, part of the water infiltrates into the soil. In the model, a distinction between compacted and non-compacted areas is made. In case the infiltration capacity is smaller than the throughfall (left precipitation after interception), then infiltration excess occurs.

The fluxes between the unsaturated and saturated zone are included in the model by 'transfer' and 'capillary rise'. The magnitude of these fluxes depends on soil properties and are determined by pedotransfer functions.

As can be seen in Figure 5, the open water areas in the basin are incorporated in the model as well. There is both open water evaporation and open water runoff. Also the evaporation of water in the river, main reservoirs and lakes is included in the model.

2.4 The role of vegetation in hydrological modelling

As indicated earlier, interception evaporation and transpiration are important fluxes in the hydrological cycle. The magnitude of these fluxes is dependent on the density of vegetation and the type of vegetation. Previous research (Thompson, et al., 2011) shows that vegetation has a substantial influence on the amount of water that is discharged to the river. An increase in vegetation leads to more interception and transpiration. As a result, there are lower discharges (on yearly basis) and less ground water replenishment (Cheng, et al., 2017). Next to that, when having more vegetation, water can more easily infiltrate into the soil before being discharged. This leads to a more flattened discharge peak (Gao, Holden, & Kirkby, 2016)

Next to the interception, vegetation influences the hydrological response of river basins through the storage capacity of the root-zone. (Gao, et al., 2014). The root-zone storage capacity, $S_{r,max}$, determines the maximum amount of water available for transpiration to the roots of vegetation in the unsaturated soil between field capacity and wilting point (Wang-Erlandsson, et al., 2016). In the wflow_sbm model, the root-zone storage capacity is parameterized as the Rooting Depth. This is the maximum depth to which the roots reach, also in mm.

A large root-zone storage capacity means that a lot of water is available for transpiration of vegetation. In winter, because temperatures are low and deciduous trees have lost their leaves, differences in storing capacity do not have a lot of effect since the potential evaporative losses are very small. In summer, a large root-zone storage capacity implies a higher amount of water available for transpiration. As a result, the discharge might be lower than when having a small root-zone storage capacity.

Ecosystems tend to respond to water stress by adapting their root systems to the local conditions. (Gao, 2014). Because of climate change, local conditions change. As an example, the drier conditions of the recent years in Austria are assumed to have led to an adaption in the root system of vegetation. This means the root-zone storage capacity increased gradually (Merz, Parajka, & Blöschl, 2011). Climate change therefore is an important factor for the root-zone storage capacity. The root-zone storage capacity is especially related to the difference in precipitation and potential evaporation (Kleidon & Heimann, 1998).

2.5 Estimating the root-zone storage capacity

The root-zone storage capacity thus is an important factor in hydrological modelling. Despite its importance, estimating the root-zone storage capacity at the catchment scale is very uncertain and difficult to measure in the field.

Currently, the root-zone storage capacity in the wflow_sbm model is estimated using look-up tables relating rooting depth to land-use. Within a grid cell, the land-use is determined by a static land-use map. After that, the look-up table is used to relate the land-use type to a certain rooting depth. The values in the look-up table are determined using literature which is partly based on field experiments (Vittal & Subbiah, 1984). The current estimations of the Rooting Depth in the Moselle catchment can be found in Figure 30 of Appendix A. The average Rooting Depth in the current version of the model is 318 mm, ranging between 1.4 and 433mm, with a median of 340mm and a standard-deviation of 88mm. This method of estimating the root-zone storage capacity has various limitations (Wang-Erlandsson, et al., 2016). First of all, it is difficult to measure the rooting profile in the field. Especially in case of large study areas, root profile measurements are difficult to conduct. Secondly, when rooting profiles would be largely available, it is difficult to translate a rooting profile to a root-zone storage capacity. Thirdly, this method assumes that a single rooting depth is valid across a land-use type. However, the root-zone storage capacity is changing constantly, adapting to local circumstances and climate change. Using the root-zone storage capacity from field measurements therefore is not a very certain option.

As an alternative for the static estimation of the root-zone storage capacity, a more dynamic approach was designed: The root-zone storage capacity at the catchment scale can also be estimated using a water balance approach. An advantage of this approach is that specific information about the soil and vegetation is not required. As a result, this method can be applied on a larger scale more easily with readily available data (Wang-Erlandsson, et al., 2016). Using precipitation and evaporation data to estimate the root-zone storage capacity instead of using soil-derived root-zone storage capacity values was also recommended based on the study of de Boer-Euser et al. (2016).

2.6 Data

For this research, observed climate and discharge data are used.

2.6.1 Observed climate data

For the observed climate data, the HYRAS v2.0 data set was used. This gridded dataset is developed by the German Weather Service and uses a database of approximately 6000 stations in the KLIWAS domain (Osnabrugge, Weerts, & Uijlenhoet, 2017). The dataset has a spatial resolution of 1 km^2 (Rauthe, Steiner, Riediger, Mazurkiewicz, & Gratzki, 2013). The period of the dataset is from 1979 to 2019 (41 years).

2.6.2 Observed discharge data

The observed discharge dataset that was used (Osnabrugge, Weerts, & Uijlenhoet, 2017), provides hourly observed discharge data at 727 locations in the Rhine catchment. For this research, 26 locations are selected. The period for which observed discharge values were available for each of the locations can be found in Table 2 of Appendix C.

3. Methodology

The approach of the research is as follows: first I study whether the root-zone storage capacity is an influential parameter in the model. To evaluate this, a sensitivity analysis is conducted (section 3.1). Successively in section 3.2, the method used to determine the root-zone storage capacity using the water balance approach is explained. This root-zone storage capacity is then translated to a rooting depth in order to apply it in the wflow_sbm model. The method of this step can be found in section 3.3. After that, both versions of the model are compared, as explained in section 3.4.

3.1 Determination of sensitivity of the model to a change in the rooting depth

Plant transpiration is the largest continental water flux (Jasechko, 2018) and storage volumes such as the root-zone storage capacity are key for hydrological functioning (Sprenger et al, 2019b), as they provide a buffer against hydrological extremes. It was therefore expected that the discharge is very sensitive to a change in root-zone storage capacity and thus that it was important to estimate this parameter as accurately as possible. However, the hydrological response of a change in catchment characteristics differs for different flow regimes (Ranatunga, Tong, & Yang, 2017). It therefore was important to assess if the discharge of the Moselle is also sensitive to changes in the root-zone storage capacity, and when this is the case. For this, a sensitivity analysis of this parameter on the predicted discharges was conducted.

3.1.1 Output Locations

The first step of the sensitivity analysis was to select output locations across the study area. At these output locations, which are points in the river Moselle or one of its tributaries, discharge simulated by the model was extracted. Also, average actual and potential evaporation and precipitation data of the catchment area upstream of the output location was retrieved.

In total, 5 output locations were selected (Figure 6). To obtain a broad overview of the influence of a change in root-zone storage capacity on the model output, the selected locations are spread over the study area, such that locations with different vegetational and geographical characteristics are considered. For consistency in the next steps of this research, only locations for which observed discharge data was available for at least 10 years were used.

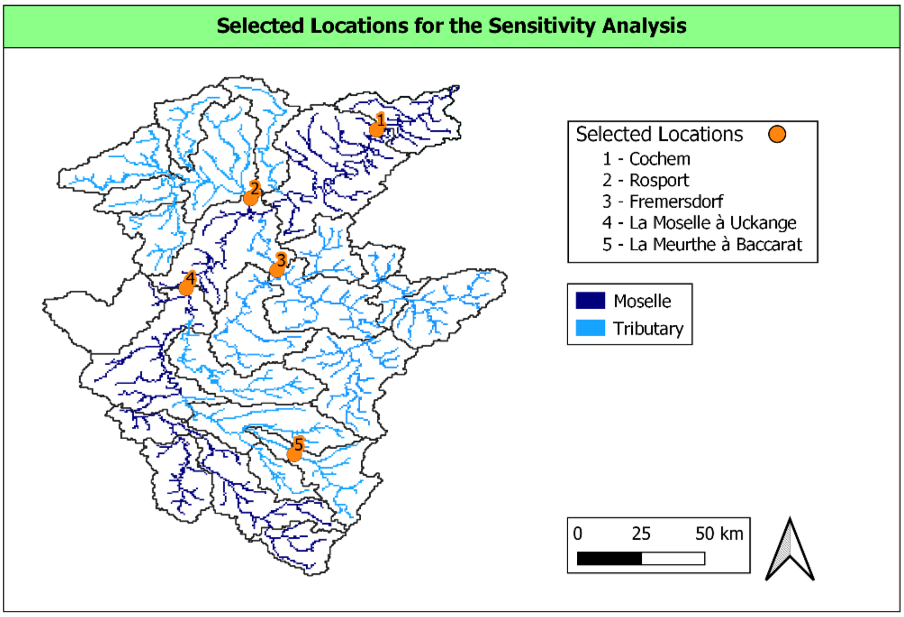

Figure 6: Selected locations for the Sensitivity Analysis

The first location is Cochem, which is the most downstream location for which observed discharge data is available. This location is selected to obtain an idea of the influence of a change in root-zone storage capacity on the model output considering the entire basin. The second location is near Rosport, which is located on the Sauer tributary just upstream of the confluence between the Sauer and the Moselle. The most downstream location of the Saar tributary, near Fremersdorf (location 3), was selected as well. By selecting these two locations, the sensitivity of these two most important tributaries of the Moselle to changes in root-zone storage capacities was determined. To analyse the sensitivity in the French part of the Moselle basin, location 4, La Moselle à Uckange was selected. This location is near the border between France and Germany. The last location of interest was La Meurthe à Baccarat (location 5), located far upstream in the south-eastern part of the Moselle basin. As stated earlier (Section 2.1), the dominant land-use type of the area upstream of this location (coniferous forest) differs from the average dominant land-use type in the Moselle basin (cropland), which is the reason for choosing this location.

3.1.2 Scenarios

The next step was to create different scenarios. For each scenario, the root-zone storage capacity was changed, while all other parameters in the model as well as the forcing data of the model were kept constant. The root-zone storage capacity in the wflow_sbm model is parametrized as the Rooting Depth (section 2.4). To assess the sensitivity, the Rooting Depth map of the wflow_sbm model was multiplied with different values. In total, 11 different scenarios were considered in the sensitivity analysis. Next to the reference scenario (0), the Rooting Depth was multiplied and divided by factors of 1.5, 2, 4, 8 and 10 (Figure 7). The values for the rooting depth in the different scenarios are not chosen in order to be realistic but are made more extreme to obtain a broad view (within two orders of magnitude) of the influence of a change in rooting depth on the model output.

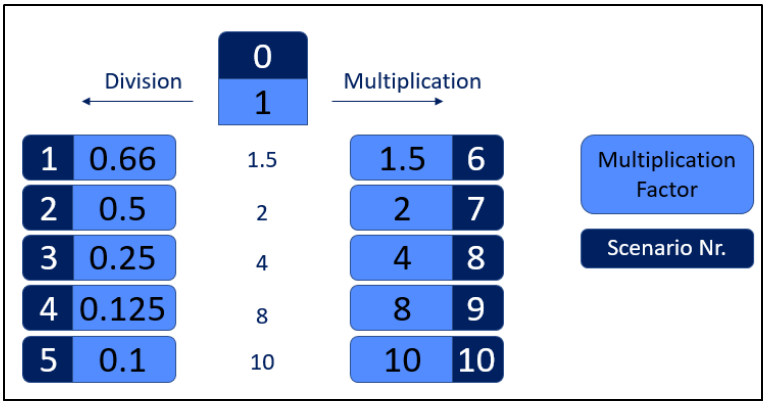

Figure 7: Overview of the different scenarios considered in the sensitivity analysis. Dark blue indicates the number of the scenario, whereas the light blue values show the factor with which the Rooting Depth parameter was multiplied

3.1.3 Running the model

Once the output locations and scenarios were defined, output data was generated by running the wflow_sbm model with the data mentioned in Section 2.6. For each output location, the modelled discharges in m^3/s per day were obtained. Next to that, the average precipitation and potential evaporation of the catchment area upstream the selected location in mm/day were obtained, as well as the average interception evaporation and transpiration in mm/day. For further analyses with this data, a warm-up period was defined. This warm-up period was based on the modelled hydrograph of Cochem (Appendix B). The simulated discharge data within this warm-up period was not included in the analysis to take into account the time it takes for the model to get into realistic conditions.

3.1.4 Metrics

To analyse the obtained data, different metrics are used. First of all, two metrics are used to analyse the change in average performance of the model.

1. **Run-off coefficient:**
   It was expected that a change in root-zone storage capacity would lead to a change in average annual discharge. In case the root-zone storage capacity increases, there will be more water available for vegetation for transpiration in dry periods. As a result, the actual evaporation will increase and using the long-term water balance ($\bar{P} = \bar{Q} + \overline{E_a}$), this means the annual discharge will in general decrease. To measure this effect, the run-off coefficient was used (Goel, 2011). The run-off coefficient (C) relates the long-term discharge to the long-term precipitation (Eq. 1).

$$C = \frac{\bar{Q}}{\bar{P}} \qquad \text{Eq. 1}$$

   $\bar{Q}$ is the average annual discharge (mm/year)
   $\bar{P}$ is the average annual precipitation (mm/year)

   To determine the run-off coefficient of the simulation scenarios, the long-term discharge is the average simulated discharge per hydrological year in mm/year, whereas the long-term precipitation is the average precipitation per hydrological year in mm/year. A hydrological year starting from the 1st of October and ending at the 30th of September was used. For the observed run-off coefficient, observed discharge data per hydrological year in mm/year was used.

2. **Long-term ratio $\overline{E_a}/\bar{P}$ as function of $\overline{E_p}/\bar{P}$ in Budyko Framework**
   As it was expected that the actual evaporation will increase in case the root-zone storage capacity increases, also the long-term ratio $\overline{E_a}/\bar{P}$ as function of $\overline{E_p}/\bar{P}$ was used as a metrics. This ratio is plotted in the Budyko framework. In the Budyko framework, the evaporative index ($\overline{E_a}/\bar{P}$) is plotted against the aridity index ($\overline{E_p}/\bar{P}$). The Budyko curve (Budyko, 1974) in this framework is an empirically derived curve which estimates the evaporative index ($\overline{E_a}/\bar{P}$) as function of the aridity index ($\varphi = \frac{\overline{E_p}}{\bar{P}}$). There are multiple Budyko curves (Gerrits, Savenije, Veling, & Pfister, 2009), but for this research the curve derived by Budyko (Budyko, 1974) is used (Eq. 2).

$$\left(\frac{\overline{E_a}}{\bar{P}}\right) = \sqrt{\varphi \cdot \tanh\left(\frac{1}{\varphi}\right) \cdot (1 - \exp(-\varphi))} \qquad \text{Eq. 2}$$

   In the Budyko framework, also the energy limit and water limit are plotted. An example of the Budyko framework can be found in Figure 15. The expectation is that $\overline{E_a}/\bar{P}$ will increase and will therefore become closer to 1. When plotting the ratio $\overline{E_a}/\bar{P}$ as function of $\overline{E_p}/\bar{P}$ in the Budyko framework, the relative influence of a change in rooting depth will become visual. The long-term actual evaporation ($\overline{E_a}$), long-term potential evaporation ($\overline{E_p}$) and long-term precipitation ($\bar{P}$) are the averages of total actual evaporation, potential evaporation and precipitation per hydrological year (30th of September – 1st of October).
   To determine the observed aridity index, the actual evaporation ($\overline{E_a}$) is estimated by subtracting the observed long-term discharge ($\overline{Q_{obs}}$) from the long-term precipitation ($\bar{P}$), which is based on the long-term water balance ($\bar{P} = \bar{Q} + \overline{E_a}$).

Because the root-zone storage capacity was expected to be especially a critical parameter in the dry period, two metrics that evaluate the model performance in the dry period are used.

3. **The runoff volume during the dry season**
In case the root-zone storage capacity increases, more water will be available for transpiration in the dry period. As a result, it is expected that the discharge volume during the dry season will decrease. The runoff volume during the dry season (1st of April to the 30th of September) can thus be used as a metrics to assess the sensitivity to a change in root-zone storage capacity. The runoff volume (in mm) is calculated by summing the discharges (mm/day) between each first of April to the 30th of September.

4. The average annual minimum average discharge of seven consecutive days
The average annual minimum discharge was determined as a metrics as well. This minimum flow was determined by taking the average annual minimum average runoff of seven consecutive days (Hanus, et al., 2021). Since the dry periods are mainly in winter (Vormoor, Lawrence, Heistermann, & Bronstert, 2015) (Jenicek, Seibert, & Staudinger, 2018), a year from the 1st of April to the 30th of March was taken, to prevent that a dry period was located at the turns of the year.

The behaviour of the peaks and its change due to a changing root-zone storage capacity, so the model performance on event time scale, was evaluated using a visual inspection of the hydrographs. This is the fifth metrics.

5. Visual inspection of the hydrograph
The hydrograph for an average year, dry year and wet year were analysed. To determine which years can be defined as average, dry and wet, precipitation data was used. The year with the highest precipitation as an average over the area upstream of Cochem is defined as the wet year, the lowest precipitation as the dry year and the average year is defined as the year in which the precipitation of that year is the nearest to the average precipitation over all years.

   The visual inspection concentrated on the first peak after a dry period, both its height and timing. In case the root-zone storage capacity was increased, it was expected that the magnitude of the first peak after a dry period would decrease. At the end of a dry season, the water buffer in the soil is almost empty. In case there is precipitation again, the root-zone will be filled. Only after the water buffer is filled, water will be transferred to the unsaturated zone or excess precipitation will be discharged. A larger root-zone storage capacity would mean it takes longer before the water buffer is filled. As a result, the first discharge peak after a dry period would be later and lower.

A last metric that is used in this research is the standard deviation of the annual discharges. In this way, the influence of a change in root-zone storage capacity on the variability of discharges between different years is researched.

6. **Relative standard deviation of the annual discharge**
A change in root-zone storage capacity may lead to a change in the discharge variability between years (Boer-Euser, McMillan, Hrachowitz, Winsemius, & Savenije, 2016). To quantify the discharge variability between years, the standard deviation of the annual discharge ($\sigma(Q_{years})$) is taken. This standard deviation is divided by the long-term discharge ($\bar{Q}$), to obtain the relative standard deviation of the annual discharge (σ_{rel}) (Eq. 3).

$$\sigma_{rel} = \frac{\sigma(Q_{years})}{\bar{Q}} \qquad \text{Eq. 3}$$

3.2 Estimation of the root-zone storage capacity using the water balance approach

The next step of the research was to estimate the root-zone storage capacity using the water balance approach. When using the water balance approach, the root-zone storage capacity at the catchment scale is estimated using water-balance data. Various studies have shown this approach for estimating the root-zone storage capacity is promising (Nijzink, et al., 2016) (Hrachowitz, et al., 2020). First, you estimate the transpiration from observed discharge, precipitation and evaporation data and based on this, you estimate the storage deficits stored in the root-zone. It is assumed that this volume is a good estimation of the root-zone storage capacity, since root systems adapt their roots in such a way that they can survive critical dry periods with a certain return period. The root-zone storage capacity $S_{r,max}$ can be determined by taking the minimum storage deficit that corresponds with the return period of the dry period. In this research, the root-zone storage capacity is estimated using the water balance approach for 26 different areas, after which the values of the root-zone storage capacity at each point in the study area are estimated by using the values of the different areas.

Thus, to estimate the root-zone storage capacity in the Moselle catchment, the following steps were taken (Figure 8):

Estimation of the root-zone storage capacity in the Moselle catchment

- **A** For each area, estimate the root-zone storage capacity
  - **1** Estimate the vegetation storage deficit per day
    - **a** Estimate the long-term transpiration
      - *Using observed discharge data at the outlet point of the area, average precipitation and potential evaporation and modelled interception evaporation data*
    - **b** Estimate the daily transpiration
      - *Scaling the long-term transpiration using daily and long-term modelled interception and potential evaporation data*
    - **c** Estimate the vegetation storage deficit per day
      - *Using daily differences in effective precipitation and transpiration*
  - **2** Determine the minimum vegetation storage deficit per year
    - *Using a year from the 1st of April to the 30th of March*
  - **3** Translate the minima per year to a root-zone storage capacity
    - *Using a Gumbel distribution and different return periods*
- **B** Estimate the root-zone storage capacity across the study area
  - **4** Combine the root-zone storage capacity values
    - *Using the root-zone storage capacity values of different areas to estimate the root-zone storage capacity at each point in the study area*

Figure 8: Overview of the steps to be taken in order to estimate the root-zone storage capacity in the Moselle catchment using the water balance approach

3.2.1 Step A1: Estimate the vegetation storage deficit per day

The first step of the water balance approach was thus to determine the vegetation storage deficits at each day. For this, first the long-term transpiration is estimated, which is scaled to a daily transpiration to estimate the vegetation storage deficit at each day.

A1a: Estimation of the long-term transpiration

First, the long-term water balance (Eq. 4) was used to estimate the long-term transpiration. The long-term water balance indicates that, on the long-term, all precipitation ($\overline{P}$) (mm/year) will be either evaporated ($\overline{E_a}$) (mm/year) or discharged ($\overline{Q}$) (mm/year), as storage changes are assumed to be negligible over long-term period.

$$\bar{P} = \bar{Q} + \overline{E_a} \quad \text{Eq. 4}$$

The total actual evaporation ($\overline{E_a}$) (mm/year) is the sum of interception evaporation ($\overline{E_\iota}$) (mm/year), soil evaporation ($\overline{E_s}$) (mm/year) and transpiration ($\overline{E_r}$) (mm/year) (Eq. 5). It is difficult to make a distinction between soil evaporation and transpiration. Therefore, the soil evaporation will be included in the transpiration.

$$\overline{E_a} = \overline{E_\iota} + \overline{E_s} + \overline{E_t} = \overline{E_\iota} + \overline{E_r} \quad \text{Eq. 5}$$

To determine the transpiration, Eq. 6 can thus be used to determine the long-term transpiration.

$$\overline{E_r} = \bar{P} - \bar{Q} - \overline{E_\iota} \quad \text{Eq. 6}$$

To obtain the long-term precipitation ($\bar{P}$), precipitation data in mm/day as an average over the whole area upstream the outlet point was used. For each hydrological year (1st of October – 30th of September), the total amount of precipitation in mm/year was determined, after which an average of these years was taken as the long-term precipitation ($\bar{P}$) in mm/year.

Approximately the same approach was used for the long-term discharge ($\bar{Q}$) and long-term interception evaporation ($\overline{E_\iota}$). For the long-term discharge, hourly observed discharge data was obtained at the outlet point of each area in m^3/s. For each day, an average of this hourly discharge data was determined. This discharge in m^3/s was then translated to mm/day, using the area of the catchment upstream the outlet point. The discharge in mm/year was then determined by summing the discharges in mm/day. In some years, observed discharge data at some days was missing. It was chosen to only include a year in the calculation in case at least 95% of the days, observed discharge data was available. An average of these discharges in mm/day was taken as the long-term observed discharge ($\bar{Q}$). A warm-up period was used to exclude the data at the start of the model run. For the long-term interception evaporation, modelled interception evaporation data per day was in the same way as the precipitation calculation summed to mm/year and then averaged. In all the calculations, the leap years are considered.

Estimation of daily transpiration

To take into account seasonality, the long-term transpiration ($\overline{E_r}$) (mm/year) was translated to a daily transpiration ($E_r(t)$) (mm/day). This was done by scaling the long-term transpiration with the ratio of mean daily potential evaporation ($E_p(t)$) (mm/day) minus the daily interception evaporation ($E_i(t)$) (mm/day) over the mean annual potential evaporation (E_p) (mm/year) minus the mean interception evaporation $\overline{E_\iota}$ (mm/year) (Eq. 7).

$$E_r(t) = \frac{E_p(t) - E_i(t)}{\overline{E_p} - \overline{E_\iota}} \cdot \overline{E_r} \quad \text{Eq. 7}$$

The daily potential evaporation is input data, whereas daily interception evaporation was obtained in the model. For estimating the long-term potential evaporation, the same approach was used as for estimating the long-term interception evaporation.

Estimation of the effective precipitation

To determine the storage deficit, also effective precipitation ($P_e(t)$) (mm/day) is needed. The effective precipitation was determined by subtracting the interception evaporation $E_i(t)$ (mm/day) from the total precipitation ($P(t)$) (mm/day) (Eq. 8). The effective precipitation therefore indicates the amount of precipitation that actually reaches the soil.

$$P_e(t) = P(t) - E_i(t) \quad \text{Eq. 8}$$

Estimation of the vegetation storage deficit

Now that both the effective daily precipitation and daily transpiration are known, the cumulative vegetation storage deficit can be estimated. The vegetation storage deficit was determined by taking the cumulative differences between effective precipitation ($P_e(t)$, mm/day) and transpiration ($E_r(t)$, mm/day) for each day (Eq. 9). The cumulation started at T_0, the moment that the storage deficit became negative, and ended at T_1, when the storage deficit was positive again.

$$S_{r,def}(t) = \int_{T_0}^{T_1} \big(P_e(t) - E_r(t)\big)dt \qquad \text{Eq. 9}$$

For this calculation, the flowchart of Figure 9 was used:

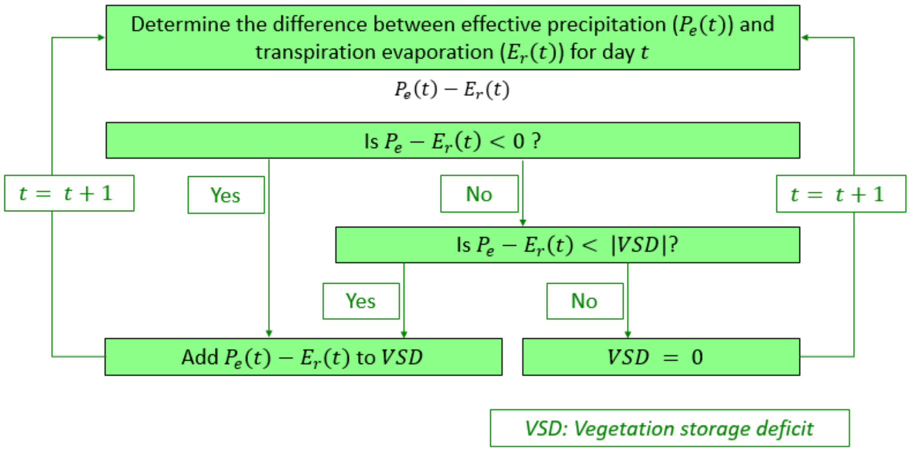

Figure 9: Flowchart used to determine the vegetation storage deficit (VSD) at each day

3.2.2 Step A2: Determine the minimum vegetation storage deficit per year

When the cumulative vegetation storage deficits per day are known, the minimum vegetation storage deficit per year is determined by taking the minimum value of the vegetation storage deficits in a hydrological year from the 1st of April to the 30th of March. A year from the 1st of April to the 30th of March is taken, since it is assumed that the 1st of April, the end of the wet period, the vegetation storage deficit is almost always 0.

3.2.3 Step A3: Translate the minima per year to a root-zone storage capacity

To estimate the root-zone storage capacity of an area, the minimum vegetation storage deficits of each year are used. The reason for this, is explained below.

In Figure 10, the vegetation storage deficit and the situation in the root-zone for a period of 3 years, in a fictional situation is schematized. In Figure 10A, the vegetation storage deficit (mm) is plotted against time (the values are fictional). In the Figure, seven characteristic points are indicated. In Figure 10B, the water deficit within the unsaturated zone of the soil at each characteristic point is schematized. The black line represents the upper boundary of the unsaturated zone. The orange blocks indicate the magnitude of the water deficit within the soil for that situation. In Figure 10B, the water deficit is schematized directly below the surface. In reality however, in case there is a water deficit, the location of the pores filled with air (indicating the water deficit) however is not per se the upper part of the soil but is instead divided over the whole unsaturated soil. The schematization therefore only gives the magnitude of the water deficit and not the location of the water deficit within the root-zone storage.

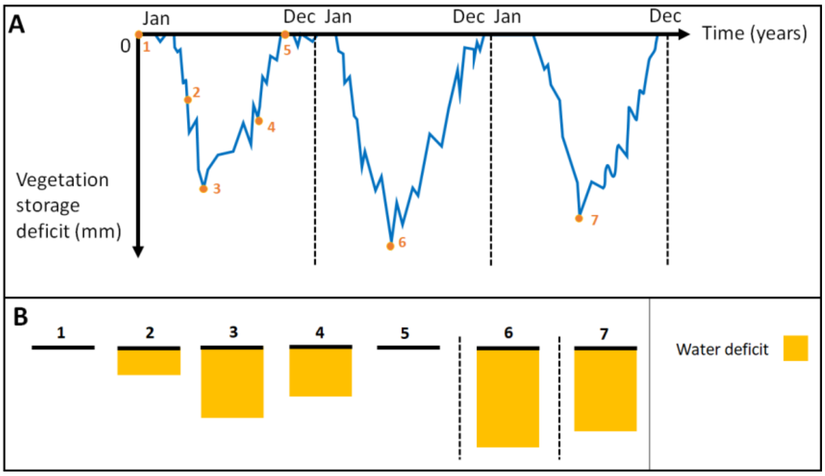

Figure 10: (A) Schematization of the vegetation storage deficit through time (fictional case), 7 characteristic points are indicated. (B) schematizes the water deficit in the root-zone for these 7 characteristic points

In situation 1, in a wet period, the vegetation storage deficit is 0 or higher, which means that the root-zone storage is completely filled with water and so all excess precipitation is immediately discharged. Between situation 1 and 2, the transpiration was higher than effective precipitation. As a result, a part of the buffer of the root-zone was evaporated and so the storage deficit decreased below 0. This means there is a water deficit (indicated in orange). The same happens between situation 2 and 3, leading to a further decrease in storage deficit. Since after situation 3, the storage deficit increases again, the minimum storage deficit of the first year is reached in situation 3. Between situation 3 and 4, the effective precipitation is higher than the transpiration. As a result, the storage deficit increased with respect to situation 3. The orange area of situation 4 shows that there is still a water deficit, but less than in situation 3. In situation 5, the storage deficit is 0 or higher again, the water deficit in the root-zone is not present anymore. The same process happens in year 2 and 3. In situation 6 and 7, the minimum storage deficits of corresponding year 2 and 3 are shown.

To determine the root-zone storage capacity $S_{r,max}$ (mm) of this area, the minimum vegetation storage deficits of multiple years are needed. For example, for year 1, 2 and 3, situation 3, 6 and 7 can be used. By determining the minimum vegetation storage deficits for multiple consecutive years, the root-zone storage capacity can be estimated using a Gumbel distribution. The minimum vegetation storage deficit that corresponds with a certain recurrence time is taken as the root-zone storage capacity. Important to mention is that for the determination of the annual minimum vegetation storage deficits, it is assumed that the root-zone is infinitely big. Another important assumption of this methodology is that vegetation taps its water from the unsaturated zone and not from the saturated zone.

Thus, to translate the minimum vegetation storage deficits per year to a root-zone storage capacity for that area, the annual minimum vegetations storage deficits are fitted to an extreme value distribution of Gumbel. With this Gumbel distribution, the root-zone storage capacities were estimated using different return periods. According to Nijzink et al. (2016), root systems in forested areas survive dry periods with a return period of ~20 years. For cropland and grasslands, return periods of ~2 years have been used in previous researches (Wang-Erlandsson, et al., 2016). Wang-Erlandsson et al. (2016) state that the return period differs per land-use type. However, in order to avoid artificially introduced transitions of the root-zone storage capacity between landscapes, a uniform return period across the area was used (Singh, Wang-Erlandsson, Fetzer, Rockström, & Ent, 2020). In total, four different scenarios, using return periods of 2, 5, 10 and 20 years, were chosen for this research.

3.2.4 Step B: Combine the root-zone storage capacity values to estimate $S_{r,max}$ across the area

The root-zone storage capacity was estimated for in total 26 nested sub-catchments, shown in Figure 11. The black dots indicate the outlet points, so the most downstream points, of the sub-catchments. The sub-catchment belonging to an outlet point is the total area upstream of this outlet point. As can be seen in Figure 11, the sub-catchments are divided in different levels. The two sub-catchments belonging to level 6 are located most upstream, while the level 1 sub-catchment, upstream Cochem (1A), is the most downstream sub-catchment. A catchment area of a certain level X encompasses the catchment areas of level X+1. For example, sub-catchment area 4D consist of all area upstream outlet point 4D, which is the orange part north-eastern from outlet point 4D and the two yellow areas upstream outlet points 5C and 5D. Sub-catchments 5C and 5D are thus nested within sub-catchment 4D. In Appendix C, this is elaborated further.

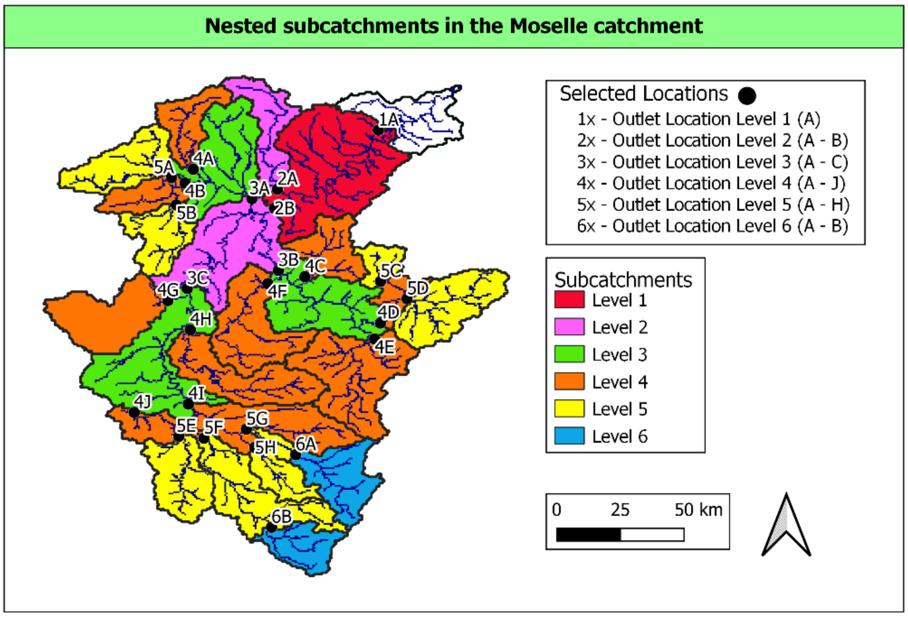

Figure 11: Nested sub-catchments in the Moselle catchment. Colours indicate the different levels, the black points indicate the outlet points of each sub-catchment

For each nested sub-catchment of Figure 11, the root-zone storage capacity is estimated using the water balance approach explained in Section 3.2. Since the sub-catchments are nested, it is needed to make a translation to a unique root-zone storage capacity for each point in the area. To determine this, the values of the nested catchments are used for the non-nested catchments. To clarify this, an example of area 4D, 5C and 5D is used (Figure 12).

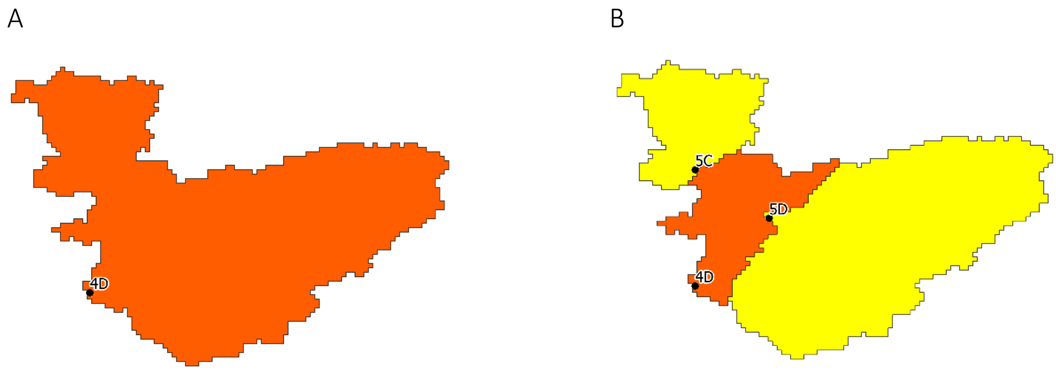

Figure 12: Example of nested catchments: Area 5C and 5D are nesting within area 4D

As said, the root-zone storage capacity value of catchment 4D belongs to the whole area upstream outlet point 4D (Figure 12A). Within this area, catchment 5C and 5D are nested. Also for these two areas, a root-zone storage capacity value was determined. The root-zone storage capacity of the remaining orange area of Figure 12B, which is from now on called the non-nested area 4D, is given the value of the root-zone storage capacity of the nested area 4D (Figure 12A). The reason for doing this can be found in Appendix E.5.

3.3 Implementation of new estimations of $S_{r,max}$ in the wflow_sbm model

As was stated in section 2.4, the root-zone storage capacity is the maximum amount of water available to the roots of vegetation in the unsaturated soil between field capacity and wilting point (Wang-Erlandsson, et al., 2016). In the wflow_sbm model, this root-zone storage capacity is parametrized as the Rooting Depth, which is the maximum depth of the roots in the soil, in mm. To translate the root-zone storage capacity values of the previous step (Section 3.2) to a Rooting Depth, soil characteristics were considered.

First of all, the saturated water content, θ_s, which is the maximum amount of water that the soil can store. It is equivalent to the porosity and differs throughout the study area (Figure 31 of Appendix A). A θ_s of 40% thus means that 40% of the volume of the soil can possibly consist of water. To translate the root-zone storage capacity to a rooting depth, it is thus important to divide the root-zone storage capacity by the value of θ_s.

However, the roots are not able to suck up all the water in the ground. Only water above the wilting point is available for the roots. Therefore, also the residual soil water content, which is the percentage of soil in which water can be stored that is not accessible for the roots, should be considered. In Figure 32 of Appendix A, these values can be found.

Thus, to translate the root-zone storage capacity values to a rooting depth, the root-zone storage capacity values should be divided by the saturated water content minus the residual soil water content (Eq. 10).

$$RD = \frac{S_{r,max}}{\theta_s - \theta_r} \qquad \text{Eq. 10}$$

In which: $S_{r,max}$ = root-zone storage capacity (mm), as determined in step 2 (Section 3.2)

θ_s = saturated water content of the soil (-)

θ_r = wilting point (-)

RD = Rooting depth (mm)

3.4 Analysis of the predictive power of both versions of the model

The last step of this research was to analyse the predictive power of the different versions of the model and see which estimations for the root-zone storage capacity are yielding the optimal predictive power of the model. After this, sub-question 4 and the main question can be answered.

As stated on page 18, in the estimations of the root-zone storage capacity using the water balance approach, four different return periods were used. As a result, there are five different versions of the model (Figure 13A). First of all, the model as it is now, with the root-zone storage capacity estimated using look-up tables relating rooting depth to land-use. Next to that, the four versions of the model, with the root-zone storage capacities estimated using the water balance approach, each with another return period.

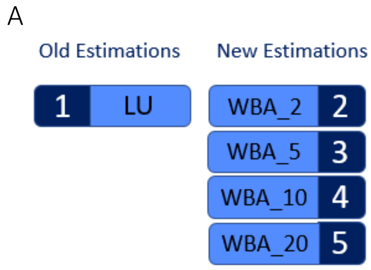

B

Overview of metrics used in the analysis of the predictive power
1. Average annual run-off coefficient
2. Long-term ratio $\overline{E_a}/\overline{P}$ as function of $\overline{E_p}/\overline{P}$ (Budyko)
3. The runoff volume during the dry season
4. The average annual minimum average discharge of 7 consecutive days
5. Average discharges per month
6. Visual inspection of the hydrograph (timing of the peaks)
7. Visual inspection of the hydrograph (height of the peaks)

Figure 13A: Overview of the different versions of the hydrological wflow_sbm model for the Moselle catchment. Figure B shows an overview of the metrics used in the analysis of the predictive power

The different versions of the model are compared with each other, but also with the observed values. For this analysis, the metrics stated in Figure 13B are used. The first 4 metrics are the same metrics as in the sensitivity analysis (described in Section 3.1). Also, the same locations for which these metrics are determined are the same as in the sensitivity analysis (Figure 6, page 10).

For the fifth metric, the average discharge per month (in mm/day) is determined. This is done for all 5 scenarios and for the observed values. The sixth and seventh metric use the hydrograph to analyse the performance of the different versions of the model on an event time scale. Both the timing and height of peaks in the hydrograph are analysed.

For the timing (metric 6), the hydrograph of different years is visually inspected and it is assessed if and how the different versions of the model differ in the timing of different peaks. For this, the hydrographs of output location 1, Cochem, are used. Since observed data is available for Cochem for the period 1990 – 2016, 117 different peaks in this period are compared in timing, for each scenario. For each peak, it is defined based on a visual inspection whether the new versions of the model (WBA_2 to WBA_20) are predicting the timing of the peak more accurately than the current version of the model (LU). Three possible outcomes are given for each peak: 'Worse', when the timing of the peak became substantially worse for the new versions of the model compared to the current version, 'Better', when the timing of the peaks substantially improved, or 'No Difference', when there is no substantial difference.

For the height of the peak (metric 7), again 117 peaks in the period 1990 – 2016 are visually inspected and given either the value 'Worse', 'No Difference' or 'Better'. In the analysis, a distinction is made between peaks falling within the dry period of the year (June – October) and the wet period of the year (November – May). Also, a distinction is made between peaks within dry years and wet years. The dry years are defined as the 7 years in the period 1979-2019 in which the annual precipitation was the lowest, the wet years are defined as the 7 years in the period 1979-2019 in which the annual precipitation was the highest.

4. Results

4.1 Sensitivity analysis

4.1.1 Variables of the sensitivity analysis

In the sensitivity analysis, different scenarios of the Rooting Depth parameter were created as described in Section 3.1. After this, for each scenario, modelled discharge data at the five selected output locations was obtained, as well as average precipitation, potential evaporation, interception evaporation and transpiration of the areas upstream these output locations.

As stated in Section 3.1, a warm-up period was determined using simulated discharge data [Appendix B]. The warm-up period in this research is defined as 1 year, which means that all simulated discharge data collected between 1-1-1979 and 1-1-1980 is not included in the analysis. This means that in total 40 years of modelled data (1980-2019) were used in the analysis. In case hydrological years are used, the year in which the hydrological year ends, is the name of that hydrological year. For example, for the hydrological year from the 1-10-1987 to 30-9-1988, this hydrological year is called '1988' in the analysis.

4.1.2 Average annual performance

To assess the average annual performance of the model, the average annual run-off coefficient was determined for each scenario, for the 5 selected locations. In Figure 14, the relative change in a scenario's average annual run-off coefficient compared with the base situation can be found, for all five selected locations.

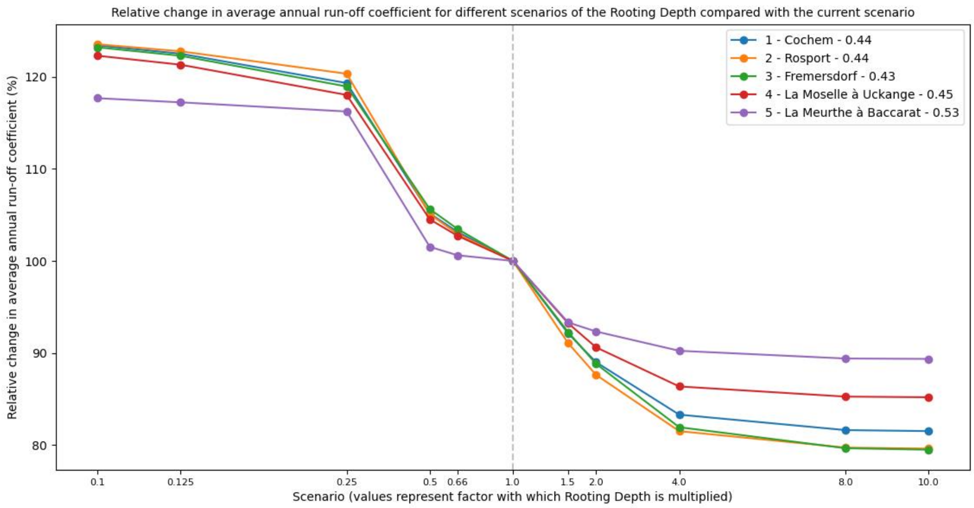

Figure 14: Relative change in average annual run-off coefficient for different scenarios of the Rooting Depth compared with the current scenario, for each selected location. The value behind the name in the Legend represents the average annual run-off coefficient in the base scenario. For example, for selected location 4, the average annual run-off coefficient changed to 85% when multiplying the Rooting Depth with 8 compared to the base scenario. The average annual run-off coefficient of that location, for that scenario was thus 85% of 0.45

As can be seen in Figure 14, an increase in the rooting depth leads to a decrease in run-off coefficient for all the selected locations. When the rooting depth is doubled, the average decrease of the average annual run-off coefficient for all 5 selected locations is 10.3%. The rooting depth thus has substantial influence on the average annual run-off coefficient. The direction of the change in run-off coefficient can be explained by an increase of the water that roots are able to access in case of an increase in rooting depth. As a result, roots will be able to evaporate more, which via the long-term water balance ($\bar{P} = \overline{E_a} + \bar{Q}$) leads to less discharge on the long term.

However, Figure 14 also shows there is a limit to a substantial change in average annual run-off coefficient in case of a change in rooting depth. For example, the red line (location 4, 'La Moselle à Uckange) between scenario 4 and 10 is almost horizontal: the average annual run-off coefficient changes by only 1.4% while increasing the rooting depth with 150%. At the other side of the graph, between scenario 0.1 and scenario 0.25, the differences in average annual run-off coefficient are very limited as well. For all the selected locations, the change in rooting depth is thus especially affecting the average annual run-off coefficient when this change is between a factor 0.25* and 4* the reference scenario. Between this range, the average annual run-off coefficient changes, as an average over all locations, with 28,5%, while this percentage only increases to 31.9% when increasing the range from 0.1* to 10* the reference scenario. The rooting depth parameter for the Moselle catchment affects the annual average run-off coefficient the most when the average Rooting Depth is between 80 and 1300mm (Table 3 of Appendix D.1).

It is not unreasonable that there is a limit to a change in average annual run-off coefficient when changing the rooting depth. In case the rooting depth is already sufficiently large, the roots may already be able to access enough water to evaporate. Increasing the amount of water that the roots can reach may not have influence on the evaporation and thus the run-off anymore. This line of reasoning was checked by comparing the actual and potential evaporation in different scenarios (Appendix D.1). Figure 44 of this Appendix shows that indeed the actual evaporation approaches the potential evaporation when having large rooting depth values. However, the actual evaporation does not reach the potential evaporation value. A reason for this may lay in the way transpiration and potential evaporation are related in the wflow_sbm model. On the other side, when the rooting depth already is too small for the vegetation to evaporate a significant amount of water, decreasing this rooting depth even more does not have influence on the amount of water that is evaporated and thus not on the run-off coefficient.

When examining the differences between the selected locations, Figure 14 and Table 1 show that the influence of a change in rooting depth on the average annual run-off coefficient at location 5 is smaller than for the other locations. This may be since the average annual run-off coefficient at this location (0.53) in the base scenario is substantially higher than the average annual run-off coefficients at the other locations (all between 0.43 and 0.45). As can be seen in rows 3 and 4 of Table 1, this is due to both a higher average annual discharge as well as a higher precipitation. The higher precipitation may have as an effect that there is more often excess precipitation which leads to more discharge. Another important factor may be the slope of the areas, which is for location 5 twice as high as for the other locations (Table 1). As a result, water will be discharged faster, before it can be evaporated. Hence, because of the higher run-off coefficient, the rooting depth plays a less important role.

Table 1: Characteristics of the areas upstream the five selected locations. In the first row, the percentual difference in run-off coefficient between scenario 0.1 and 10 can be found. The average annual run-off coefficient, precipitation and discharge of the base scenario (mm/year) are shown in row 2, 3 and 4 respectively. The average slope of the area upstream the locations is shown in the last row

	1– Cochem	2– Rosport	3– Fremersdorf	4– La Moselle à Uckange	5– La Meurthe à Baccarat
$\%\Delta\,\bar{C}$ ($Sce\ 0.1 \leftrightarrow Sce\ 10$)	33.9	35.5	35.5	30.3	24.1
$\bar{C}_{base\ scenario}$	0.44	0.44	0.43	0.45	0.53
$\bar{P}$ (mm/year)	923	904	900	980	1234
$\bar{Q}_{base\ scenario}$ (mm/year)	403	394	390	440	653
Slope	0.10	0.09	0.09	0.08	0.19

To evaluate the average annual performance for the different scenarios, also the ratio $\overline{E_a}/\bar{P}$ as function of $\overline{E_p}/\bar{P}$ is shown in the Budyko space for each scenario at each location (Figure 15A). The green box of Figure 15A is enlarged in Figure 15B. With the red crosses, the observed evaporative index as function of the aridity index is estimated.

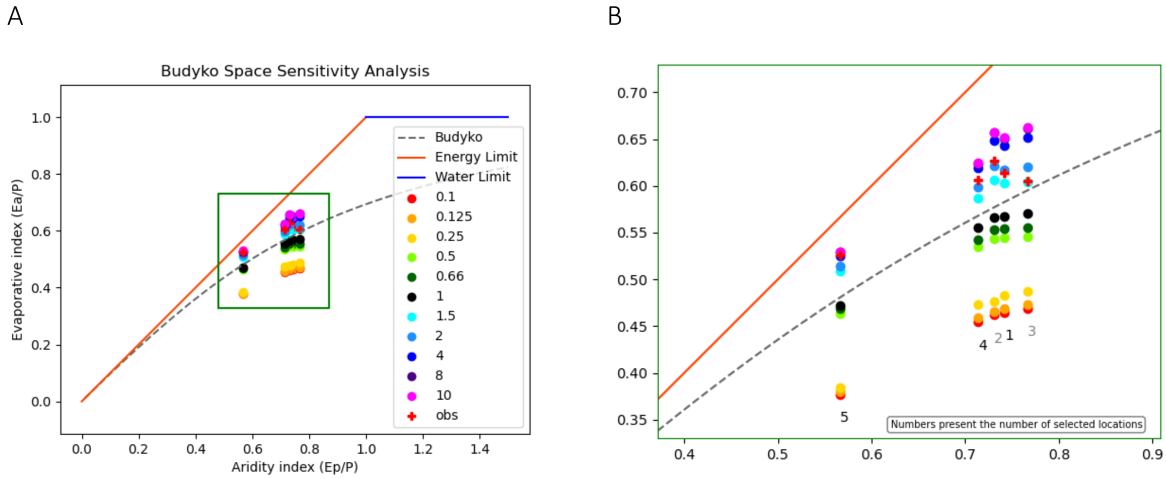

Figure 15: Budyko Space showing the ratio $\overline{E_a}/\bar{P}$ as function of $\overline{E_p}/\bar{P}$ for each scenario at each selected output location. The grey dotted line presents the Budyko curve, the red and blue line the energy and water limit. The green box is enlarged in Figure B. The numbers below the dots in Figure B present the number of the output locations (1 = Cochem, 2 = Rosport, 3 = Fremersdorf, 4 = La Moselle à Uckange, 5 = La Meurthe à Baccarat).

Again, location 5 stands out from the other locations because of the low aridity index because of the high precipitation. As a result, also the evaporative index of location 5 is lower than the evaporative indexes of other locations.

For each location, the relationship between the rooting depth and the evaporative index is the same: As the rooting depth increases, also the evaporative index increases. In case the rooting depth is multiplied with 10 compared with the base scenario, the evaporative index for station 1 (Cochem) is 0.65, with an aridity index of 0.74. This is 10.5% higher than the expected evaporative index for an aridity index of 0.74 using the Budyko curve (0.58) and 6.1% higher than the observed evaporative index (0.61). The rooting depth thus again has substantial influence on the average performance of the model.

Studying at Figure 15B, again it is visible that there is a limit on the change in average model output when changing the rooting depth. For example, the yellow and red dots (showing the evaporative indexes of scenarios 0.1 and 0.25) are close to each other.

4.1.3 Average performance in dry periods

The root-zone storage capacity was expected to especially have influence on the discharges in the dry period, since then precipitation is relatively low and potential evaporation high (Figure 4 on page 5). As a result, the root-zone was expected to play a more important role. To check this, the average annual run-off volume during the dry season and the average annual minimum average discharge of seven consecutive days were used as metrics. The relative changes in the metrics of different scenarios compared with the base scenario can be found in Figure 45 and Figure 46 in Appendix D. The same trend is visible as for the average annual run-off coefficient (Figure 15), namely that the metric decreases in case of an increase in rooting depth.

When comparing the average annual run-off coefficient, average annual run-off volume during the dry season and the average annual minimum discharge (Figure 16), it can be seen that the effect of a change in rooting depth is more extreme for the annual minimum discharge than it is for the other metrics. The difference in average annual minimum discharge between scenario 0.1 and scenario 10 is 70%, while it is 45% for the annual run-off volume during the dry season and even lower (34%) for the annual average run-off coefficient. A possible reason for this could be that for the data used for the annual minimum discharge (the 7 consecutive days with the lowest average discharge), the roots are heavily dependent on the water in the soil, while for the average annual run-off coefficient also days are used in which the roots are not dependent on the water in the soil. Furthermore, as relative differences are given in this graph, due to a small discharge value, the values may be blown up.

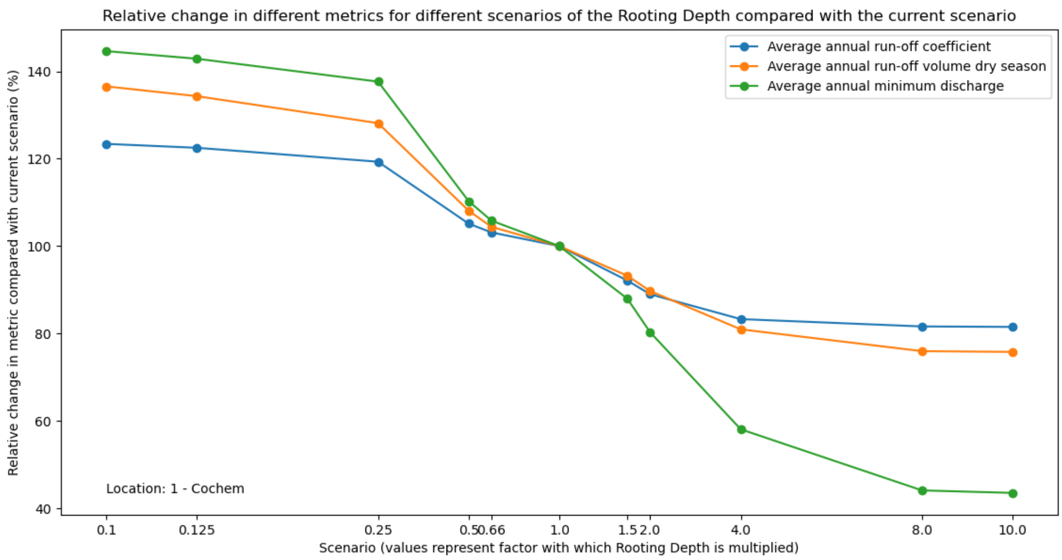

Figure 16: Relative change in different metrics (see legend) for different scenarios of the Rooting Depth, compared with the current scenario (%). Location = Cochem (1)

When having a look at Figure 16, it can also be seen that the average annual minimum discharge at Cochem is decreasing between scenario 4 and 8 more than when exploring the average run-off coefficient. The average annual minimum discharge changes with 24% when changing the rooting depth from scenario 4 to scenario 8, while the average annual run-off coefficient only changes by 2%. This effect is also visible for the other locations (Figure 47Figure 48 to Figure 51 of Appendix D).

4.1.4 Performance in peak periods

As can be seen in the hydrographs of Figure 17, the rooting depth also influences the model performance at event time scale. In Figure 17, the hydrographs at Cochem (location 1) are plotted for five different scenarios of the Rooting Depth (0.1, 0.5, 1, 2 and 10). This is done for an average year (2018), dry year (1996) and wet year (1983). The hydrographs at the other selected locations can be found in Appendix D.

A B C

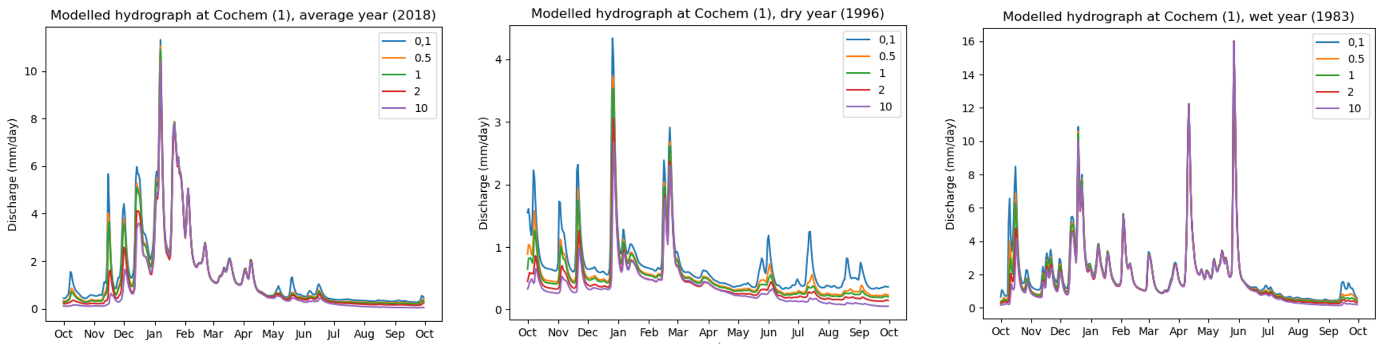

Figure 17: Modelled hydrographs at Cochem (location 1) for an average year (2018) (fig. A), dry year (1996) (fig. B) and wet year (1983) (fig. C), for 5 scenarios of the Rooting Depth (0.1, 0.5, 1, 2, 10)

A change in rooting depth influences discharge peaks for all types of years (Figure 17). This shows that the influence of the rooting depth on the discharge is not only limited to dry periods, but also occurs in the discharge peaks. The model with a lower rooting depth value leads to a more erratic pattern with higher peaks, while increasing the rooting depth leads to a more muted output.

An interesting point in the hydrographs is the first discharge peak after a dry period. For example, the peak in September 1983 (Figure 18) is differing for each scenario in both timing and height.

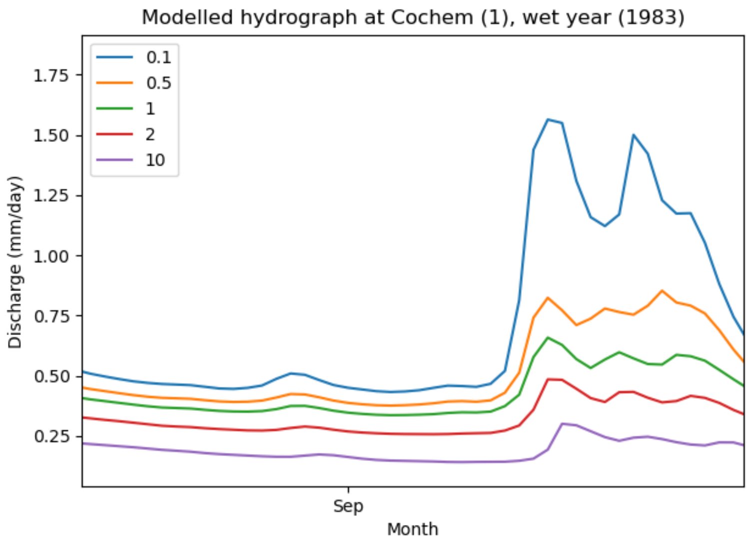

Figure 18: Modelled hydrograph at Cochem (1983), zoomed in on the peak in September 1983

Comparing this peak for scenario 0.1 and 10, the peak of scenario 0.1 is 4 days earlier and 5.7 times higher than the peak of scenario 10. This phenomenon is also visible at the peaks after the dry periods in other years and at other locations. A possible explanation could be that the first discharge peak after a dry period occurs after the root-zone is saturated by a precipitation event. In case of a larger root-zone storage capacity, it takes longer for the root-zone to be saturated again and as a result, the discharge peak will be later. Next to that, the discharge peak will be spread over a longer period, resulting in a lower peak.

4.1.5 Performance of variability between years

A last metric that is used to evaluate the model performance when changing the rooting depth, is the relative standard deviation of the annual discharge (Eq. 3 of Section 3.1.4). In Figure 19, the relative change in this metric can be found for each of the selected locations and for each scenario, compared with the current scenario.

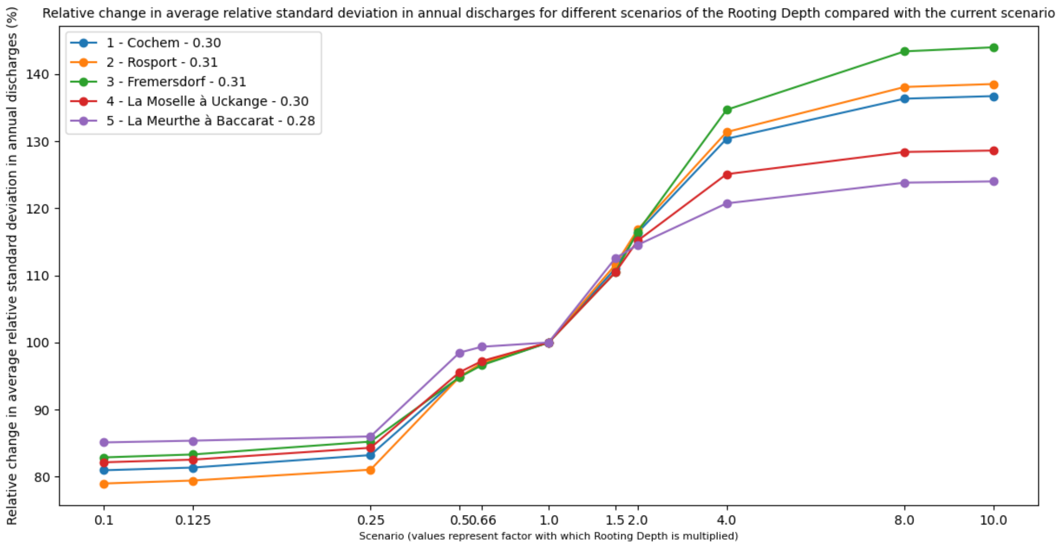

Figure 19: Relative change in relative standard deviation of the annual discharges for different scenarios of the Rooting Depth compared with the current scenario, for each selected location. The value behind the name in the Legend represents the relative standard deviation of the annual discharges in the base scenario

The relative standard deviation of the annual discharges increases on average with 15.9% in case of doubling the rooting depth of the current scenario. This will mainly be because the average discharges of the dry years become lower (roots can access more water, will evaporate more water and thus less discharge), while the average discharges of the wet years are also becoming lower, but to a smaller extent. As a result, the differences between dry and wet years are becoming bigger, resulting in a higher flow variability between different years. In Appendix D.5 (Figure 57 and Figure 58) this is elaborated further.

4.2 Root-zone storage capacity according to the water balance approach

In step 2 of this research, the root-zone storage capacity was estimated using the water balance approach. Since four different return periods were used (2, 5, 10 and 20 years), there are four different results (Figure 20). Some general statistics of these maps can be found in Appendix E.6.

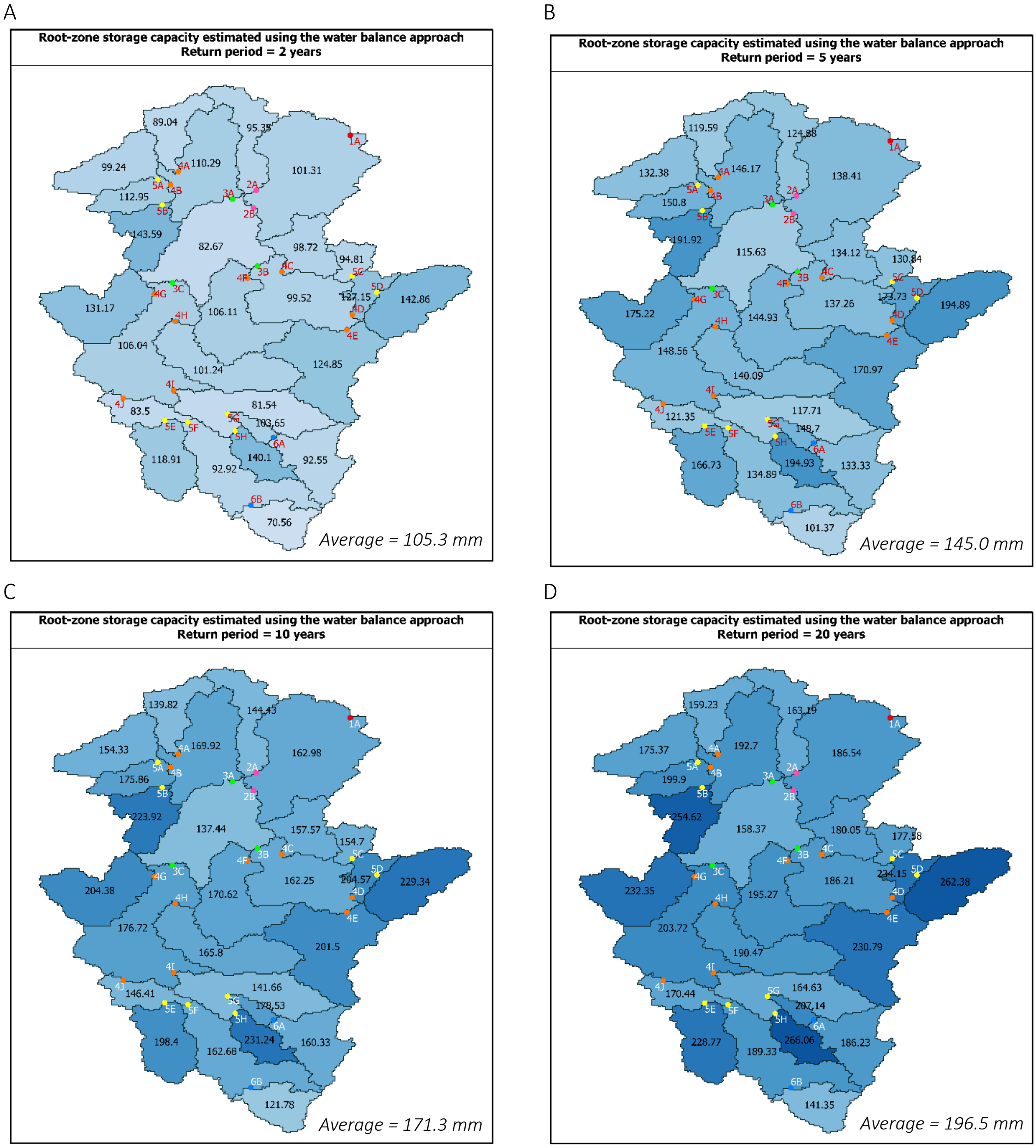

Figure 20: Estimated root-zone storage capacity values (mm) using the water balance approach, for different return periods. Figure A presents the $S_{r,max}$ values that were determined using a return period of 2 years, Figure B, C and D show the values using return periods of 5, 10 and 20 years respectively

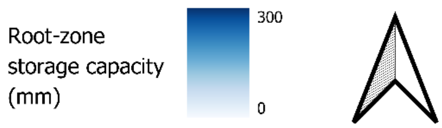

In Appendix E, the intermediary results of the water balance approach can be found. First of all, the long-term values used to determine the vegetation storage deficits. Then, the vegetation storage deficits and the minimum annual vegetation storage deficits. Then, the Gumbel plots used to estimate the $S_{r,max}$ using different return periods, for each catchment area.

4.3 Implementation of the water balance approach in the wflow_sbm model

In step 3 of this research, the root-zone storage capacity values of step 2 were translated to a Rooting Depth (mm), using the method described in Section 3.3. Since four different return periods were used (2, 5, 10 and 20 years), there are four different results (Figure 21).

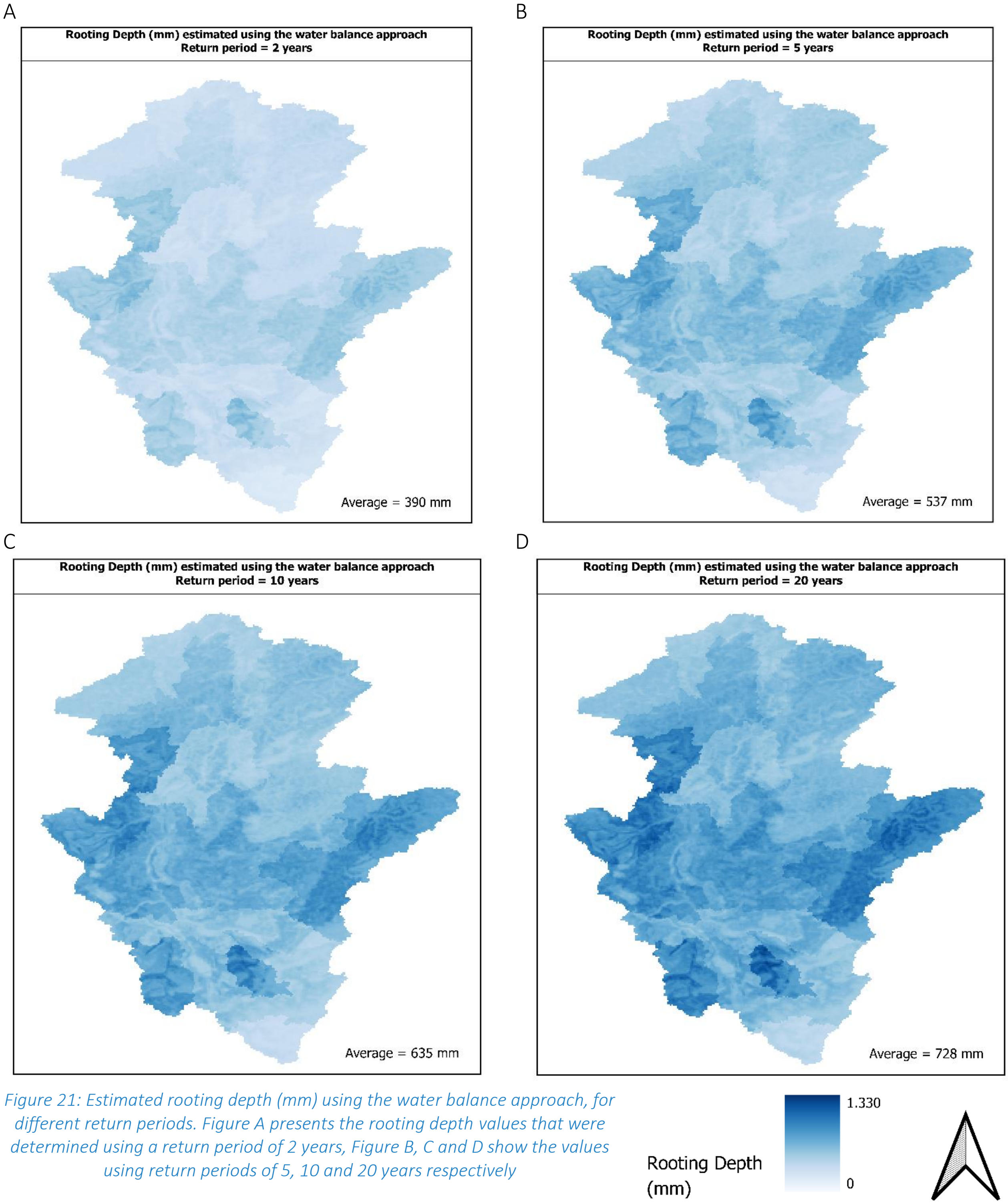

Figure 21: Estimated rooting depth (mm) using the water balance approach, for different return periods. Figure A presents the rooting depth values that were determined using a return period of 2 years, Figure B, C and D show the values using return periods of 5, 10 and 20 years respectively

In Appendix F, a comparison between the rooting depth maps of Figure 21 and the rooting depth map in the current model (Figure 30 in Appendix A) can be found. Also, basic statistics for these rooting depth maps can be found here.

4.4 Comparison predictive power of different versions of the model

In this Section, the results of the comparison of the different scenarios of the model (Section 3.4) are discussed. The different scenarios are compared with observed discharge data. To obtain the results, again a warm-up period of 1 year was used.

4.4.1 Average annual performance

For the five selected scenarios (described in section 3.4) and the five selected locations (Figure 6), the average annual run-off coefficient was determined. In Figure 22, for each scenario, the relative difference in average annual run-off coefficient compared with the observed average annual run-off coefficient can be found. The scenarios are named the same as in Figure 13: LU stands for the scenario with the current estimation of the Rooting Depth, and the 'WBA_x' scenarios are the new scenarios, each with another return period.

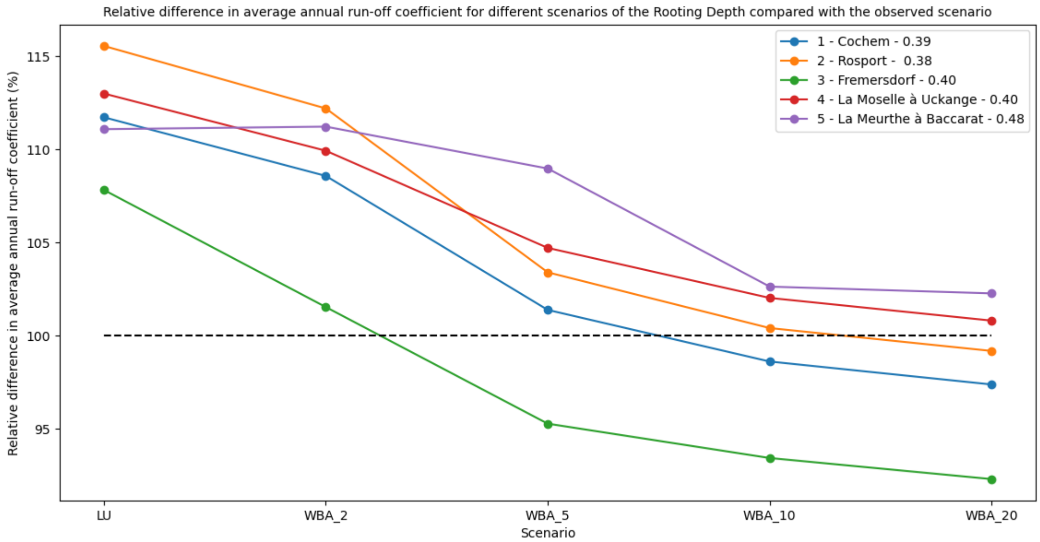

Figure 22: Relative differences in average annual run-off coefficient for different scenarios, compared with the observed average annual run-off coefficient, for each location. The black dashed line represents the observed scenario. Behind each name of the location in the legend, the average observed annual run-off coefficient is presented in mm/da

As can be seen, when using the water-balance method to estimate the Rooting Depth, the average annual run-off coefficient is closer to the average observed annual run-off coefficient for all locations. For example, for output location Cochem (1), the annual average run-off coefficient differs only 1.4% from the observed value when using the estimations of the water balance approach with a return period of 10 years, whereas this difference is 11.7% when using the current estimations of the rooting depth. The box plot in Figure 68 of Appendix G.1 shows how these values are spread out for different years.

However, it depends per location which return period is the most optimal. For example, for Cochem, the scenario in which estimations using a return period of 10 years is used is the closest to the average observed annual run-off coefficient, while for location 3, Fremersdorf, the scenario WBA_2 performs closest to the observed annual run-off coefficient. For location 5, La Meurthe à Baccarat, a return period of 20 years is most optimal to choose when examining at the annual run-off coefficient. This probably has to do with the differences in land-use. In the catchment area belonging to location 5, coniferous forest is the dominant land-use type, whereas cropland is the dominant land-use type of the catchment area belonging to location 3. Literature advises higher return periods for catchments with forested area than for catchments in which cropland is the main land-use type (Wang-Erlandsson, et al., 2016). The results of Figure 22 are thus consistent with previous studies. In Appendix G.1, Figure 69, this is elaborated further, by showing the optimal return periods for 26 different locations.

Using the average annual run-off coefficient as a metric to measure the performance of the different versions of the model shows that the water balance approach can be an improvement for the estimation of the Rooting Depth, for each selected location. On average for all locations, using a return period of 10 years leads to a deviation of 0.6% with the average observed annual run-off coefficient, while it deviates 11.8% when using the current estimations of the Rooting Depth.

The evaporative index ($\overline{E_a}/\overline{P}$) as function of the aridity index ($\overline{E_p}/\overline{P}$) for each scenario is also plotted in the Budyko framework (Figure 15). In this framework, also the observed estimated evaporative index as function of the aridity index can be found for each location.

A B

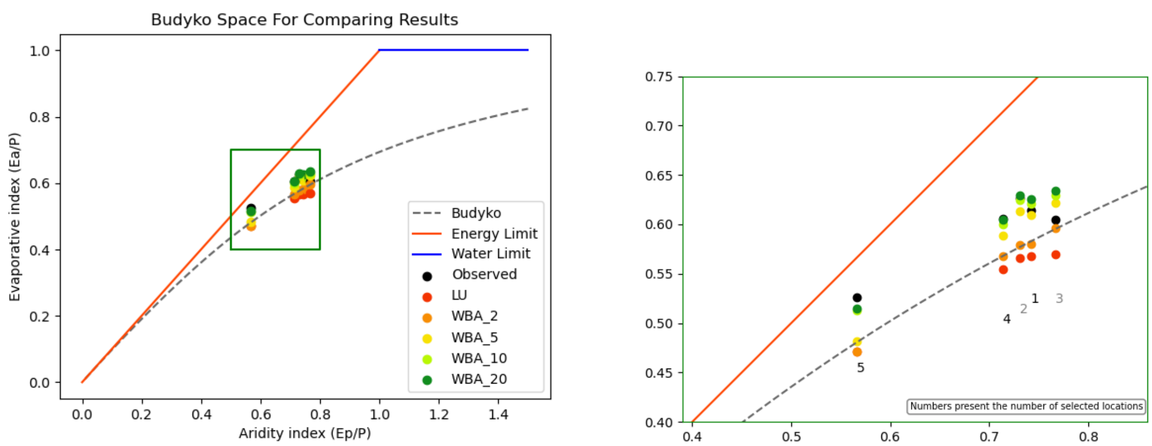

Figure 23: Budyko Space showing the ratio $\overline{E_a}/\overline{P}$ as function of $\overline{E_p}/\overline{P}$ for each scenario at each selected output location. The grey dotted line presents the Budyko curve, the red and blue line the energy and water limit. The green box is enlarged in Figure B. The numbers below the dots in Figure B present the number of the output locations (1 = Cochem, 2 = Rosport, 3 = Fremersdorf, 4 = La Moselle à Uckange, 5 = La Meurthe à Baccarat)

Studying this Budyko framework, it is visible that the points based on observed values are not closer to the Budyko curve than some points belonging to modelled scenarios. This is not necessarily unexpected, since catchments around the world plot in a scatter around the Budyko curve. The points belonging to the observed data are a good estimation, but they differ from the Budyko curve because the Budyko curve is empirically derived as an average of all catchments in the world (Gerrits, Savenije, Veling, & Pfister, 2009).

On average for all locations, the points of the scenarios in which the water balance approach is used are closer to the observed values than the points belonging to the current scenario (LU). It thus can be concluded that for this annual average performance, the water balance approach leads to a higher predictive power of the model.

4.4.2 Dry period performance

In Figure 24, the relative differences between the average annual run-off volume during the dry period of each scenario with the observed average annual run-off volume during the dry period can be found. In Figure 25, the same differences are shown, but now in average annual minimum average discharge of 7 consecutive days. As can be seen, all lines are decreasing in case the return period is increasing. This can be explained by the fact that the Rooting Depth increases in case of an increase in Return period, resulting in more evaporation and thus less discharge. For some locations (Rosport, Cochem), the descending line means the value of the metric is coming closer to the metric of the observed scenario, while for some other locations, such as Fremersdorf, the differences between the metric of the scenario and the metric of the observed discharges are deviating more.

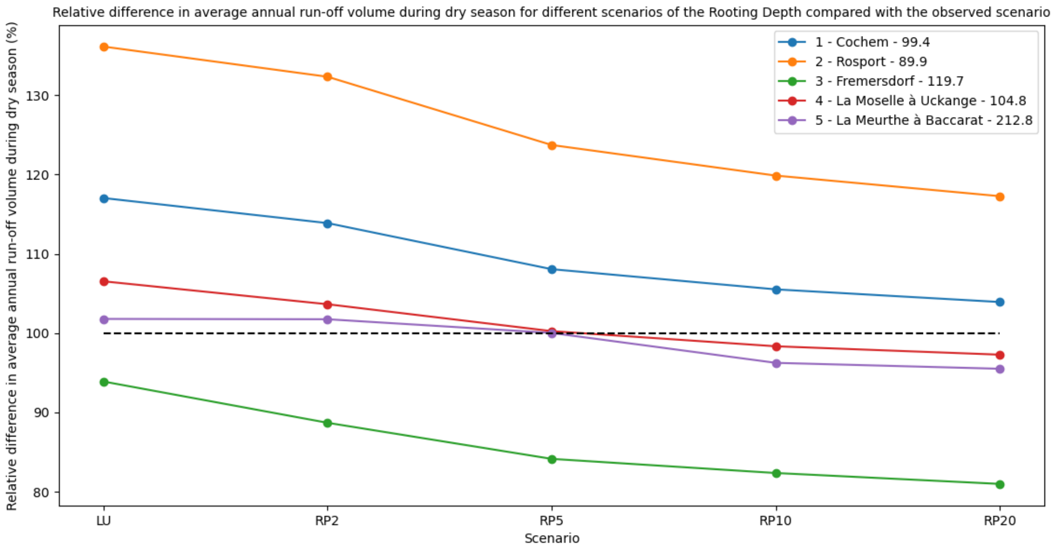

Figure 24: Relative difference in average annual run-off volume during the dry season (1st of April – 30th of September) for different scenarios of the Rooting Depth compared with the current scenario, for each selected location. The black dashed line represents the observed scenario. Behind each name of the location in the legend, the average observed annual run-off volume during the dry season is presented in mm

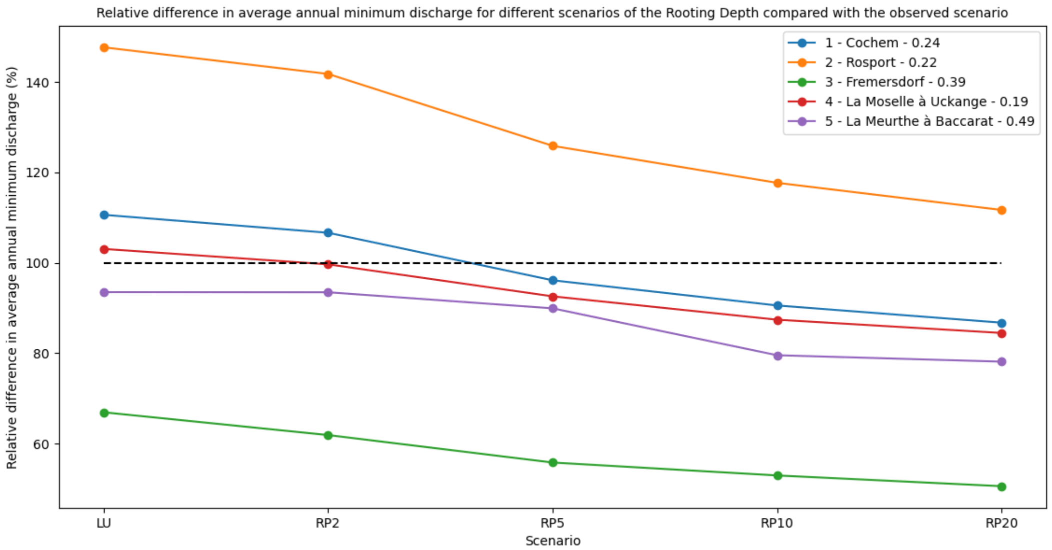

Figure 25: Relative difference in average annual minimum discharge of seven consecutive days for different scenarios of the Rooting Depth compared with the current scenario, for each selected location. The black dashed line represents the observed scenario. Behind each name of the location in the legend, the average observed annual minimum discharge is presented in mm/day

4.4.3 Average monthly performance

In Figure 26, the average discharge per month (mm/day) for each scenario can be found, as well as the average observed discharge per month. These discharges are measured or modelled at Cochem. For the other locations, the same bar charts can be found in Appendix G.

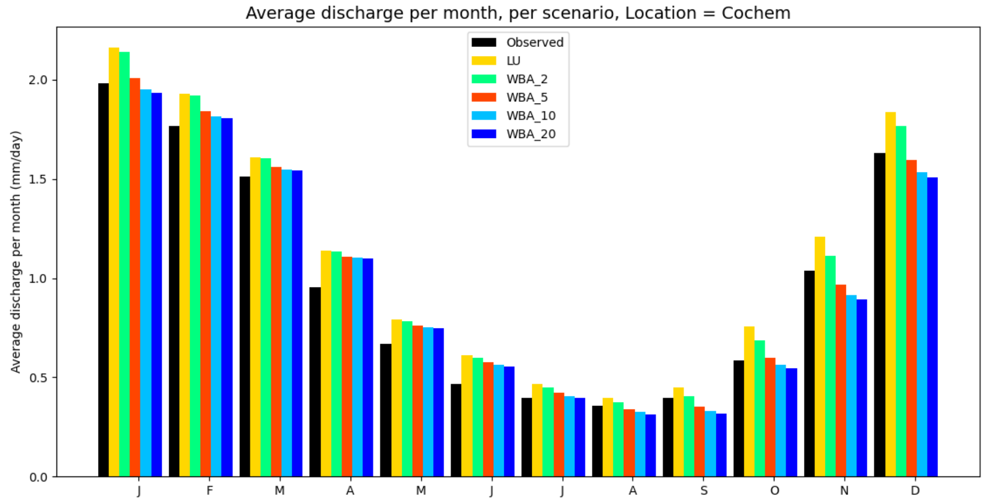

Figure 26: Average discharge per month (mm/day), per scenario, for Cochem

As can be seen in Figure 26, from February to July, the average discharge of all modelled scenarios is higher than the observed average discharge. In these six months, the average discharge of the scenario in which a return period of 20 years was used to estimate the Rooting Depth is the closest to the observed average discharge of that month. However, in the other six months, the average discharges of the scenarios 'WBA_2' and 'WBA_5' are closer to the observed average discharges.

For Cochem, the months with a high discharge are thus estimated the best with a high return period. This applies for the other locations, for example Fremersdorf (Figure 75 of Appendix G), as well.

A possible explanation could be that the current model on average overestimates the discharges in the wet period (which is mostly in the first half of the year). An example is shown in Figure 27, which is the hydrograph showing both the observed values and the modelled discharges in the current version of the model, for Cochem, 1999. In this Figure, the blue line (current model) is almost always above the observed line in the period November – April.

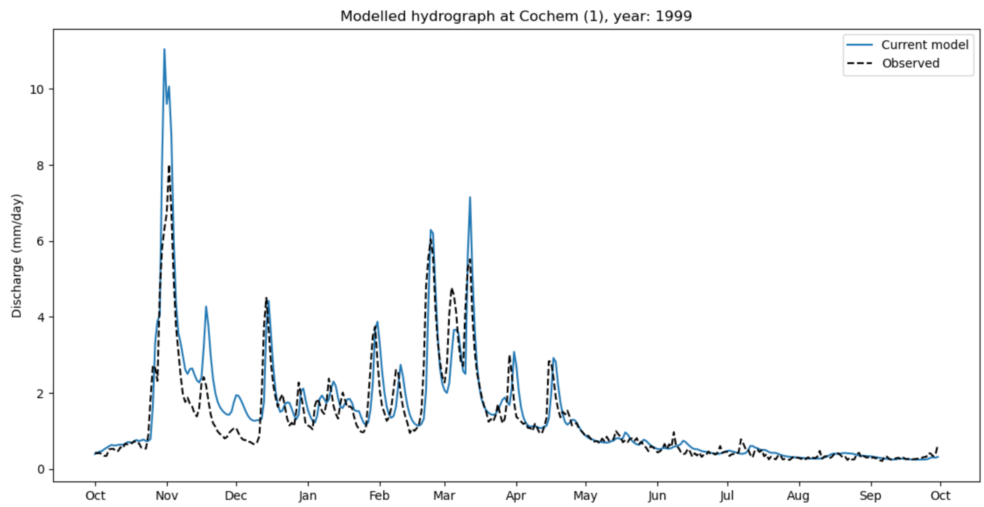

Figure 27: Hydrograph for Cochem (1), in 1999, showing the observed discharges as well as the modelled discharge values with the current version of the model

Because the current model overestimates the discharges in the wet period, the scenarios using the water balance approach to estimate the Rooting Depth will be closer to the monthly discharges. This is because in the scenarios of the water balance approach, the average Rooting Depth is higher, leading to more evaporation and thus less discharge. As a result, the discharges in the wet period are lower and less overestimating the observed values. At first it was expected that the rooting depth would especially have influence in the dry periods, as then precipitation is low and thus the vegetation is dependent on water in the root-zone. However, this graph shows the rooting depth also leads to substantial changes in discharge in the wet months. This may be the case because when the rooting depth increases, more water will be evaporated in the dry period, which means less water will be recharged to the saturated zone. As a result, in the wet periods, the system is not completely filled yet, which means in the wet periods also water is recharged instead of only discharged, which means lower discharge peaks.

Concluding, examining the monthly performance of the different scenarios, the predictive power of those scenarios in which the water balance approach is used, is higher than the predictive power of the current scenario.

4.4.4 Performance in peak periods

In this research, not only the average performance of the different versions of the model are compared, but also the performance at event time scale. For this, I performed a visual inspection of several peak periods of different hydrographs.

Timing of the peaks

In total, 117 peaks within the period 1990 – 2016 in the hydrograph at Cochem were analysed. For all peaks, the timing of the peaks was not improved by the new version of the model compared with the current version of the model. For the peaks within the wet period, there was no substantial difference in timing between the peak of the current version of the model and the peaks of the new versions of the model (example shown in Figure 28A). For the discharge peaks that were located just after a long dry period, the timing of the peaks of the new versions was worse than the timing of the peak of the current version of the model (example shown in Figure 28B). A possible explanation for this could be that a peak in the wet period is so high, that they occur at the moment of a large precipitation event anyway, even though the saturated zone is not completely full yet. The precipitation in this case is larger than the amount of water recharged to the saturated zone. In peaks just after a long dry period, the precipitation is not always higher than the amount of water that needs to be recharged to the saturated zone. As a result, there is a delay in the peak (Section 4.1.1). Since the rooting depth of the scenarios in which the water balance approach was used is bigger than the rooting depth of the current version of the model, the peak is later (Section 4.1.1). In Appendix G.4, the results for all peaks can be found.

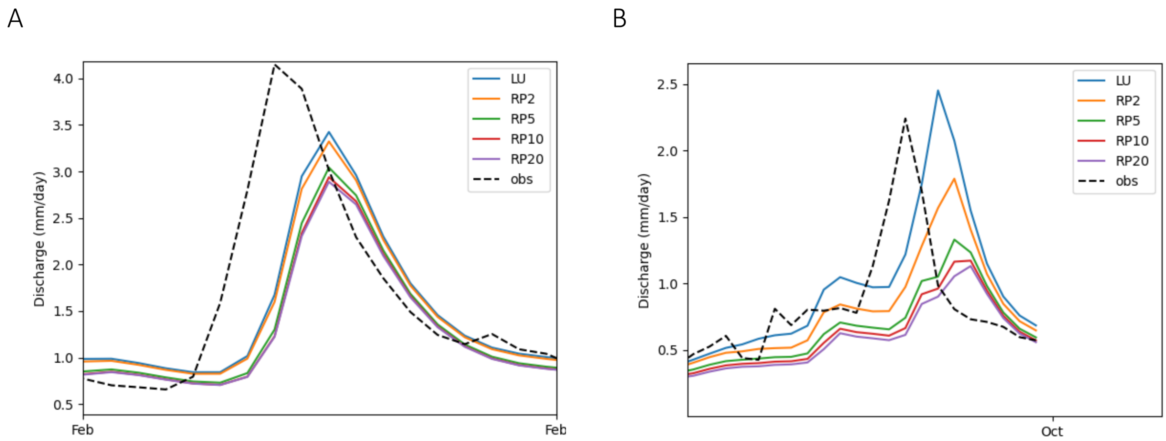

Figure 28: (A) Example of peak within a wet period (February 2005) of which the timing is not substantially differing for the different modelled scenarios. (B) Example of peak after a dry period (October 2001) of which the timing is worse in the scenarios in which the water balance approach was used (RP2 – RP20) compared to the current version of the model (LU)

The predictive power of all versions of the model regarding the timing of the peak is not very strong. The peaks modelled with the current version of the model are on average 3 days later than the observed peaks. For the new versions of the model, this is even bigger. A possible reason for this would be the measurement errors at stations. This was especially likely to be the case when the observed peaks in precipitation are later than observed discharge peaks. However, as elaborated in Appendix G.5., this is not the case.

Height of the peaks

The same 117 peaks in the hydrograph of Cochem were used to analyse the predictive power of the height of the peaks for the different versions of the model. As can be seen in Figure 29, for the total of 117 peaks, 47% of the peaks was predicted more accurately by the new versions of the model, while 36% of the peaks was predicted more accurately by the current version of the model.

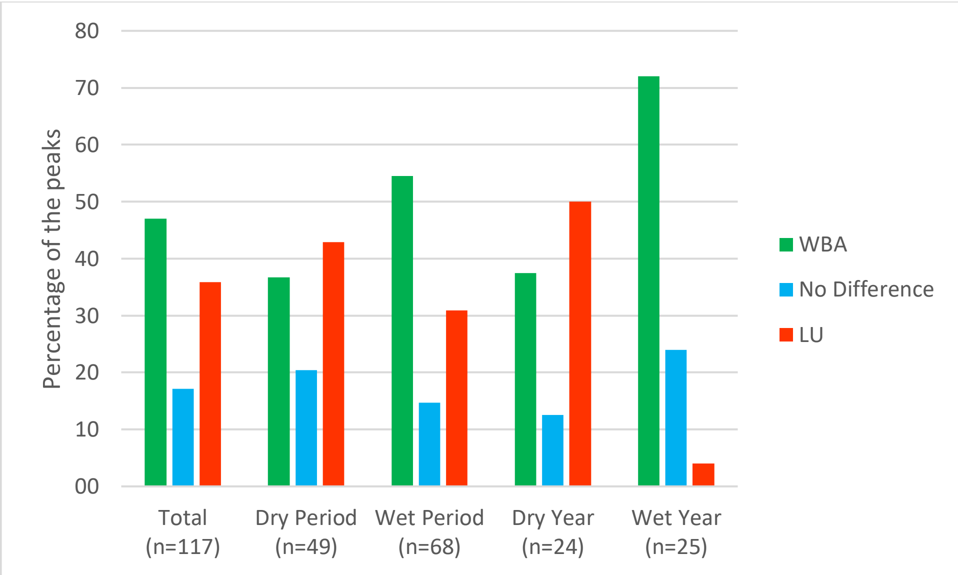

Figure 29: Percentage of the considered peaks for which the versions of the model with the new estimations of the Rooting Depth predicted the height of the observed peak better (green) or worse (red) than the model with the current estimations of the Rooting Depth. In blue, the percentage of peaks for which there was no substantial difference between both versions is given

What stands out is that the height of the peaks falling within the 6 wettest years is substantially better predicted by the versions of the model using the water balance approach (72%) to estimate the root-zone storage capacity than the current version of the model (4%). A possible explanation for this could be that the peaks in the wet years are currently overestimated and that the water balance approach leads to a lower estimation (Section 4.4.3). Especially the peaks in the wet period of the wet peaks are closer to the observations when using the water balance approach to estimate the root-zone storage capacity.

5. Discussion

To improve the wflow_sbm model of the Moselle basin, in this research, the role of the root-zone storage capacity in this model was evaluated and it was assessed whether another method, the water balance approach, for estimating the root-zone storage capacity would improve the predictive power of the model.

5.1 Sensitivity analysis

First of all, the results of Section 4.1 show the Rooting Depth has a substantial role in the model performance of the wflow_sbm model, which is also concluded in Imhoff, Verseveld, Osnabrugge & Weerts (2020). Since the Rooting Depth (parameter in the wflow_sbm model) is closely related to the root-zone storage capacity (Singh, Wang-Erlandsson, Fetzer, Rockström, & Ent, 2020), this implies the model is sensitive to a change in the root-zone storage capacity. From the sensitivity analysis, it follows that a larger rooting depth leads to a lower discharge and a higher actual evaporation, especially for dry periods. (Wang-Erlandsson, et al., 2016) and (Bouaziz, et al., 2021) indicate the same relationship. However, according to Figure 14, there is a limit to this trend: changing the average value of the rooting depth between 80 and 1300 mm gives a substantial difference in annual run-off coefficient, but when the average rooting depth is more than 1300 mm or less than 80 mm, changing the rooting depth does not lead to a substantial change in annual model performance. As the average rooting depth in the current model is 318 mm and it is physically unlikely that the average rooting depth in the Moselle basin becomes higher than 1300 mm or lower than 80 mm, the rooting depth thus is a sensitive parameter to the average annual output in the Moselle basin.

5.2 Water balance approach

The results of the estimation of the root-zone storage capacity using the water balance approach (Figure 20) are in the same order of magnitude as the estimations of Wang-Erlandsson, et al. (2016) and Schenk, et al. (2009). However, uncertainties in the estimation of the root-zone storage capacity remain. A first important reason for this is the limited data availability of observed discharge data. To determine the long-term discharge, the average of annual discharges is determined. However, the period in which observed discharge data was available was for some locations very short (Table 2 of Appendix C). As a result, the amount of years for which 95% of the days observed discharge data is available, for location 4A is only 11 years (Table 2 of Appendix C). The long-term discharge is thus based on a short period and is thus uncertain. In case the long-term discharge would increase with 10%, the root-zone storage capacity would decrease with 16.3%, while an increase of 10% in long-term discharge leads to an increase with 17.7% of the root-zone storage capacity[1].

Secondly, uncertainties in precipitation and evaporation data may lead to uncertain estimates of the root-zone storage capacity. In the Rhine river, stations for precipitation observations are often irregularly spatially and temporally distributed, leading to substantial uncertainties (Rauthe, Steiner, Riediger, Mazurkiewicz, & Gratzki, 2013).

Thirdly, there are uncertainties in the estimations of the root-zone storage capacity using the water balance approach, as the water balance approach is based on certain assumptions which are not always true in the Moselle basin. For example, in the water balance approach it is assumed that vegetation systems adapt their roots in such a way that they can survive critical periods (Merz, Parajka, & Blöschl, 2011). However, from the area for which cropland is the dominant land-use, 78% is arable land (European Environment Agency, 2018), which means the land is under temporary crops

[1] Average over all return periods

and ploughed regularly. As a result, root systems of these crops cannot adapt in such a way that they can survive critical periods, as this is a process of years.

5.3 Translating the root-zone storage capacity to a rooting depth

The values that were obtained after having translated the root-zone storage capacity to a rooting depth (Figure 21, page 28) are on average higher than the current rooting depth values, but still within a realistic range (Canadell, et al., 1996): For each return period that is used, the average and median rooting depth is higher than the average and median rooting depth of the current model (Appendix F). However, especially in the steeper, more forested areas, the rooting depth of the current model is higher than the estimations using the water balance approach with a low return period (Figure 62 and Figure 63).

In the translation step (Section 3.3) it was assumed that an increase in root-zone storage capacity would lead to an increase in rooting depth (in vertical direction). However, it may also be possible that the roots develop in horizontal direction in reality. This leaves room for improvement. Another important assumption of the water balance approach is that vegetation only taps its water from the unsaturated zone and not from the saturated zone. In the wflow_sbm model, if the roots are able to reach the saturated zone, first the transpiration is taken from the saturated zone, but if the roots are above the groundwater level the unsaturated zone is used (Schellekens, wflow Documentation, 2020).

5.4 Comparison between models

Comparing the predictive power of the new versions of the model with the predictive power of the current version of the model shows that the average annual performance of the new versions of the model are closer to the annual observed data than the current version of the model (Figure 22). The return period that is recommended however depends per location (Figure 69).

Especially for the wet months, in which the current version of the model is overestimating the discharge, the new versions of the model perform better (Figure 26). Regarding the height of discharge peaks on event time scale, when assessing wet years (Figure 29), the predictive power of the new versions of the model perform substantially better than the current version of the model. This is remarkable, as the model comes to better results in these important peak periods without any further calibration of the model. When considering peaks in all years, there is not one model version that performs substantially better than another version (Figure 29).

Regarding the timing of peaks, the peaks of the current version of the model are on average 3 days later than observed peaks. For the new versions of the model, the timing is even later. It was assessed if an unrealistic timing between precipitation event and corresponding discharge peak was the cause of this, but this was not the case (Appendix G).

In the analysis of the results there is however uncertainty regarding the observed values. First of all, the observed values with which the simulated values are compared are sometimes based on a small period, as explained earlier and indicated in Table 2 of Appendix C. Next to that, the validity of these observed data can be doubted, because of measurement errors in the data. On an annual level, in case the observed discharge data increases with 5%, still the model version in which the water balance approach is used has a higher predictive power (Figure 70 of Appendix G.1)

6. Conclusion and recommendations

6.1 Conclusion

The aim of this research was to evaluate the differences between two methods to estimate the root-zone storage capacity in the hydrological wflow_sbm model and to recommend one of the methods for application in operational water management and water management planning. In this conclusion, first the four sub-questions are answered, after that a conclusion to the main question is formulated.

1. How sensitive is the simulated discharge of the Moselle to changes in root-zone storage capacity?

In this study, the rooting depth of the wflow_sbm model is multiplied with different values and the model output at different locations for each scenario was determined. The results show the root-zone storage capacity is a key parameter in the hydrological model of the Moselle. Doubling the rooting depth leads to a decrease in annual discharge of 10.3% (Section 4.1). On event time scale, an increase in the root-zone storage capacity leads to later and lower discharge peaks.

2. How large is the root-zone storage capacity for catchments within the Moselle basin according to the water balance approach and how much does it differ from the current estimation based on look-up tables related to land-use?

The root-zone storage capacity was estimated using the water balance approach using four different return periods. The root-zone storage capacity values differ within the basin and differ for each return period but are within a range of 70 to 266 mm (Table 7, p.60). For return periods 2, 5, 10 and 20 years, the average root-zone storage capacities are 105, 145, 171 and 196 mm respectively (Section 4.2). Only after translating this root-zone storage capacity to a rooting depth (sub-question 3), the root-zone storage capacity could be compared with the current estimations.

3. How can the method for estimating the root-zone storage capacity from water balance data best be implemented in the hydrological wflow_sbm model of the Moselle?

The root-zone storage capacity value was implemented in the hydrological wflow_sbm model by translating it to a rooting depth, using estimates of the saturated and residual water contents (Section 3.3). The resulting rooting depth values differ within the basin and per return period but are within a range of 179 to 1304 mm (Table 8, p.62). Using a return period of 10 years, the average rooting depth is 99.7% higher than the current estimations of the rooting depth.

4. What are the differences in predictive power of both versions of the hydrological wflow_sbm model of the Moselle?

As the new estimations of the rooting depth are higher than the current estimations, the versions of the model in which the water balance approach was used gave lower annual discharges and later and lower discharge peaks.

Comparing both versions of the model with observed discharge data, it turned out that the version in which the root-zone storage capacity was estimated using the water balance approach had a higher predictive power for the annual and monthly metrics. The average annual run-off coefficient of the version of the model in which the water-balance method was used to estimate the root-zone storage capacity deviated 1.38% from the observed annual run-off coefficient, whereas this is 11.7% for the current version of the model.

At event time scale, no such conclusion can be drawn. However surprisingly, in wet years, especially in the wet periods of these years, the model version in which the water balance approach is used is simulating the peaks closer to observations than the current version. This is remarkable, as the model comes to better results in these important peak periods without any further calibration of the model.

"Which of the two methods for estimating the root-zone storage capacity yields the best predictive power of the hydrological wflow_sbm model of the Moselle?"

Following from the answers to the sub-questions, the water balance approach for estimating the root-zone storage capacity is recommended for the Moselle basin, regarding both water management planning and operational water management.

6.2 Recommendations

6.2.1 Practical recommendations for predicting discharges in the Moselle basin

When predicting discharges in the Moselle basin, it is recommended to use the water balance approach for estimating the root-zone storage capacity, instead of using look-up tables relating rooting depth to land-use.

Especially regarding annual metrics, the wflow_sbm model with estimations of the root-zone storage capacity for which the water balance approach was used gives a better prediction (Figure 22, page 29). This makes the water balance approach a suitable approach for estimating the root-zone storage capacity in the field of water management planning.

The version of the model in which the water balance approach was used to estimate the root-zone storage capacity also has a higher predictive power of the heights of discharge peaks in wet years (Figure 29, page 34). The water balance approach is thus also recommended for operational water management, when focusing on high flows. When the focus of a study is on low flows, not a specific version of the model performs better.

When using the water balance approach for the Moselle basin, it is recommended to assume vegetation systems adapt their roots such that they can survive a dry period with a return period of 10 years. Using other return periods model performance improved as well, however as a return period of 10 years led to the best model performance at Cochem (Figure 22, page 29), the most downstream location in the Moselle basin, this return period is recommended.

The water balance approach especially led to better model performance in sub-catchments with a high percentage of forest. Thus, when the focus of the study is on these areas, the water balance approach is highly recommended.

6.2.2 Recommendations for further research

As the water balance approach seems a promising approach for the Moselle, this topic is important to do further research on. In this section, some recommendations for further research are given.

First of all, as mentioned in Section 4.4.4, the predictive power of all versions of the model regarding the timing of peaks is not very strong. The simulated peaks at Cochem (downstream) are on average minimal 3 days later than the observed discharge peaks in all versions of the model. It was already preliminary checked if an unrealistic timing between observed precipitation and discharge peaks could be the cause (Appendix G.5.1), but this was not the case. Another possible cause could be the uncertainty in estimating the kinematic wave (Appendix G.5.2), as the approach that is currently used in the wflow_sbm model especially has limitations in non-steep terrain (Schellekens, 2013). As it is important to be able to predict the timing of peaks on operational water management level, it is important to do further research on the cause of late peak estimations in the wflow_sbm model.

Secondly, as stated in Section 4.4.1, it was expected that the actual evaporation would be equal to the potential evaporation in case the rooting depth was infinitely big. This was however not the case (Appendix D.1). A reason for this may lay in the way soil transpiration and potential evaporation are related in the wflow_sbm model. The actual soil transpiration is dependent on the potential soil evaporation, which is determined by subtracting the actual interception evaporation from the total potential evaporation (Schellekens, The wflow_sbm Model, 2013). It could be that the actual evaporation is not equal to the potential evaporation in case the interception evaporation is not potential. To obtain more insight in the role of the root-zone storage capacity in the wflow_sbm model, checking why the actual evaporation is not equal to the potential evaporation in case the rooting depth is infinitely big could be helpful.

As the water balance approach for estimating the root-zone storage capacity is a promising approach, it would be interesting to see how these findings in the Moselle translate to basins in other parts of the world. For example, basins with a tropical climate, with a short wet season and a long dry season, could be interesting. Gao, et al. (2014) already showed that ecosystems are adjusting their root systems to their environment in diverse catchments in Thailand. As land-cover is changing rapidly in Indonesia (Agaton, Setiawan, & Effendi, 2016), the water balance approach, which is independent on land-cover maps, could be a good approach for estimating the root-zone storage capacity. Testing the findings of this research in a catchment in Indonesia could therefore be valuable.

A last recommendation for further research is to assess if the water balance approach for estimating the root-zone storage capacity will also be useful in basins in which observed discharge data is available at less locations. In the Moselle catchment, the limited availability of observed discharge data already leads to uncertainty in the estimations of the root-zone storage capacity using the water balance approach. In other basins however, it could be that observed discharge data is even more limited. It would thus be interesting to see if using only the most downstream location in the basin in the water balance approach would lead to an improved model performance as well. As elaborated in Appendix H, it is expected that the water balance approach could still improve model performance, but it is important to check this.

7. Bibliography

Agaton, M., Setiawan, Y., & Effendi, H. (2016). Land use/land cover change detection in an urban watershed: a case study of upper Citarum Watershed, West Java Province, Indonesia. *Procedia Environmental Sciences, Vol 33*, 654-660. doi:10.1016/j.proenv.2016.03.120

Behrmann-Godel, J., & Eckmann, R. (2003). A preliminary telemetry study of the migration of silver European eel in the River Moselle, Germany. *Ecology of Freshwater Fish*, 12: 196-202. doi:10.1034/j.1600-0633.2003.00015.x

Boer-Euser, T. d., McMillan, H. K., Hrachowitz, M., Winsemius, H. C., & Savenije, H. H. (2016). Influence of soil and climate on root zone storage capacity. *Water Resources Research, 52*, 2009-2024. doi:10.1002/2015WR018115

Booij, M. (2019). Water Supply. In M. Booij, *Water Management* (pp. 58-78). University of Twente Engineering Technology.

Bouaziz, L., Aalbers, E., Weerts, A., Hegnauer, M., Buiteveld, H., Lammersen, R., . . . Hrachowitz, M. (2021). The importance of ecosystem adaptation on hydrological model predictions in response to climate change. *Hydrology and Earth System Sciences Discuss. [preprint]*. doi:https://doi.org/10.5194/hess-2021-204

Budyko. (1974). *Climate and Life, Volume 18, 1st Edition.*

Canadell, J., Jackson, R., Ehleringer, J., Mooney, H., Sala, O., & Schulze, E. (1996). Maximum rooting depth of vegetation types at the global scale. *Oecologia, 108*, 583-595.

Castillo, A., Castelli, F., & Entekhabi, D. (2015). Gravitational and capillary soil moisture dynamics for distributed hydrologic models. *Hydrology and Earth System Sciences, 19*, 1857-1869. doi:10.5194/hess-19-1857-2015

Cheng, L., Zhang, L., Chiew, F., Canadell, J., Zhao, F., Wang, Y., . . . Lin, K. (2017). Quantifying the impacts of vegetation changes on catchment storage-discharge dynamics using paired-catchment data. *Water Resources Research, 53*, 5963-5979. doi:10.1002/2017WR020600

Deltares. (n.d.). *About us*. Retrieved 2021, from Deltares: https://www.deltares.nl/en/about-us/

Deltares Github. (2021). *wflow_sbm*. Retrieved from deltares.github.io: https://deltares.github.io/Wflow.jl/stable/model/sbm/

Demirel, M., Booij, M., & Hoekstra, A. (2013). Effect of different uncertainty sources on the skill of 10 day ensemble low flow forecasts for two hydrological models. *Water Resources Research*, 4035-4053. doi:doi:10.1002/wrcr.20294.

Demirel, M., Booij, M., & Hoekstra, A. (2015). The skill of seasonal ensemble low-flow forecasts in the Moselle River for three different hydrological models. *Hydrology and Earth System Sciences*, 19, 275-291. doi:10.5194/hess-19-275-2015

European Environment Agency. (2018). *Corine Land Cover (CLC) 2018, version 2020_20u1*. Retrieved from https://land.copernicus.eu/pan-european/corine-land-cover

Gao, H., Hrachowitz , M., Schymanski, S., Fenicia, F., Sriwongsitanon, N., & Savenije, H. (2014). Climate controls how ecosystems size the root zone storage capacity at catchment scale. *Geophysical Research Letters 41*, 7916-7923. doi:10.1002/2014GL061668.

Gao, J., Holden, J., & Kirkby, M. (2016). The impact of land-cover change on flood peaks in peatland basins. *Water Resources Research 52*, 3477-3492. doi:10.1002/2015WR017667

Gerrits, A., Savenije, H., Veling, E., & Pfister, L. (2009). Analytical derivation of the Budyko curve based on rainfall characteristics and a simple evaporation model. *Water Resources Research, Vol. 45*. doi:doi: 10.1029/2008WR007308

Goel, M. (2011). Runoff Coefficient. In V. Singh, P. Signh, & U. Haritashya, *Encyclopedia of Snow, Ice and Glaciers.* Dordrecht: Springer. doi:https://doi.org/10.1007/978-90-481-2642-2_456

Hanus, S., Hrachowitz, M., Zakollari, H., Schoups, G., Vizcaino, M., & Kaitna, R. (2021). Timing and magnitude of future annual runoff extremes in contrasting Alpine catchments in Austria. *Hydrology and Earth System Sciences*. doi:10.5194/hess-2021-92

Heuver, E. (2018). *Moesel.*

Hrachowitz, M., Stockinger, M., Coenders-Gerrits, M., Ent, R. v., Bogena, H., Lücke, A., & Stumpp, C. (2020). Deforestation reduces the vegetation-accessible water storage in the unsaturated soil and affects catchment travel time distributions and young water fractions. *Hydrology and Earth System Sciences Discussions*, 1-43. doi:10.5194/hess-2020-293

Hurkmans, R., Terink, W., Uijlenhoet, R., Moors, E., Troch, P., & Verburg, P. (2009). Effects of land use changes on streamflow generation in the Rhine basin. *Water Resources Research, 45(6)*. doi:10.1029/2008WR007574

Imhoff, R., Verseveld, W. v., Osnabrugge, B. v., & Weerts, A. (2020). Scaling Point-Scale (Pedo)transfer Functions to Seamless Large-Domain Parameter Estimates for High-Resolution Distributed Hydrologic Modeling: An Example for the Rhine River. *Water Resources Research, 56*. doi:https://doi.org/10.1029/2019WR026807

IPCC. (2014). *AR5 Climate Change 2014: Impacts, Adaptation, and Vulnerability - Part B: Regional Aspects.* Cambridge University Press. Retrieved from https://www.ipcc.ch/site/assets/uploads/2018/02/WGIIAR5-PartB_FINAL.pdf

Jasechko, S. (2018). Plants turn on the tap. *Nature Climate Change*, 562-563. doi:10.1038/s41558-018-0212-z

Jenicek, M., Seibert, J., & Staudinger, M. (2018). Modeling of Future Changes in Seasonal Snowpack and Impacts on Summer Low Flows in Alpine Catchments. *Water Resources Research, 54*, 538-556. doi:doi: 10.1002/2017WR021648

Kleidon, A., & Heimann, M. (1998). A method of determining rooting depth from a terrestrial biosphere model and its impacts on the global water and carbon cycle. *Global Change Biology*, 275-286. doi:10.1046/j.1356-2486.1998.00152.x

Merz, R., Parajka, J., & Blöschl, G. (2011). Time stability of catchment model parameters: Implications for climate impact analyses. *Water Resources Research, 47*. doi:10.1029/2010WR009505

Nijzink, R., Hutton, C., Pechlivanidis, I., Capell, R., Arheimer, B., Freer, J., . . . Hrachowitz, M. (2016). The evolution of root-zone moisture capacities after deforestation: a step towards hydrological predictions under change? *Hydrology and Earth System Sciences*, 4775–4799. doi:0.5194/hess-20-4775-2016

Osnabrugge, B. v., Weerts, A., & Uijlenhoet, R. (2017). genRE: A method to extend gridded precipitation climatology data sets in near real-time for hydrological forecasting purposes. *Water Resources Research, 53*, 9284-9303. doi:https://doi.org/10.1002/2017WR021201

Peel, M., & Blöschl, G. (2011). Hydrologic modelling in a changing world. *Progress in Physical Geography 35(2)*, 249-261. doi:10.1177/0309133311402550

Petrow, T., Zimmer, J., & Merz, B. (2009). Changes in the flood hazard in Germany through changing frequency and persistence of circulation patterns. *Natural Hazards and Earth System Sciences, 9(4)*, 1409-1423.

Pushpalatha, R., Perrin, C., Moine, N. L., Mathevet, T., & Andréassian, V. (2011). A downward structural sensitivity analysis of hydrological models to improve low-flow simulation,. *Journal of Hydrology, Vol 411, Issues 1-2*, 66-76. doi:https://doi.org/10.1016/j.jhydrol.2011.09.034

Ranatunga, T., Tong, S., & Yang, Y. (2017). An approach to measure parameter sensitivity in watershed hydrological modelling. *Hydroloigcal Science Journal 62(1)*, 76-92. doi:10.1080/02626667.2016.1174335

Rauthe, M., Steiner, H., Riediger, U., Mazurkiewicz, A., & Gratzki, A. (2013). A Central European precipitation climatology - Part I: Generation and validation of a high-resolution gridded daily data set (HYRAS). *Meteorologsche Zeitschrift, Vol. 22, No.3*, 235-256.

Savenije, H., & Hrachowitz , M. (2017). Hess Opinions "Catchment as meta-organisms - a new blueprint for hydrological modelling". *Hydrology and Earth System Sciences 21(2)*, 1107-1116. doi:10.5194/hess-21-1107-2017

Schellekens, J. (2013). *The wflow_sbm Model*. Retrieved from wflow docs: https://wflow.readthedocs.io/en/latest/wflow_sbm.html

Schellekens, J. (2020). *wflow Documentation.*

Schellekens, J. (2020B). *wflow_funcs Module.* Retrieved from https://wflow.readthedocs.io/en/latest/wflow_funcs.html#rainfall-interception

Schenk, H., Jackson, R., Hall, F., Collatz, G., Meeson, B., Los, S., . . . Landis, D. (2009). *ISLSCP II Ecosystem Rooting Depths. ORNL DAAC*. doi:https://doi.org/10.3334/ORNLDAAC/929

Singh, C., Wang-Erlandsson, L., Fetzer, I., Rockström, J., & Ent, R. v. (2020). Rootzone storage capacity reveals drought coping strategies along rainforest-savanna transitions. *Environmental Research - 15*, 124021.

Thompson, S., Harman, C., Konings, A., Sivapalan, M., Neal, A., & Troch , P. (2011). Comparative hydrology across AmeriFlux sites: The variable roles of climate, vegetation, and groundwater. *Water Resources Research Vol. 47*, 17. doi:0043-1397/11/2010WR009797

Uehlinger, U., Wantzen, K., Leuven, R., & Arndt, H. (2009). The Rhine River Basin. *Rivers of Europe / Klement Tockner*, 199-254. doi:10.1016/B978-0-12-369449-2.00006-0.

Vertessy, R., & Elsenbeer, H. (1999). Distributed Modeling of Storm Flow Generation in an Amazonian Rain Forest Catchment: Effects of Model Parameterization. *Water Resources Research Vol. 35*. doi:10.1029/1999WR900051

Vittal, K., & Subbiah, B. (1984). Identification of rooting depth and measurements of plant root activity in situ and in toto under field conditions using a gamma probe technique. *Experientia 40*, 585-587.

Vormoor, K., Lawrence, D., Heistermann, M., & Bronstert, A. (2015). Climate change impacts on the seasonality and generation processes of floods - projections and uncertainties for catchments with mixed snowmelt/rainfall regimes. *Hydrology and Earth System Sciences, 19*, 913-931. doi:doi:10.5194/hess-19-913-2015

Vriend, H. d., Havinga, H., Visser, P., & Wang, Z. (2006). *Rvierwaterbouwkunde.* Delft: Faculteit Civiele Techniek en Geowetenschappen. doi:06917300005

Wang-Erlandsson, L., Bastiaanssen, W., Gao, H., Jägermeyr, J., Senay, G., Dijk, A. v., . . . Savenije, H. (2016). Global root zone storage capacity from satellite-based evaporation. *Hydrology and Earth System Sciences 20*, 1459-1481. doi:10.5194/hess-20-1459-2016

Wind, H., Nierop, T., Blois, C. d., & Kok, J. d. (1999). Analysis of flood damages from the 1993 and 1995 Meuse floods. *Water Resources Research, Vol. 35, No. 11*, 3459-3465. doi:0043-1397/99/1999 WR900192509.00

Wong, W., Stein, B., Torill, E., Ingjerd, H., & Hege, H. (2011). Climate change effects on spatiotemporal patterns of hydroclimatological summer droughts in Norway. *Journal of Hydrometeorology, 12(6)*, 1205-1220. doi:10.1175/2011JHM1357.1

Appendices

Appendix A. Rooting depth, porosity and wilting point in the Moselle basin

In this Appendix, maps that are used in the current version of the wflow_sbm model of the Moselle can be found.

A.1 Rooting Depth

In Figure 30, the Rooting Depth map that is currently used in the wflow_sbm model of the Moselle can be found. The values are based on look-up tables, relating land-use to a rooting depth.

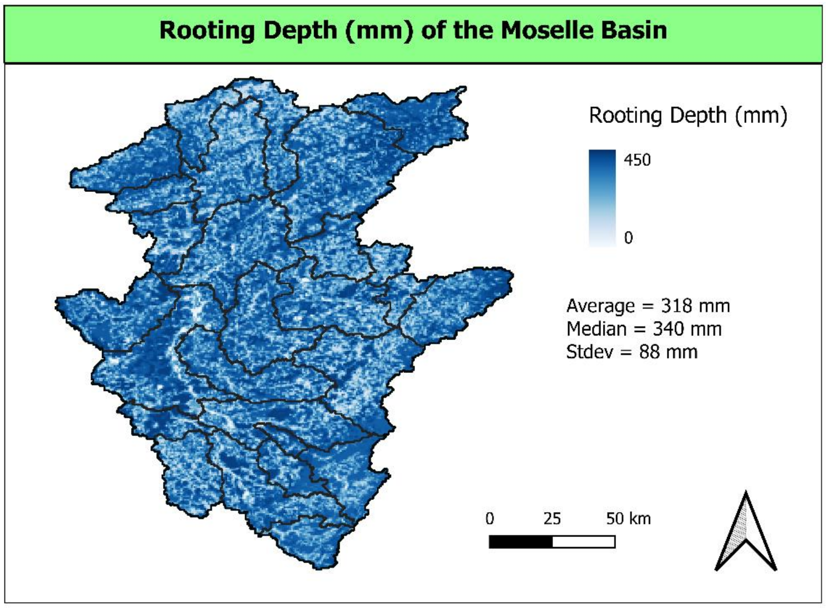

Figure 30: Rooting depth (mm) of the Moselle basin, as used in the current version of the wflow_sbm model of the Moselle

A.2 Porosity

In Figure 31, the porosity map that is currently used in the wflow_sbm model of the Moselle can be found.

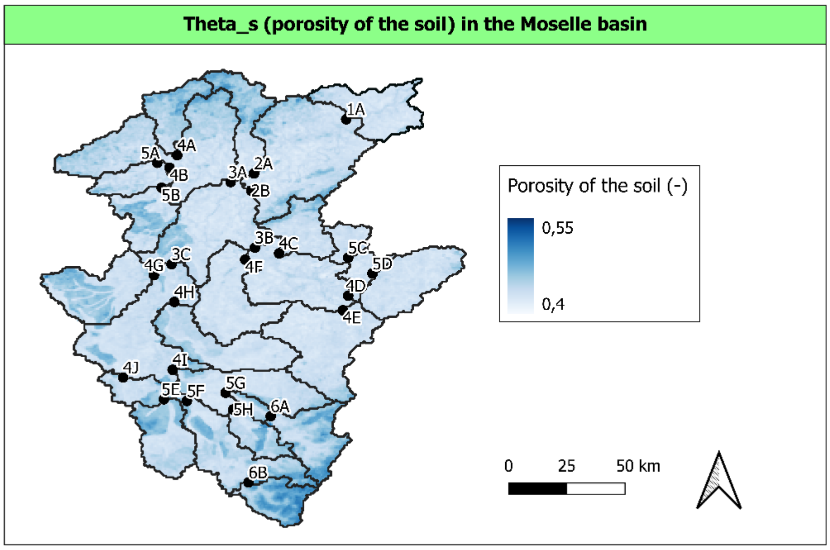

Figure 31: Porosity of the soil (-), as used in the current version of the wflow_sbm model of the Moselle

A.3 Wilting Point

In Figure 32, the wilting point map that is currently used in the wflow_sbm model of the Moselle can be found.

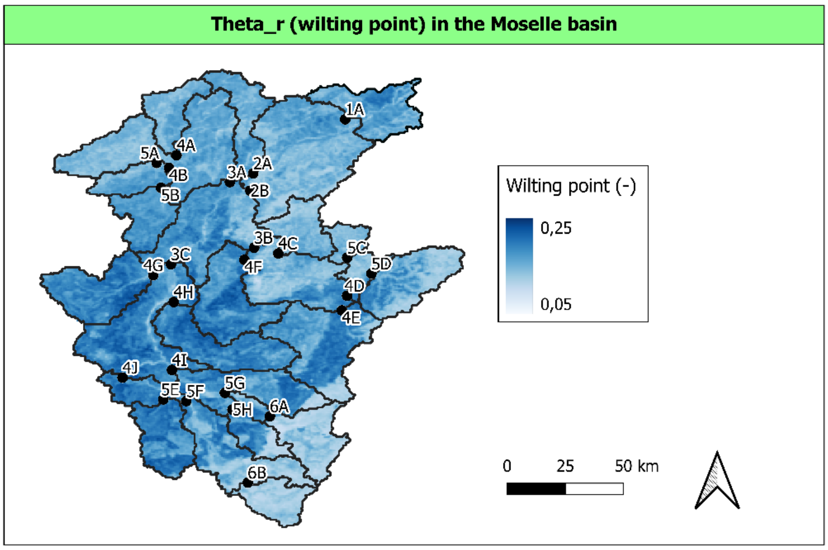

Figure 32: Wilting point (-), as used in the current version of the wflow_sbm model of the Moselle

Appendix B. Warm-up period

To define the warm-up period, the modelled hydrograph at Cochem for the first three years of the simulation period (1979 – 1981) was used (Figure 33). As can be seen in this Figure, the discharge at 1-1-1979 is 0 m^3/s, which is an unrealistic value. As can be seen, after around 50 days, the discharge is 1900 m^3/s. Studying the shape of the hydrograph of the other years, this value and shape is realistic. It is thus assumed that the model is in the right state after 50 days. To be more certain about this period, a warm-up period of 1 year was assumed.

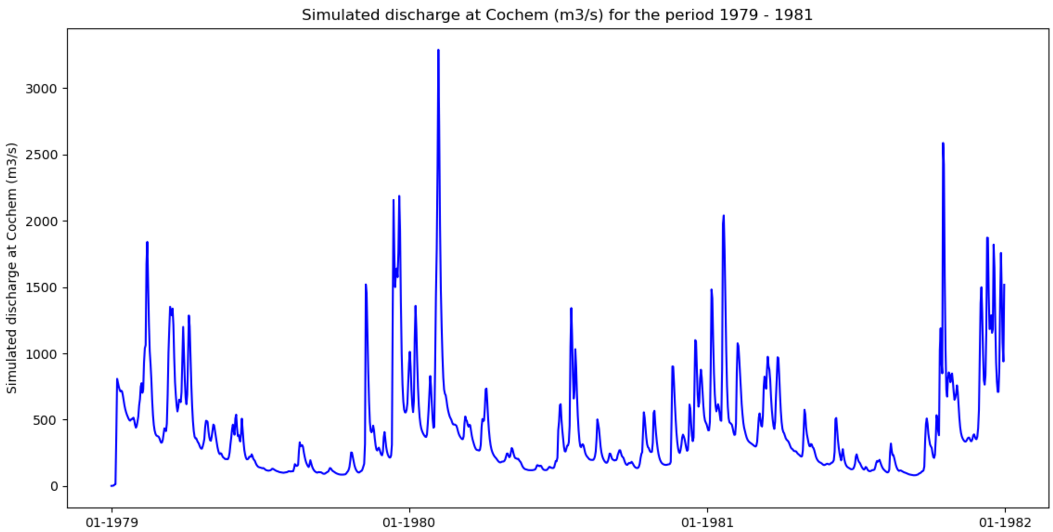

Figure 33: Modelled hydrograph at Cochem for the period 1979-1981

Appendix C. Overview of sub-catchments

In this Appendix, more information about the nested sub-catchments in which the Moselle catchment area is divided can be found.

As stated in Section 3.2.4, in total 26 nested sub-catchments are defined. In Figure 34, an overview of the locations of these catchments can be found.

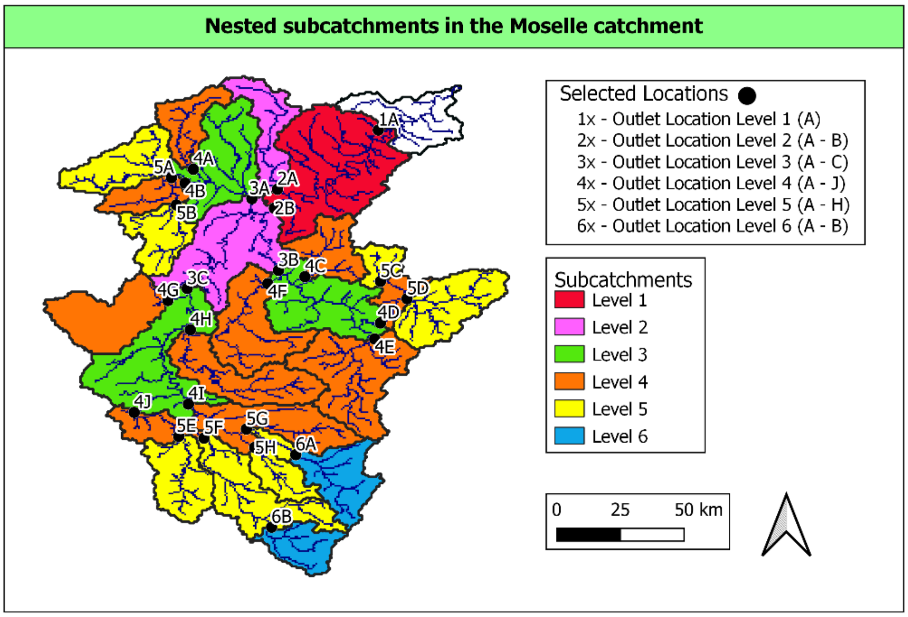

Figure 34: Nested sub-catchments in the Moselle catchment. Colours indicate the different levels, the black points indicate the outlet points of each sub-catchment

As said, the catchments are nested. This means that certain catchments of level X+1 are located within a catchment of level X. For example, catchment 5C and 5D are nesting within catchment 4D. The catchment area belonging to location 4D is thus the total of the two yellow parts and the orange part of Figure 35B.

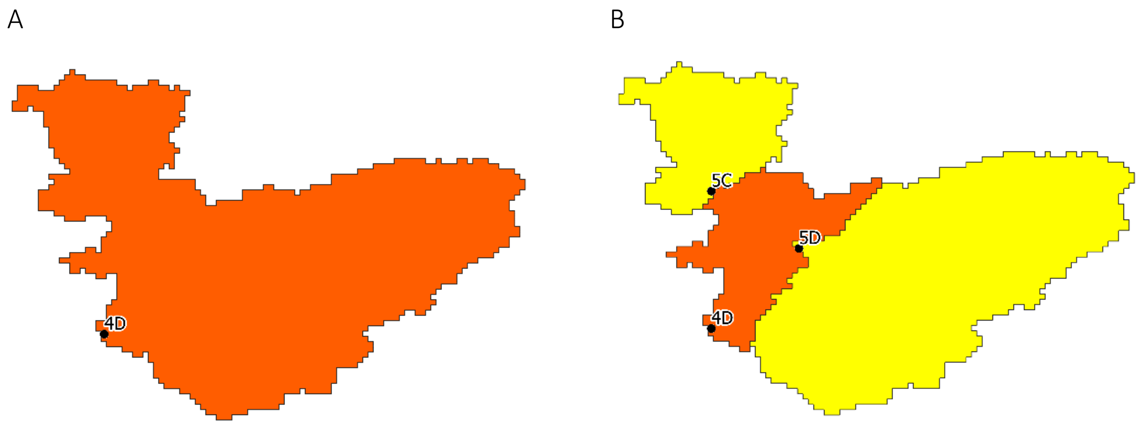

Figure 35: Example of nested catchments: Area 5C and 5D are nesting within area 4D

In the Figures below (Figure 36 to Figure 41), the full catchment areas belonging to a certain level can be found.

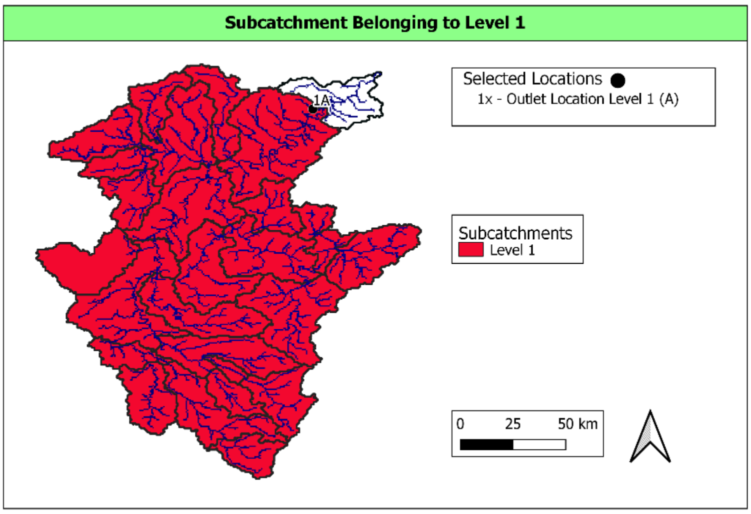

Figure 36: Sub-catchment in the Moselle catchment that belongs to level 1

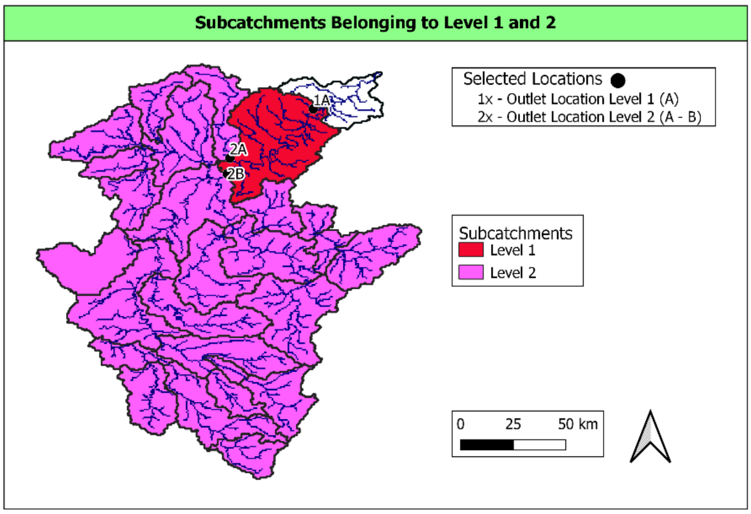

Figure 37: Sub-catchments in the Moselle catchment that belong to level 1 and 2

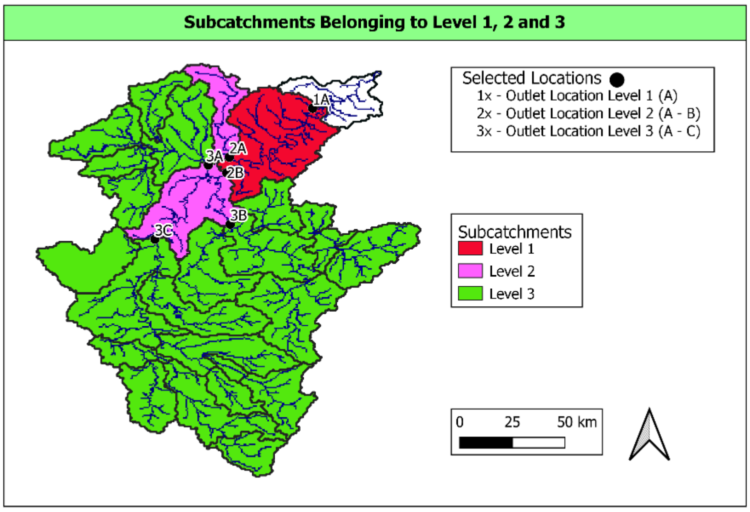

Figure 38: Sub-catchments in the Moselle catchment that belong to level 1, 2 and 3

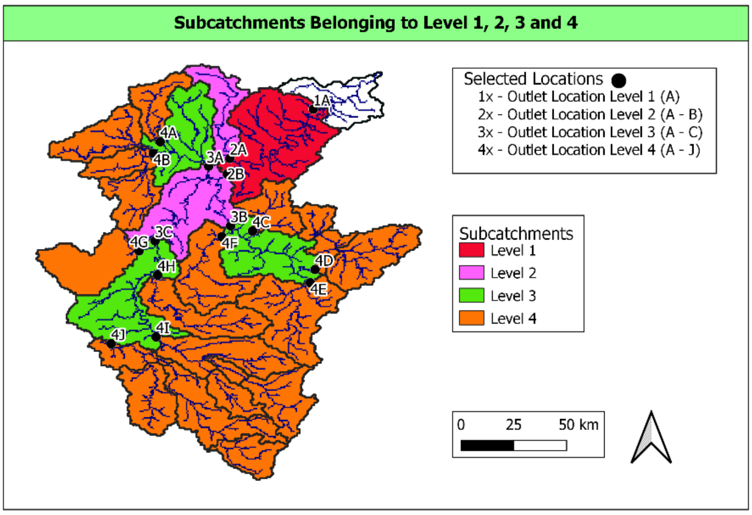

Figure 39: Sub-catchments in the Moselle catchment that belong to level 1, 2, 3 and 4

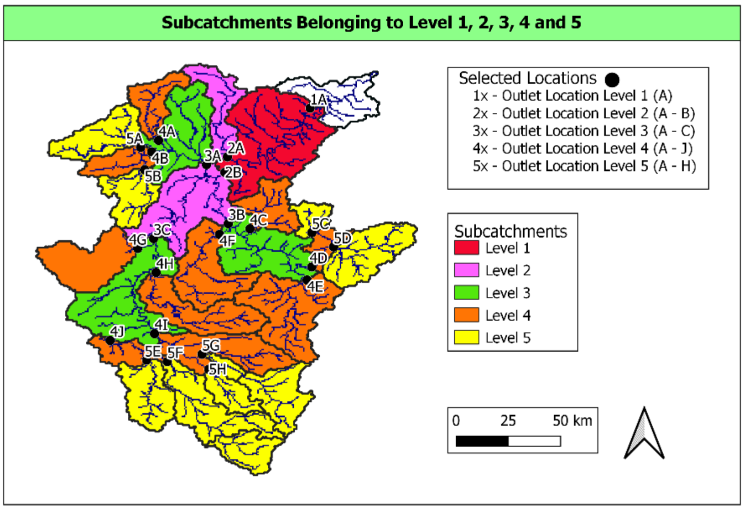

Figure 40: Sub-catchments in the Moselle catchment that belong to level 1, 2, 3, 4 and 5

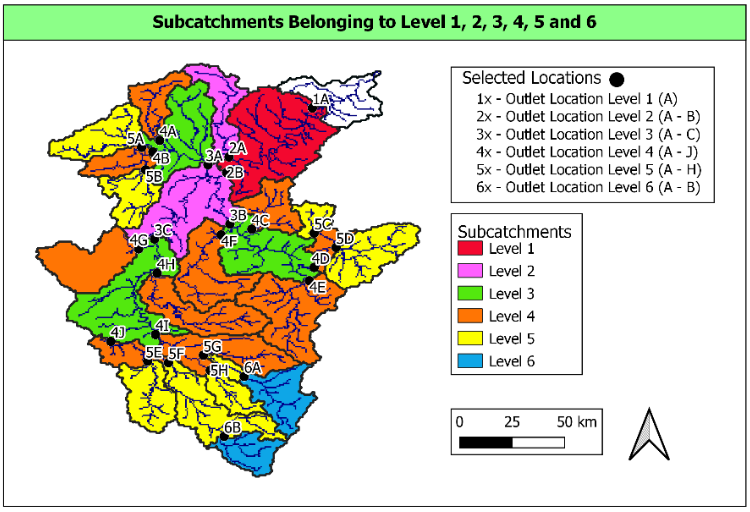

Figure 41: Sub-catchments in the Moselle catchment that belong to level 1, 2, 3, 4, 5 and 6

In Table 2, an overview of the characteristics of the different catchment areas can be found. The areas that are also selected for the sensitivity analysis are made bold.

Table 2: Overview of the characteristics of different catchment areas. The data period that is given is the period in which observed discharge data at the output locations of the catchments is available. The amount of years for which at least 95% of the days data is available, is given in the last column

#	Level	Name	Area (km^2)	Nesting areas	ID	Data	Eff. Years
1A	1	**Cochem**	27187.3	2A, 2B	694	1990-2016	25
2A	2	Kordel	819.8	-	683	1990-2016	25
2B	2	Trier	23815.0	3A, 3B, 3C	707	1990-2016	22
3A	3	**Rosport**	4268.9	4A, 4B	14	2002-2016	12
3B	3	**Fremersdorf**	6974.2	4C, 4D, 4E, 4F	711	1990-2008	17
3C	3	**La Moselle à Uckange**	10801.4	4G, 4H, 4I, 4J	373	1990-2016	25
4A	4	Vianden	636.7	-	11	2002-2016	12
4B	4	Diekirch	2183.7	5A, 5B	10	2002-2016	12
4C	4	Nalbach	718.7	-	302	1989-2016	26
4D	4	Reinheim	1806.9	5C, 5D	299	1989-2016	26
4E	4	La Sarre à Wittring	1712.5	-	368	1994-2016	21
4F	4	Niedaltdorf	1345.1	-	303	1989-2016	26
4G	4	L'Orne à Rosselange	1237.8	-	399	1990-2016	24
4H	4	La Seille à Metz	1271.6	-	726	1990-2005	13
4I	4	La Meurthe à Malzéville	2881.9	5G, 5H	365	1990-2012	11
4J	4	La Moselle à Toul	3404.2	5E, 5F	414	1990-2016	24
5A	5	Michelau	948.8	-	20	2002-2015	12
5B	5	Mersch	740.0	-	5	2002-2016	12
5C	5	Neunkirchen	319.2	-	297	1989-2016	26
5D	5	Eined	1158.9	-	328	1989-2016	26
5E	5	Le Madon à Pulligny	945.4	-	409	1990-2016	25
5F	5	La Moselle à Tonnoy	1994.1	6B	375	1990-2016	22
5G	5	La Meurthe à Luneville	1105.2	6A	391	1990-2016	20
5H	5	La Mortagne à Gerbéviller	495.8	-	394	1990-2016	25
6A	6	**La Meurthe à Baccarat**	935.7	-	374	1992-2009	15
6B	6	La Moselle à Saint-Nabord	630.7	-	413	1990-2016	23

Appendix D. Results of the sensitivity analysis (step 1)

In this Appendix, the results of the sensitivity analysis can be found.

D.1 Average Annual Performance

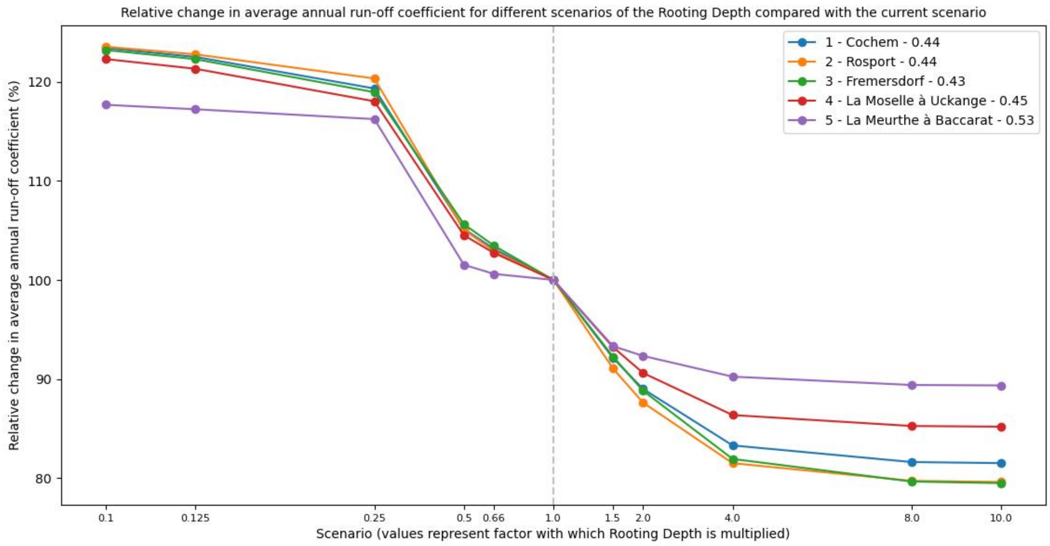

Figure 42: Relative change in average annual run-off coefficient for different scenarios of the Rooting Depth compared with the current scenario, for each selected location. The value behind the name in the Legend represents the average annual run-off coefficient in the base scenario. For example, for selected location 4, the average annual run-off coefficient changed to 85% when multiplying the Rooting Depth with 8 compared to the base scenario. The average annual run-off coefficient of that location, for that scenario was thus 85% of 0.45

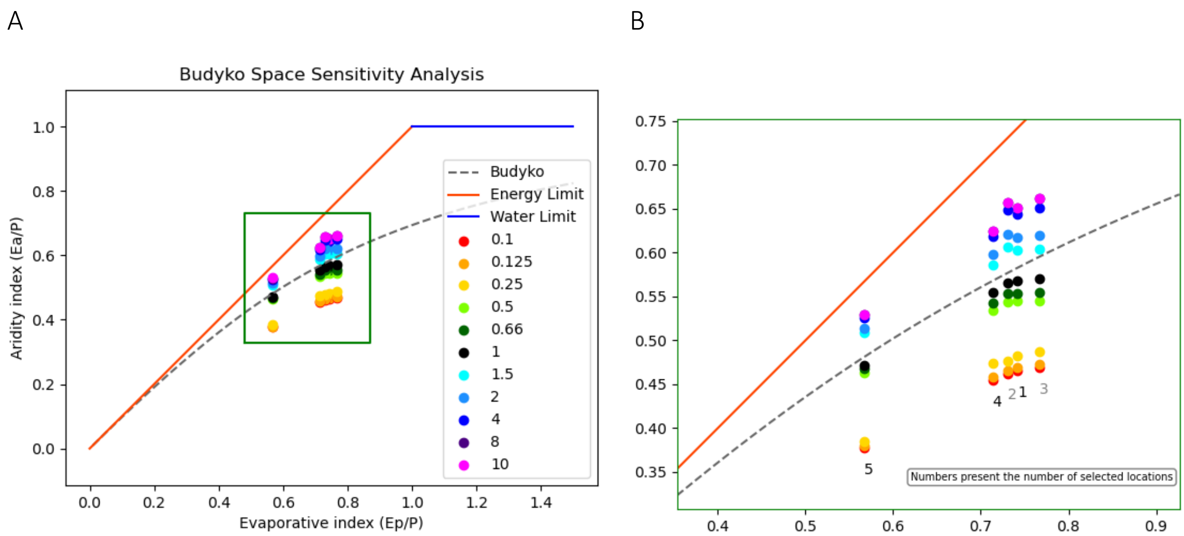

Figure 43: Budyko Space showing the ratio $\overline{E_a}/\overline{P}$ as function of $\overline{E_p}/\overline{P}$ for each scenario at each selected output location. The grey dotted line presents the Budyko curve, the red and blue line the energy and water limit. The green box is enlarged in Figure B. The numbers below the points in Figure B present the number of the output locations (1 = Cochem, 2 = Rosport, 3 = Fremersdorf, 4 = La Moselle à Uckange, 5 = La Meurthe à Baccarat)

Table 3: Average values of the rooting depth (mm) for different scenarios, namely the base scenario, scenario *0.25 and scenario *4. In blue, the range of rooting depth is given for which the model output is sensitive. In case the rooting depth value falls inside the range, this means the average annual run-off coefficient changes substantially when changing the Rooting Depth. In case the rooting depth falls outside the range, the rooting depth does not have substantial influence on the model output

#	Name	RD (base scenario)	RD * 0.25	RD * 4
1	Cochem	318	80	1272
2	Rosport	314	79	1256
3	Fremersdorf	309	77	1236
4	La Moselle à Uckange	325	81	1300
5	La Meurthe à Baccarat	333	83	1332
			80	1300

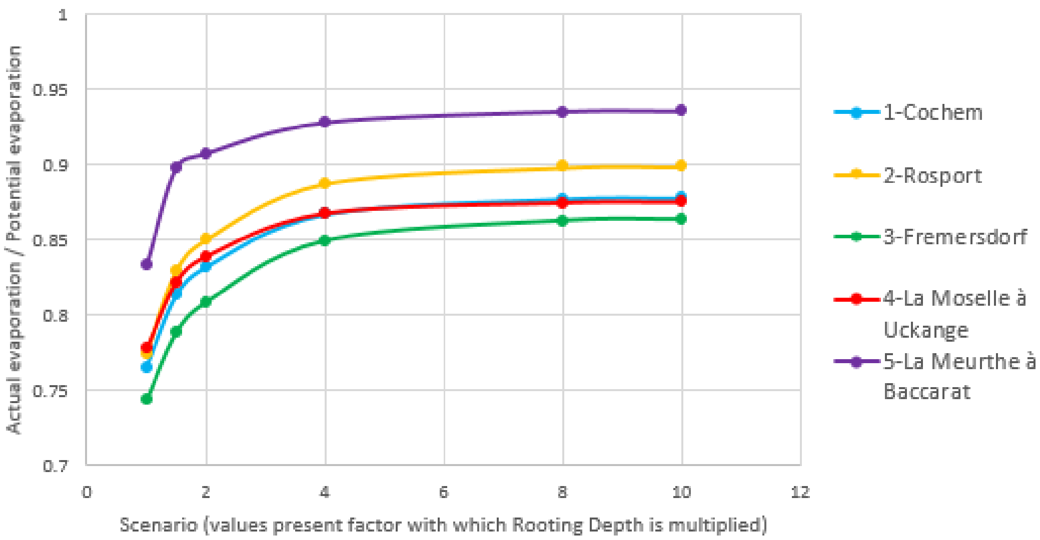

Figure 44: Actual evaporation divided by potential evaporation for different scenarios of the rooting depth (those scenarios for which the rooting depth is increased), and for different locations. As the rooting depth increases, the ratio E_a/E_p increases with a lower rate. E_a/E_p never reaches 1, which means the actual evaporation never is equal to the potential evaporation

D.2 Performance in dry period

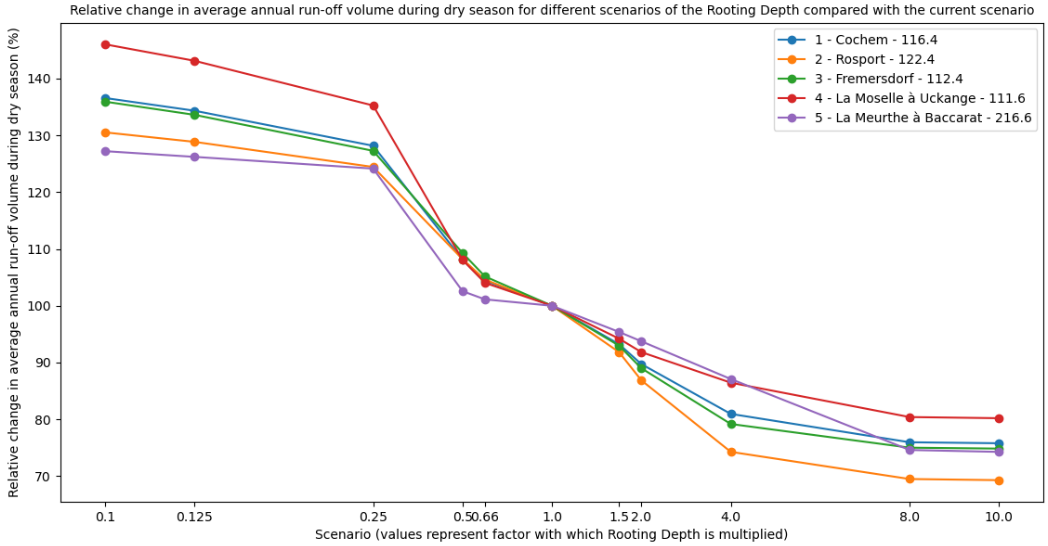

Figure 45: Relative change in average annual run-off volume during the dry season (1st of April – 30th of September) for different scenarios of the Rooting Depth compared with the current scenario, for each selected location. The value behind the name in the Legend represents the average annual run-off volume (mm) during the dry season in the base scenario

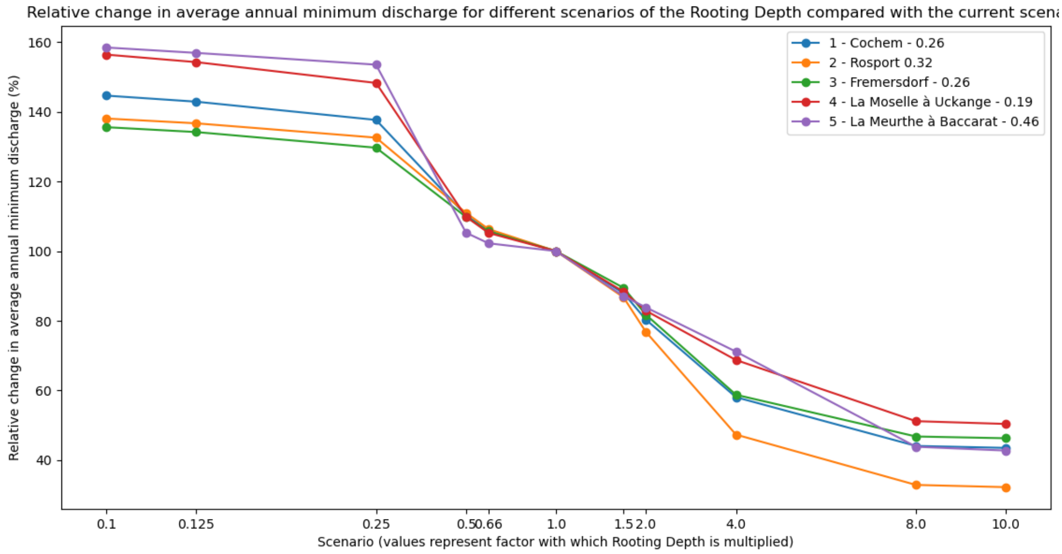

Figure 46: Relative change in average annual average minimum discharge of seven consecutive days for different scenarios of the Rooting Depth compared with the current scenario, for each selected location. The value behind the name in the Legend represents the average annual average minimum discharge of seven consecutive days (mm/day) in the base scenario

D.3 Comparison average performance and dry period, for all stations

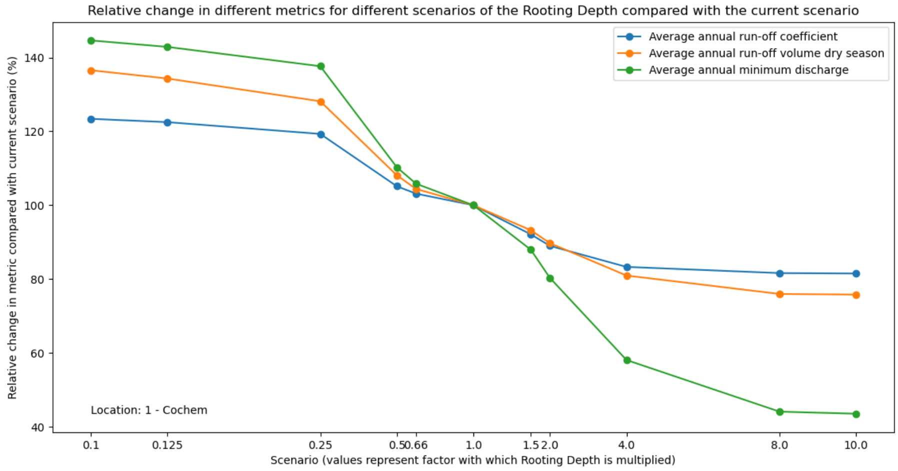

Figure 47: Relative change in different metrics (see legend) for different scenarios of the Rooting Depth, compared with the current scenario (%). Location = Cochem (1)

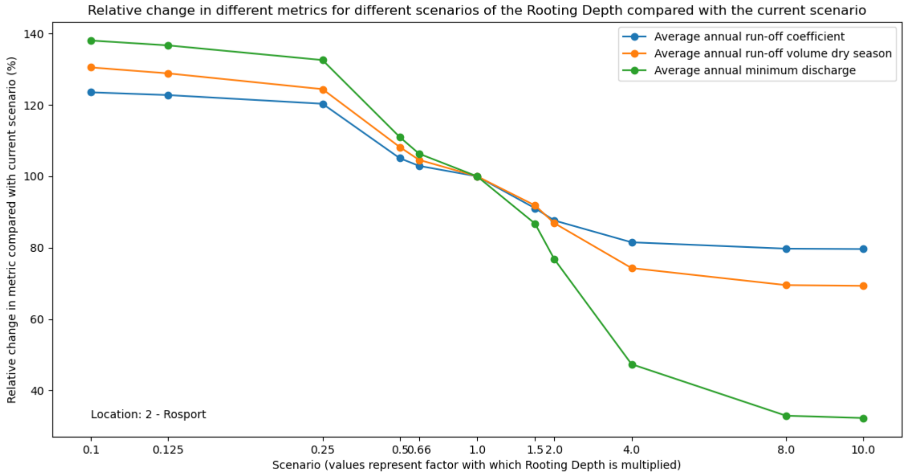

Figure 48: Relative change in different metrics (see legend) for different scenarios of the Rooting Depth, compared with the current scenario (%). Location = Rosport (2)

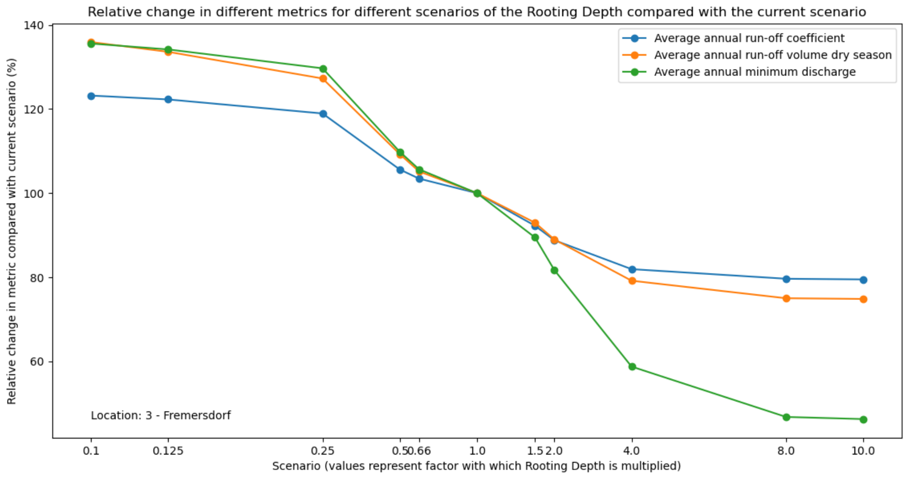

Figure 49: Relative change in different metrics (see legend) for different scenarios of the Rooting Depth, compared with the current scenario (%). Location = Fremersdorf

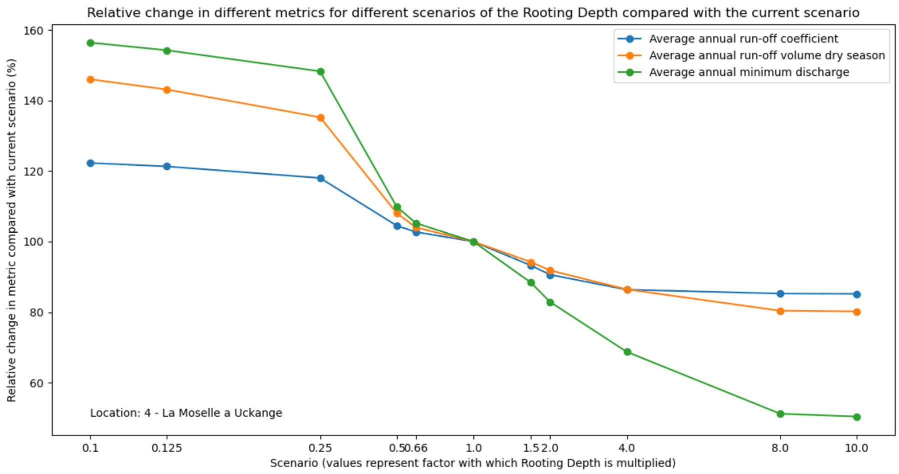

Figure 50: Relative change in different metrics (see legend) for different scenarios of the Rooting Depth, compared with the current scenario (%). Location = La Moselle à Uckange (4)

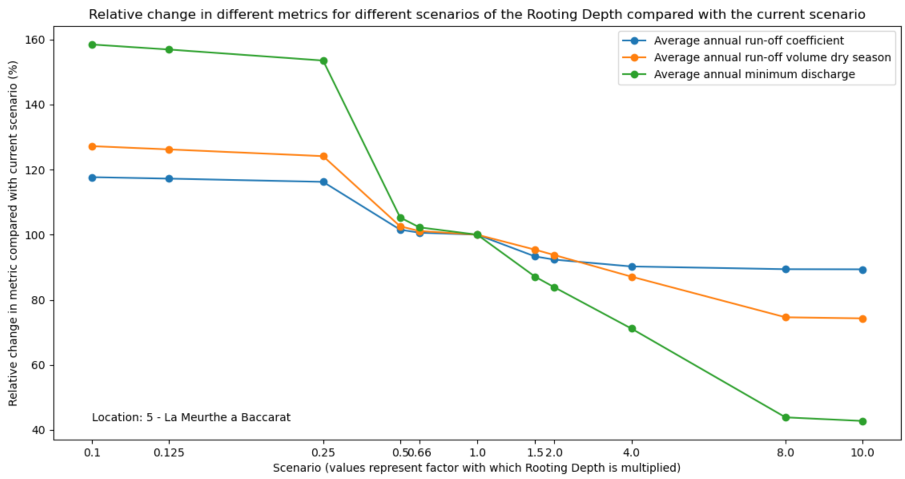

Figure 51: Relative change in different metrics (see legend) for different scenarios of the Rooting Depth, compared with the current scenario (%). Location = La Meurthe à Baccarat (5)

D.4 Hydrographs

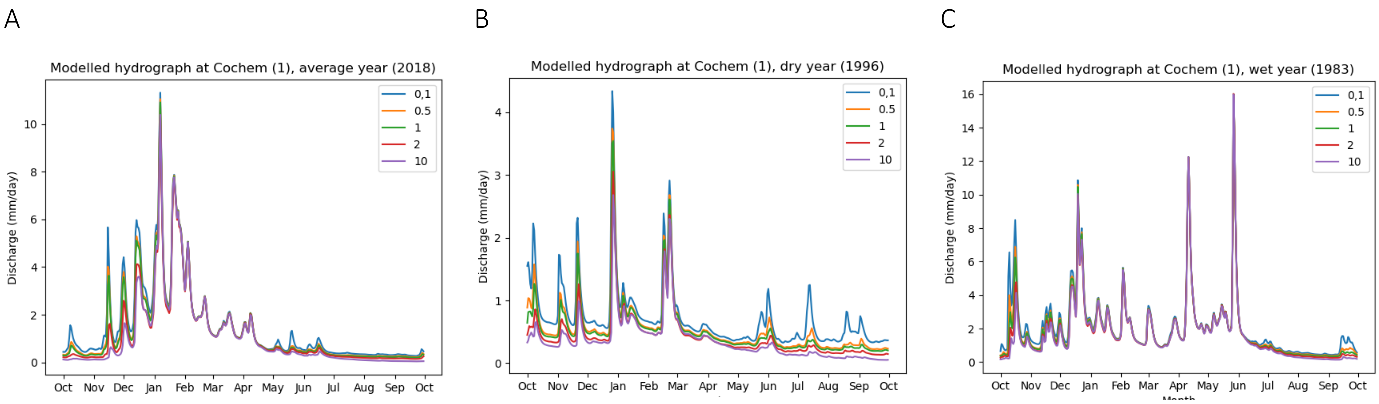

Figure 52: Modelled hydrographs at Cochem (location 1) for different years (2018, 1996, 1983), for different scenarios of the rooting depth (0.1, 0.5, 1, 2, 10)

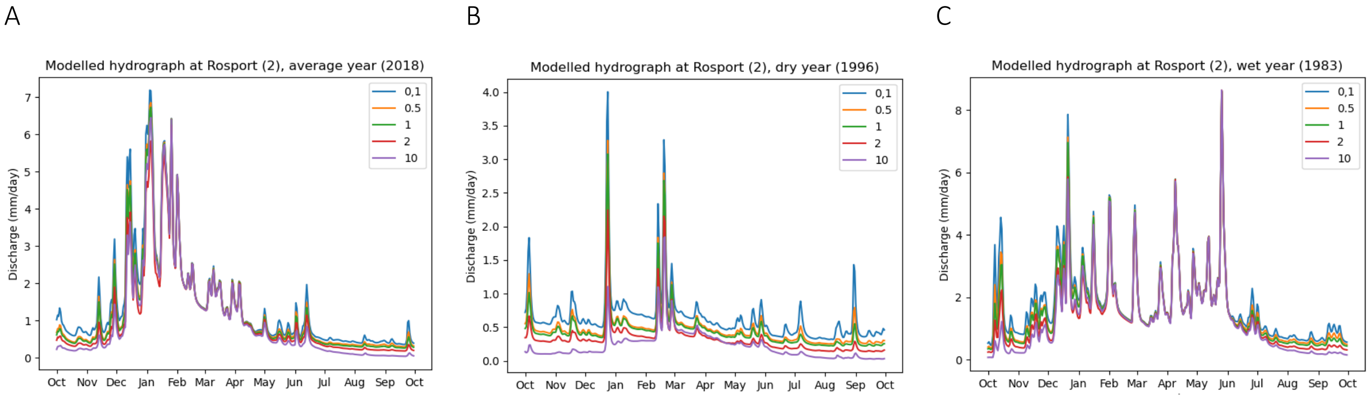

Figure 53: Modelled hydrographs at Rosport (location 2) for different years (2018, 1996, 1983), for different scenarios of the rooting depth (0.1, 0.5, 1, 2, 10)

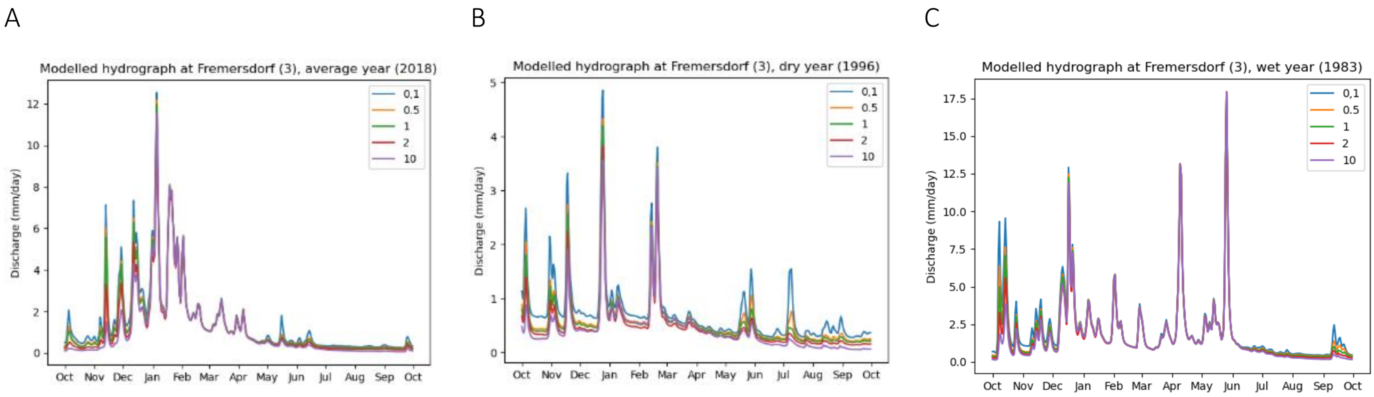

Figure 54: Modelled hydrographs at Fremersdorf (location 3) for different years (2018, 1996, 1983), for different scenarios of the rooting depth (0.1, 0.5, 1, 2, 10)

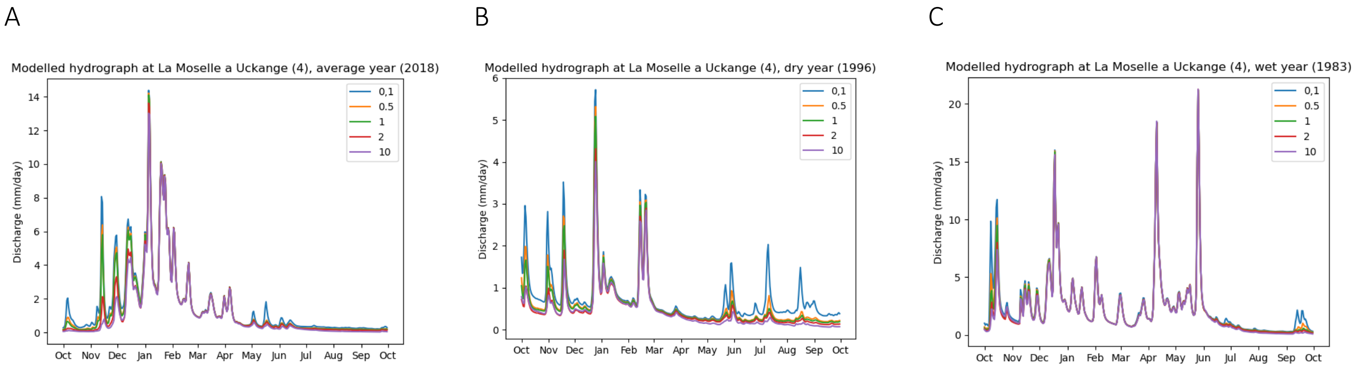

Figure 55: Modelled hydrographs at La Moselle à Uckange (location 4) for different years (2018, 1996, 1983), for different scenarios of the rooting depth (0.1, 0.5, 1, 2, 10)

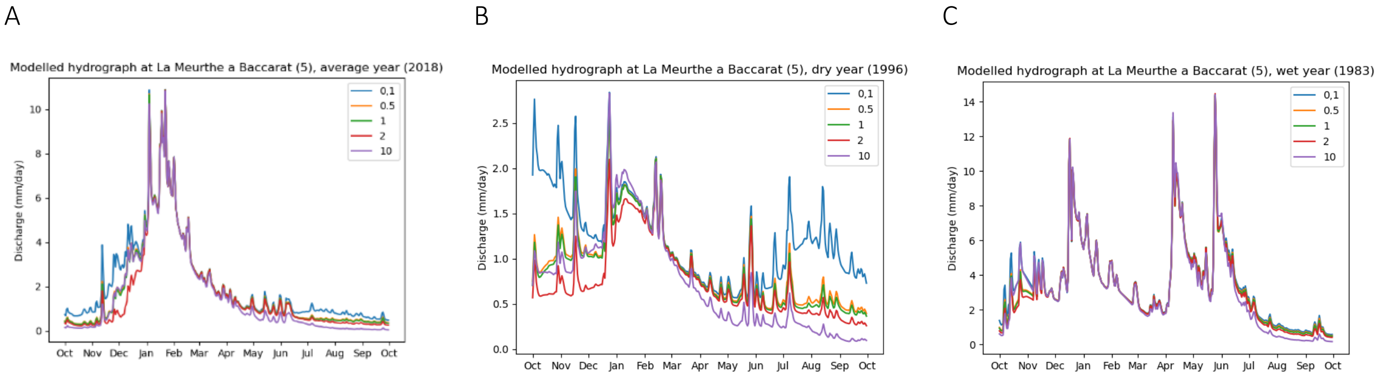

Figure 56: Modelled hydrographs at La Meurthe à Baccarat (location 5) for different years (2018, 1996, 1983), for different scenarios of the rooting depth (0.1, 0.5, 1, 2, 10)

D.5 Variability between years

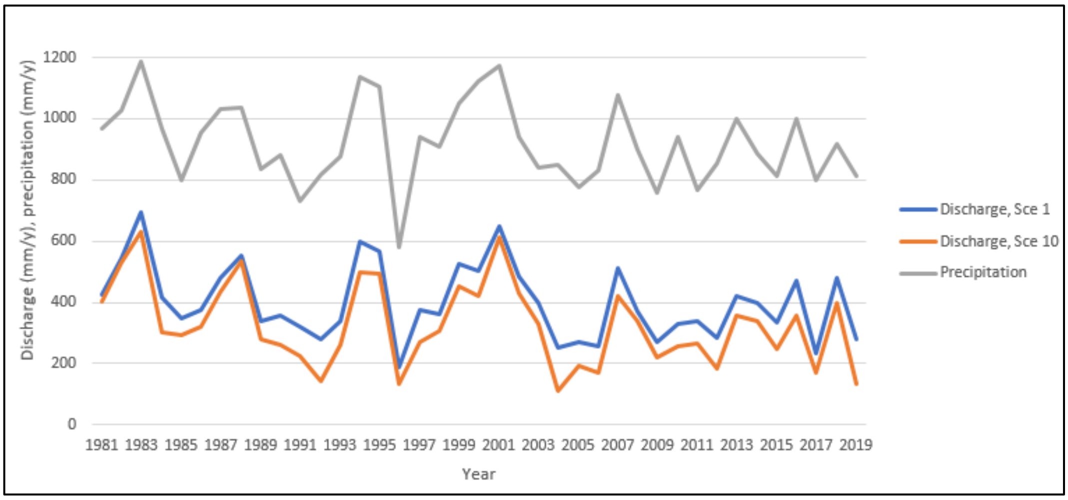

Figure 57: Annual discharge for different scenarios of the rooting depth (blue = current model, orange = Rooting depth multiplied by 10). In the graph, also the annual precipitation is plotted

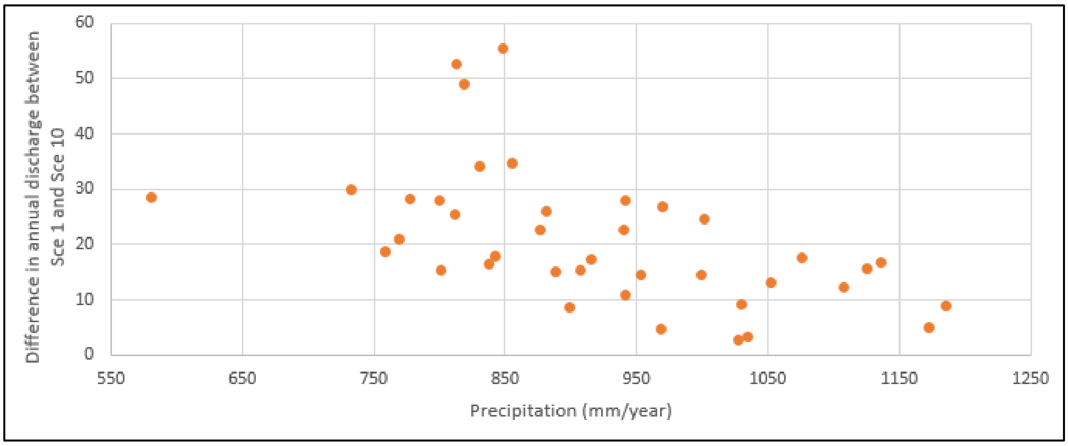

Figure 58: Difference in annual discharge between scenario RD=1 and scenario RD=10 for each year, with on the x-axis the annual precipitation of that year (mm/year). As can be seen, the difference in annual discharge between both scenarios decreases in case the precipitation increases

Appendix E. Results of the water balance approach (step 2)

To estimate the root-zone storage capacity values using the water balance approach, different steps were taken. The final results can be found in Section 0. In this Appendix, the intermediary results will be shown. First, the intermediary results of the estimation of the root-zone storage capacity in area 1A (Figure 11) are given. After that, the final estimated root-zone storage capacities of all areas are shown, as well as the final root-zone storage capacities across the study area.

E.1 Long-term values

To determine the vegetation storage deficit at each day, first the long-term annual precipitation, potential evaporation, interception evaporation and discharge were determined. The long-term precipitation and potential evaporation were determined using the data described in Section 2.6. The long-term interception evaporation was modelled using the wflow_sbm model. The long-term interception evaporation is the average annual interception evaporation between 1980 and 2019. To determine the long-term discharge, observed data was used. Only years of which for 95% of the days data was available, are used to determine this long-term discharge. In Table 4, the long-term values of area 1A can be found.

Table 4: Long-term annual discharge, precipitation, potential evaporation and interception evaporation. In row 2, the amount of years for which sufficient data was available are shown

	$\overline{Q}$ (mm/year)	$\overline{P}$ (mm/year)	$\overline{E_i}$ (mm/year)	$\overline{E_p}$ (mm/year)
Value	358.534	923.478	146.376	681.029
Years	25	40	40	40

E.2 Vegetation storage deficits

Using the long-term values of Table 4, the minimum vegetation storage deficit of each day was determined. In Figure 59A, the vegetation storage deficit in mm for each day in the period 1980 – 2019 can be found. For the hydrological year 1-4-1996 – 30-3-1997, the vegetation storage deficits of each day in mm can be found in Figure 59B. As can be seen in Figure 59B, the vegetation storage deficit is decreasing gradually and increases more steeply, because of large precipitation events in the autumn.

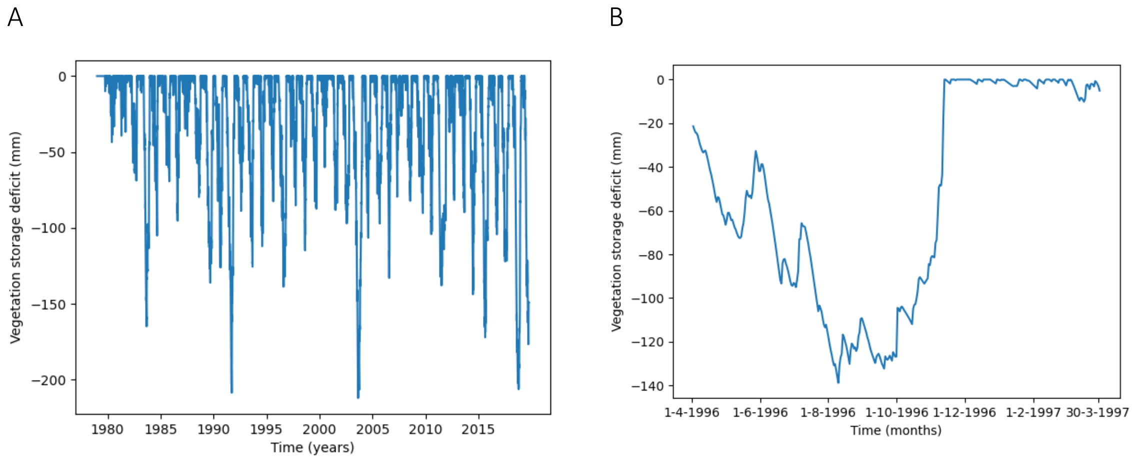

Figure 59: Vegetation storage deficit (mm) for 1980 - 2019 (Figure A) and 1-4-1996 - 30-3-1997 (Figure B)

E.3 Minimum annual vegetation storage deficits

Once the vegetation storage deficits of each day are determined, the annual minimum vegetation storage deficits are determined using hydrological years from the 1st of April to the 30th of March. For area 1A, these values are shown in Table 5.

Table 5: Minimum vegetation storage deficits for each hydrological year (1-4 to 30-3), for area 1A

Year	$S_{r,def}$ (mm)	Year	$S_{r,def}$ (mm)	Year	$S_{r,def}$ (mm)
1981	-43.5	1994	-125.6	2007	-133.0
1982	-39.3	1995	-112.1	2008	-79.5
1983	-68.8	1996	-82.5	2009	-82.2
1984	-164.9	1997	-138.8	2010	-90.3
1985	-105.1	1998	-85.2	2011	-104.2
1986	-69.3	1999	-114.9	2012	-138.0
1987	-95.3	2000	-87.5	2013	-81.7
1988	-39.3	2001	-60.0	2014	-89.7
1989	-79.7	2002	-88.2	2015	-143.8
1990	-136.1	2003	-97.1	2016	-172.1
1991	-126.1	2004	-212.1	2017	-104.3
1992	-208.7	2005	-106.5	2018	-122.1
1993	-88.9	2006	-97.1	2019	-206.3

E.4 Gumbel plots used to estimate the root-zone storage capacity

Once the minimum vegetation storage deficits are known, these values are plotted in a Gumbel plot, with the reduced variate $(-\ln(-\ln(F))$ on the x-axis. In Figure 60, the Gumbel plot for area 1A can be found. The green-dotted lines represent the reduced variates belonging to the return periods. The intersection between the red Gumbel function and the green-dotted lines are the root-zone storage capacities.

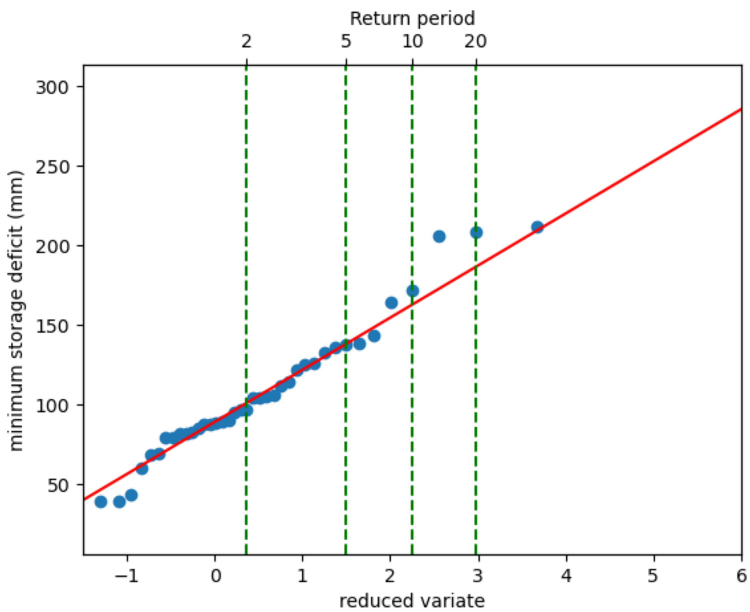

Figure 60: Gumbel Plot for determining the root-zone storage capacity, for different return periods

E.5 Translating from nested to non-nested areas

Once the root-zone storage capacities for each nested area are known (column 3 of Table 6), the root-zone storage capacities are translated using the approach described in Section 3.2.4. This means the root-zone storage capacity of a nested area X is assigned to the non-nested area X. The root-zone storage capacity values in the non-nested areas are thus equal to the values in the nested areas (column 6 of Table 6).

Table 6: Root-zone storage capacity values for the catchment areas, using different approaches

#	Nesting areas	$S_{r,max}$ (nested)	$S_{r,max}$ (non-nested) Arithmetic	$S_{r,max}$ (non-nested) Geometric	$S_{r,max}$ (non-nested) Final
1A	2A, 2B	163.0	407.2	830.6	163.0
2B	3A, 3B, 3C	137.4	278.1	9.3	137.4
3A	4A, 4B	169.9	174.2	175.8	169.9
3B	4C, 4D, 4E, 4F	162.2	53.3	88.9	162.2
3C	4G, 4H, 4I, 4J	176.7	268.4	318.0	176.7
4B	5A, 5B	175.9	145.3	157.4	175.9
4D	5C, 5D	204.6	165.7	179.4	204.6
4I	5G, 5H	141.7	75.2	96.0	141.7
4J	5E, 5F	146.4	-29.2	50.2	146.4
5F	6B	162.7	181.6	186.0	162.7
5G	6A	178.5	279.0	323.3	178.5

First of all, the root-zone storage capacities of the non-nested areas were determined using the method of the arithmetic mean.

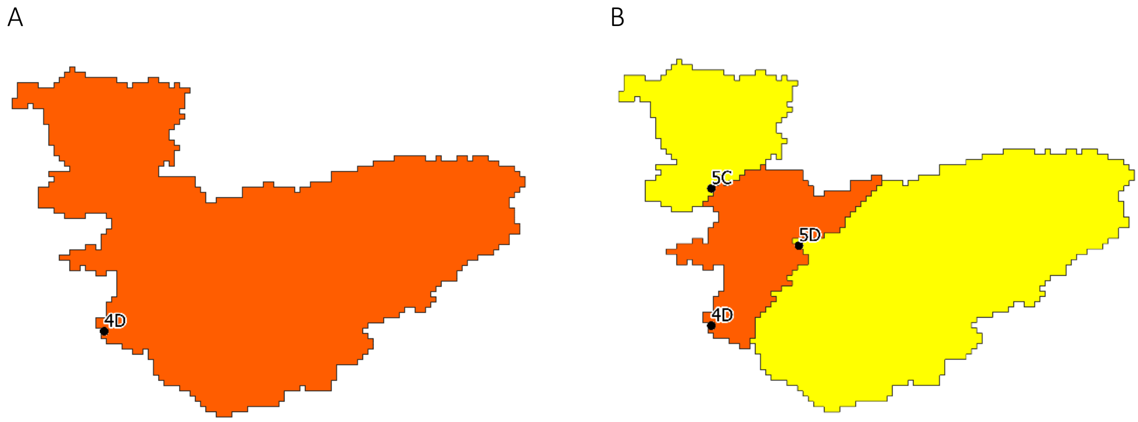

Figure 61: Example of nested catchments: Area 5C and 5D are nesting within area 4D

In Figure 61, the example of nested area 4D and its nesting areas 5C and 5D can be found. When using the method of the arithmetic mean, the root-zone storage capacity of the remaining part orange part in Figure 61B is thus estimated by assuming that the weighted mean of nested area 4D is equal to the weighted mean of area 5C, 5D and non-nested area 4D. Thus, Eq. 11 is used:

$$S_{r,\max\_4D\_nn} = \frac{S_{r,max\_4D} \cdot A_{4D} - S_{r,max\_5C} \cdot A_{5C} - S_{r,max\_5D} \cdot A_{5D}}{A_{4D} - A_{5C} - A_{5D}} \quad \text{Eq. 11}$$

In which:

- $S_{r,\max\_4D\_nn}$: Root-zone storage capacity in the non-nested area 4D (orange part Figure 5B)
- $S_{r,\max\_4D}$, $S_{r,\max\_5C}$ and $S_{r,\max\_5D}$: Root-zone storage capacities of the nested catchments
- A_{4D}, A_{5C} and A_{5D} : Areas of the nested catchments

The results of this calculation can be found in column 4 of Table 6. When analysing these values, the value of area 4J '-29.5' draws the attention. A negative root-zone storage capacity is not realistic. A possible explanation of this result is the high uncertainty in the determination of the root-zone storage capacity using the water balance approach (Section 0). As a result, when averaging the values, the value of the remaining area is getting an unrealistic value.

Since the results of column 4 could not be used, another approach was used, which was based on the geometric mean (Eq. 12).

$$S_{r,\max\_4D\_nn} = \exp\left(\frac{\ln(S_{r,max\_4D})\cdot A_{4D} - \ln(S_{r,max\_5C})\cdot A_{5C} - (S_{r,max\_5D})\cdot A_{5D}}{A_{4D} - A_{5C} - A_{5D}}\right) \qquad \text{Eq. 12}$$

The results of this approach can be found in column 5 of Table 6. As can be seen, there are no negative results anymore, however, the values are still unrealistic. For example the '9.3' value of area 2B is unrealistic. The unrealistic values of both approaches are likely related to the high uncertainties of the water balance approach, due to limited data availability. Therefore, it was chosen to have the original values of the nested catchment for the non-nested catchments.

E.6 Final Results

The results of the estimation of the root-zone storage capacity using the water balance approach can be found in Section 4.2. In Table 7, some general statistics of each scenario can be found.

Table 7: Statistics (average, median, standard deviation, minimum and maximum) of different scenarios for the root-zone storage capacity (mm)

(mm)	Average	Median	Stdev	Min	Max
WBA2	105	101	18	71	144
WBA5	145	138	23	101	195
WBA10	171	163	26	122	231
WBA20	196	189	30	141	266

Appendix F. Statistics of new rooting depth estimations (step 3)

In this Appendix, Figures in which the new estimations of the rooting depth and the current estimations of the rooting depth are compared can be found. In Table 8, some general statistics of each scenario can be found.

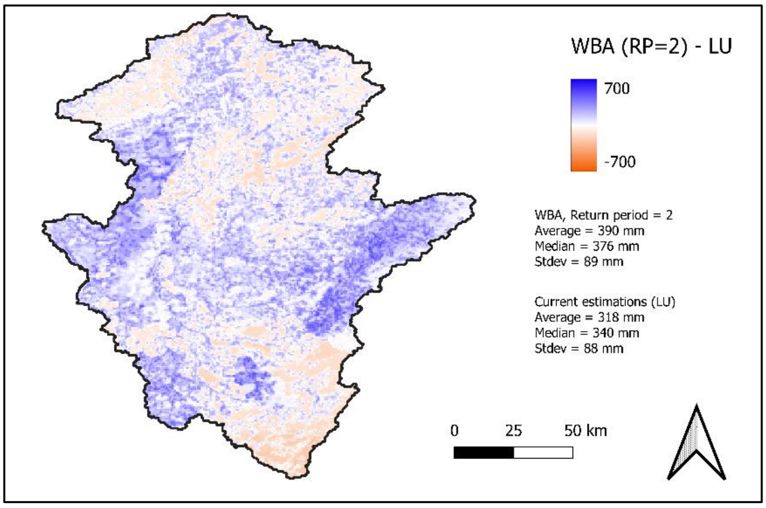

Figure 62: Different in rooting depth (mm), comparing the estimations using the water balance approach (return period of 2) and the current estimations. Blue indicates an increase compared with the current estimations

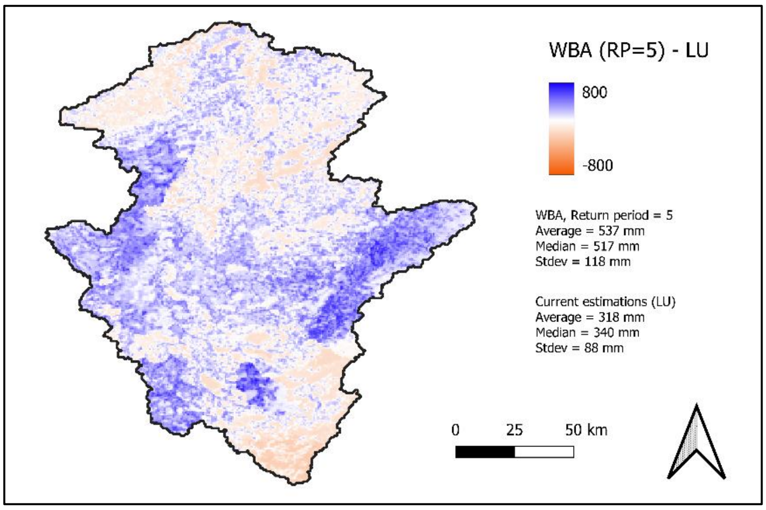

Figure 63: Different in rooting depth (mm), comparing the estimations using the water balance approach (return period of 5) and the current estimations. Blue indicates an increase compared with the current estimations

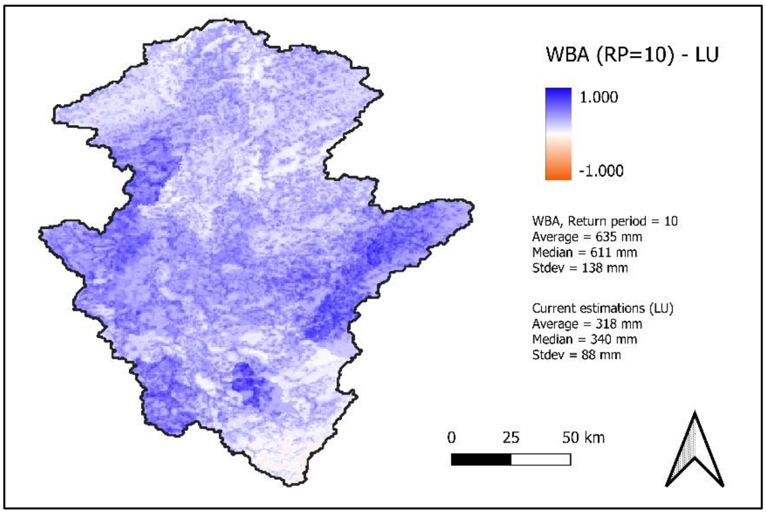

Figure 64: Different in rooting depth (mm), comparing the estimations using the water balance approach (return period of 10) and the current estimations. Blue indicates an increase compared with the current estimations

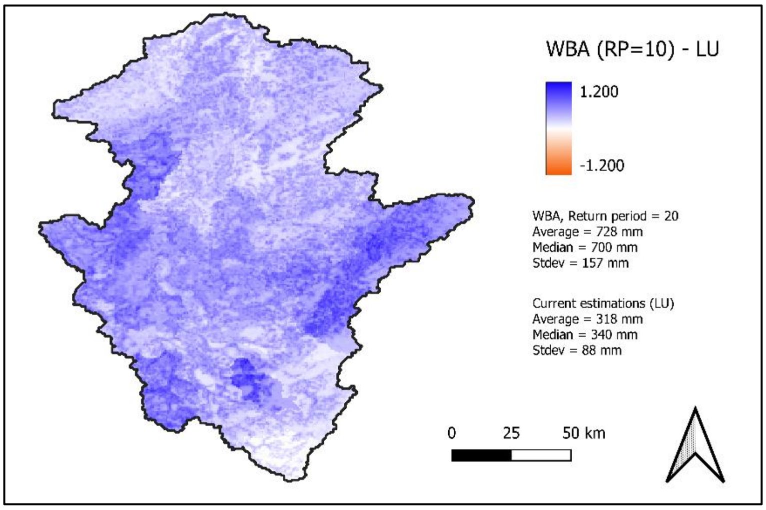

Figure 65: Different in rooting depth (mm), comparing the estimations using the water balance approach (return period of 20) and the current estimations. Blue indicates an increase compared with the current estimations

Table 8: Statistics (average, median, standard deviation, minimum and maximum) of different scenarios for the rooting depth (mm)

(mm)	Average	Median	Stdev	Min	Max
LU	318	340	87	0	432
WBA2	390	376	89	179	688
WBA5	537	517	118	257	955
WBA10	635	611	138	308	1133
WBA20	728	700	157	358	1304

Appendix G. Results of the comparison between different model versions (step 4)

In this Appendix, the results of the analysis of different versions of the model can be found.

G.1 Average Annual Performance

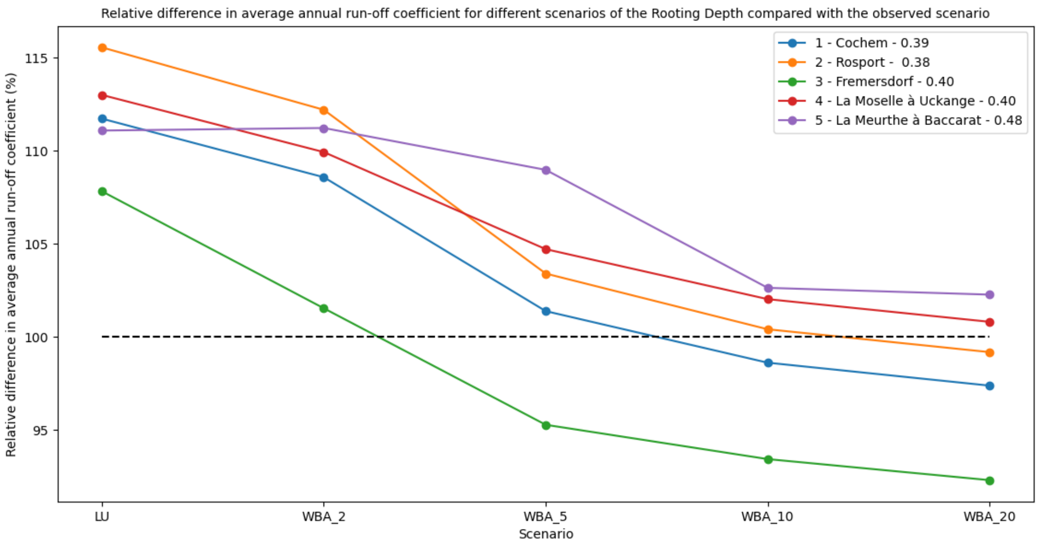

Figure 66: Relative differences in average annual run-off coefficient for different scenarios, compared with the observed average annual run-off coefficient, for each location. The black dashed line represents the observed scenario. Behind each name of the location in the legend, the average observed annual run-off coefficient is presented in mm/day

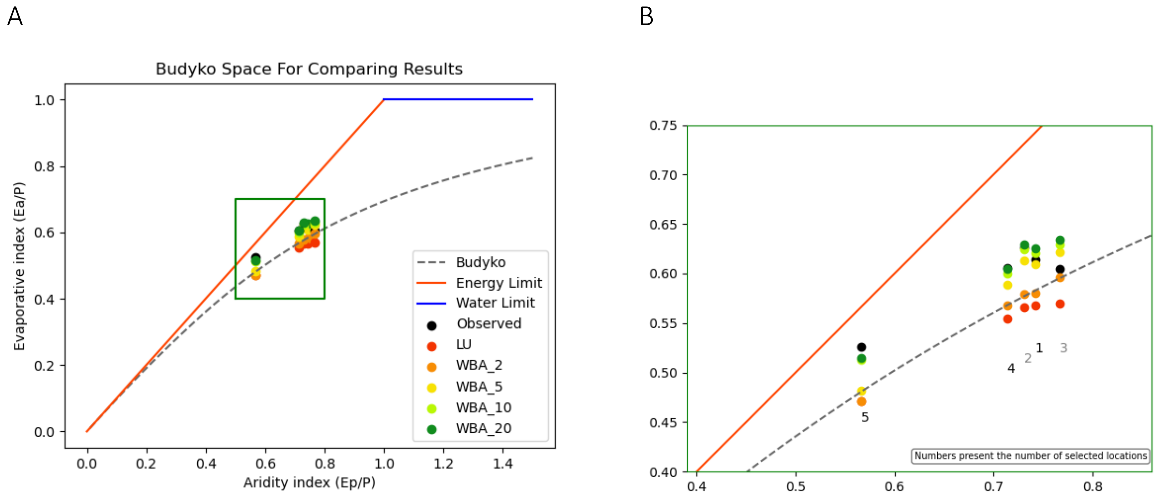

Figure 67: Budyko Space showing the ratio $\overline{E_a}/\overline{P}$ as function of $\overline{E_p}/\overline{P}$ for each scenario at each selected output location. The grey dotted line presents the Budyko curve, the red and blue line the energy and water limit. The green box is enlarged in Figure B. The numbers below the dots in Figure B present the number of the output locations (1 = Cochem, 2 = Rosport, 3 = Fremersdorf, 4 = La Moselle à Uckange, 5 = La Meurthe à Baccarat)

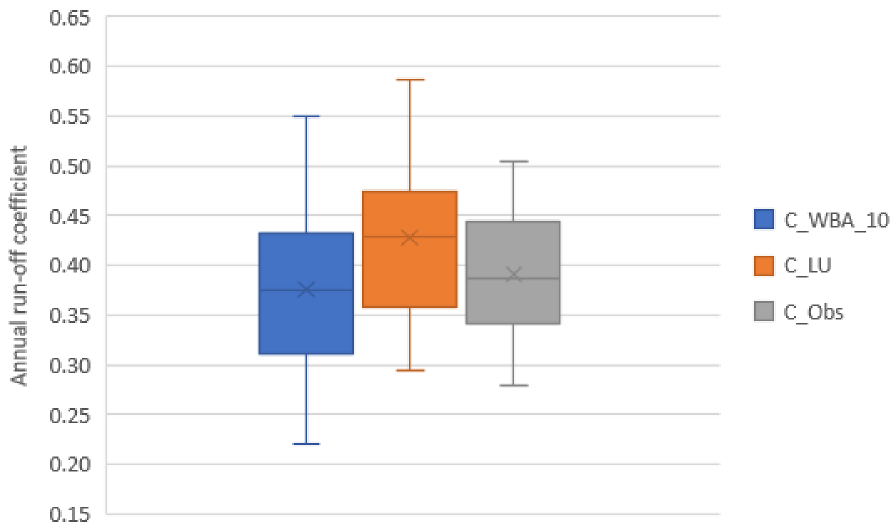

Figure 68: Boxplot showing the spread over annual run-off coefficients at Cochem (location 1), for different scenarios. In blue, the run-off coefficient for the model in which the water balance approach with a return period of 10 years was used to estimate the root-zone storage capacity. In orange, the run-off coefficient for the current version of the model, and in grey the observed annual run-off coefficients

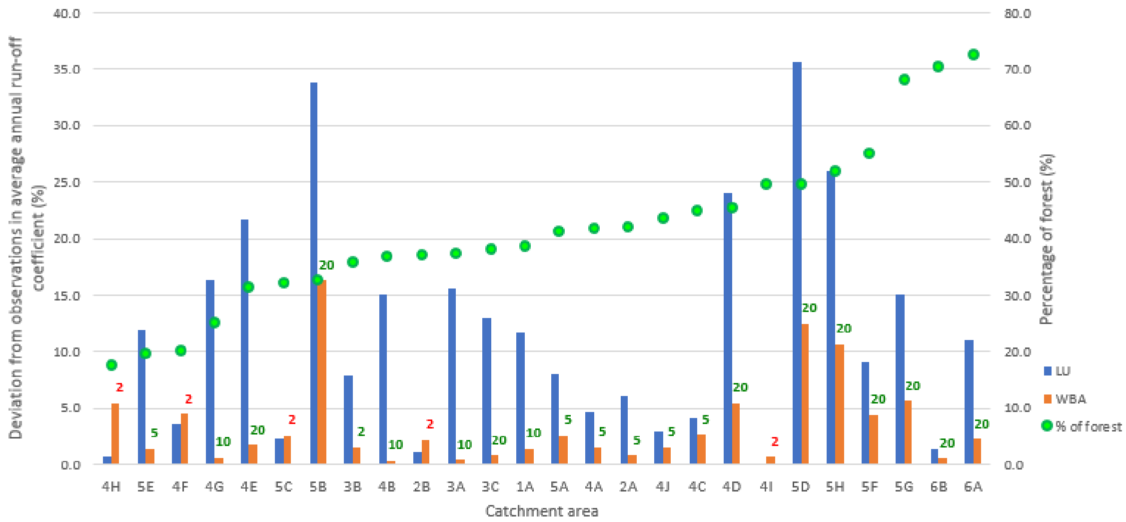

Figure 69: Deviation from the observed annual run-off coefficient for both methods for estimating the root-zone storage capacity, for each catchment area. Blue indicates the deviation from observations when using the current estimations of the rooting depth, whereas orange indicates the deviation when using the water-balance method. Above the orange bar, the return period in the water balance approach that led to the annual average run-of coefficient the closest to the observations can be found. The catchment areas (locations shown in Figure 11) are sorted in such a way that the catchment area with the lowest percentage of forest is left, while the catchment area with the highest percentage of forest is right. In green, these percentages are given

As can be seen in Figure 69, when the percentage of forest in the catchment area increases, the return period which is most optimal in the water balance approach also on average increases.

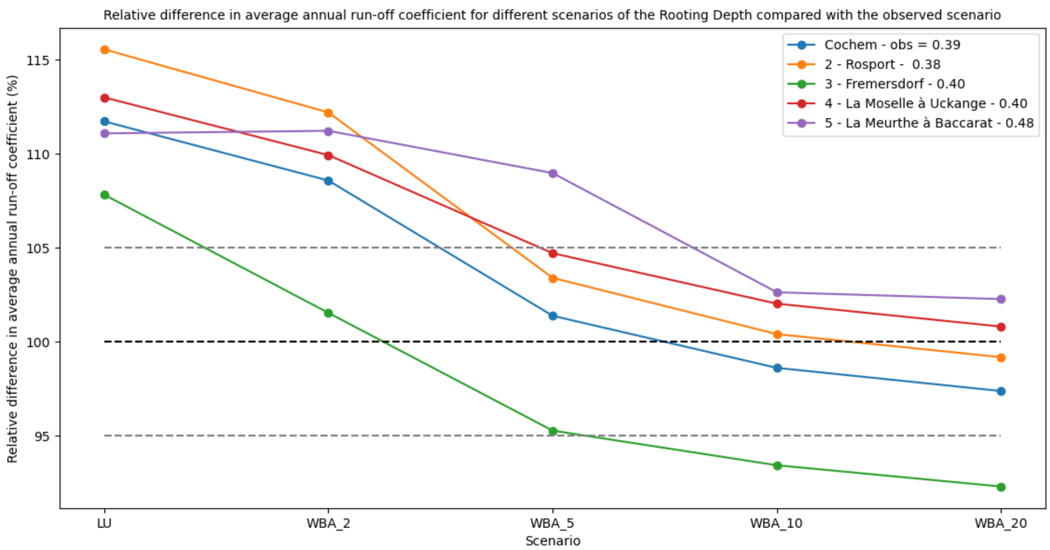

Figure 70: Relative differences in average annual run-off coefficient for different scenarios, compared with the observed average annual run-off coefficient, for each location. The black dashed line represents the observed scenario, they grey dashed lines show a deviation of +5% and -5% from the observed scenario. Behind each name of the location in the legend, the average observed annual run-off coefficient is presented in mm/day

G.2 Performance in dry period

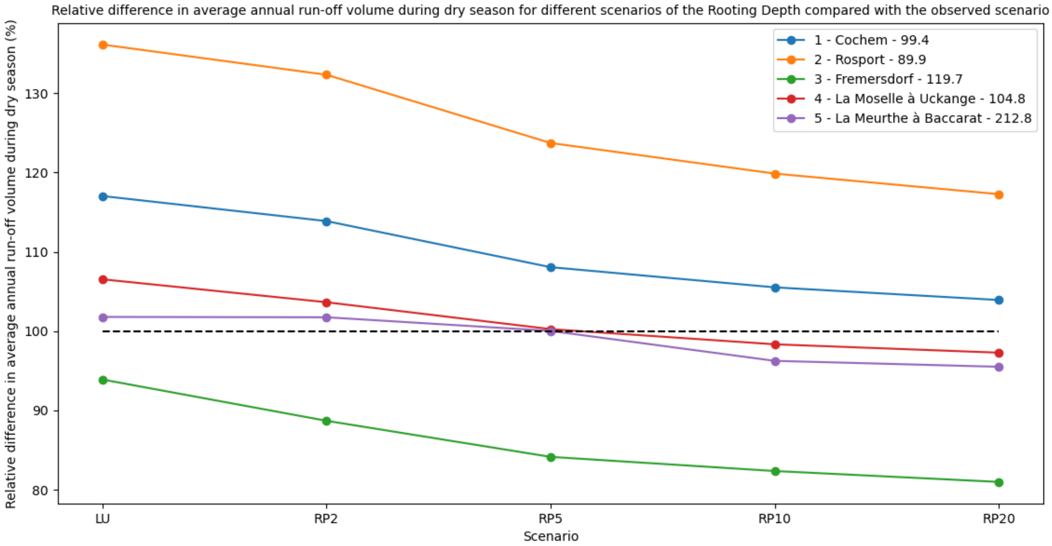

Figure 71: Relative difference in average annual run-off volume during the dry season (1st of April – 30th of September) for different scenarios of the Rooting Depth compared with the current scenario, for each selected location. The black dashed line represents the observed scenario. Behind each name of the location in the legend, the average observed annual run-off volume during the dry season is presented in mm

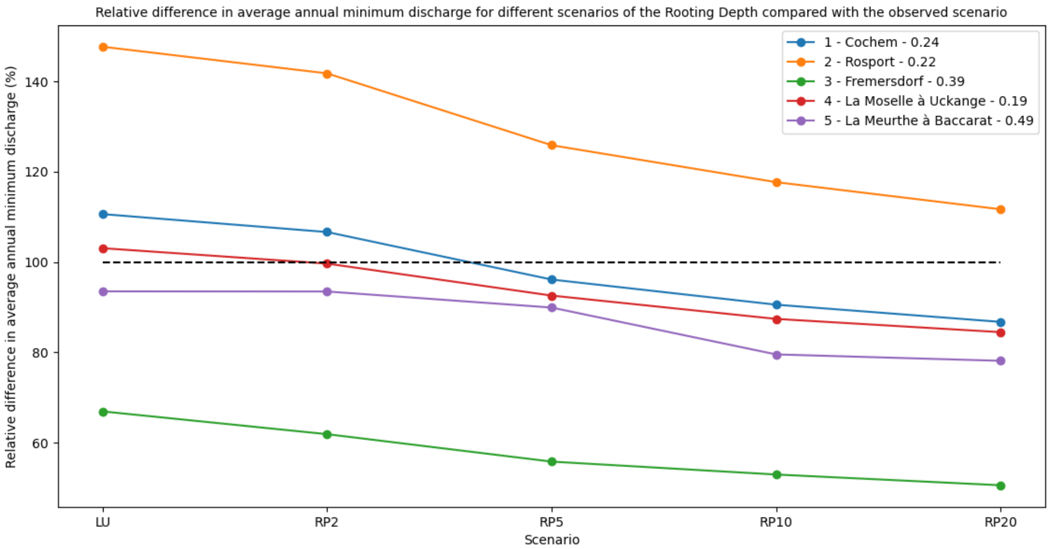

Figure 72: Relative difference in average annual minimum discharge of seven consecutive days for different scenarios of the Rooting Depth compared with the current scenario, for each selected location. The black dashed line represents the observed scenario. Behind each name of the location in the legend, the average observed annual minimum discharge is presented in mm/day

G.3 Average Monthly Performance

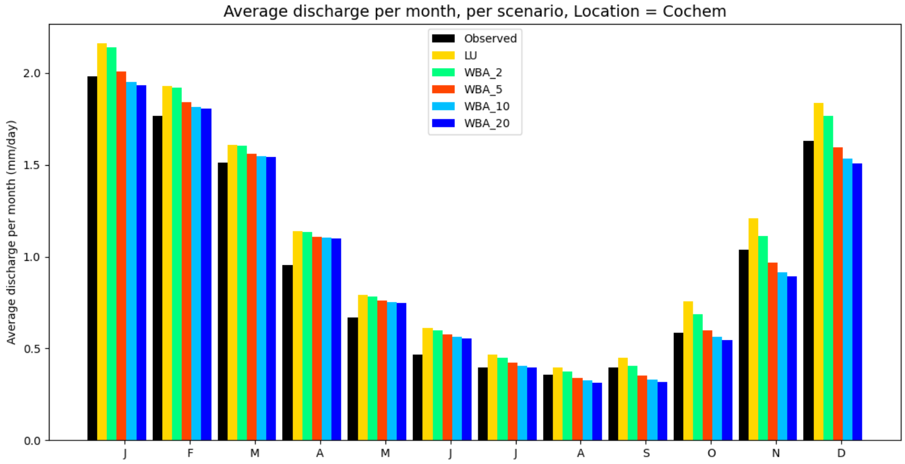

Figure 73: Average discharge per month (mm/day), per scenario, for Cochem (1)

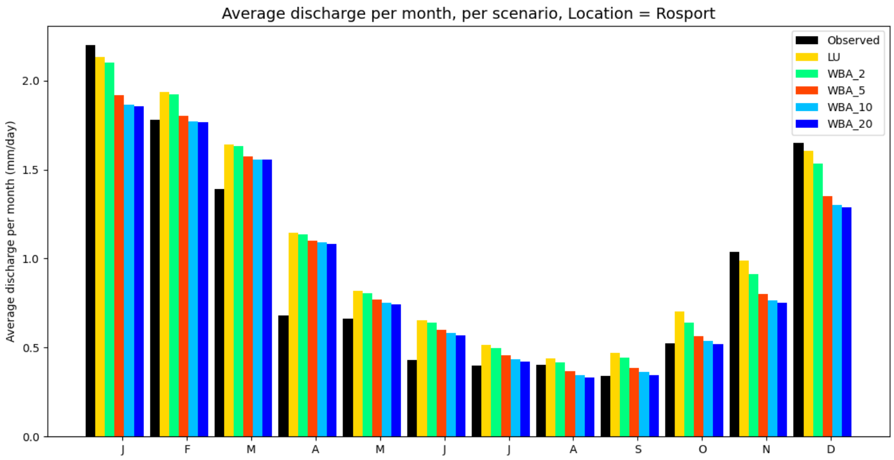

Figure 74: Average discharge per month (mm/day), per scenario, for Rosport (2)

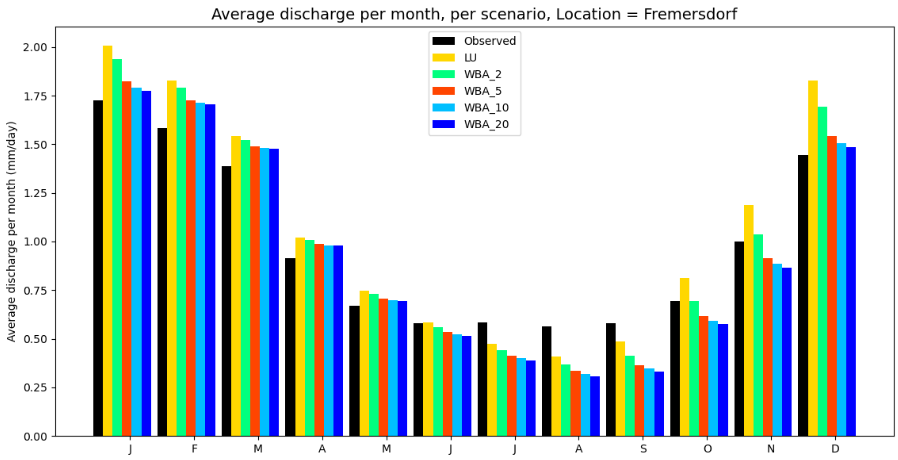

Figure 75: Average discharge per month (mm/day), per scenario, for Fremersdorf (3)

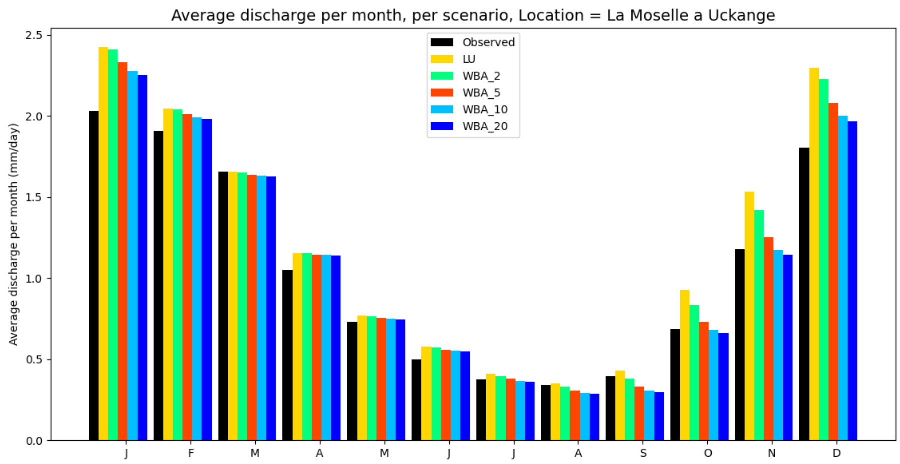

Figure 76: Average discharge per month (mm/day), per scenario, for La Moselle à Uckange (4)

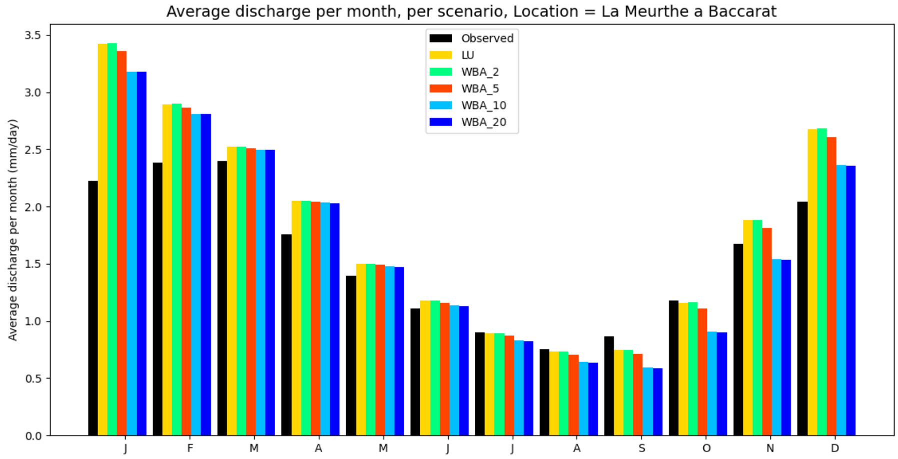

Figure 77: Average discharge per month (mm/day), per scenario, for La Meurthe à Baccarat (5)

G.4 Hydrographs

In the Figures below, the hydrographs for each scenario at Cochem (Location 1) can be found for each year. The number of the peaks are indicated in red.

A B C

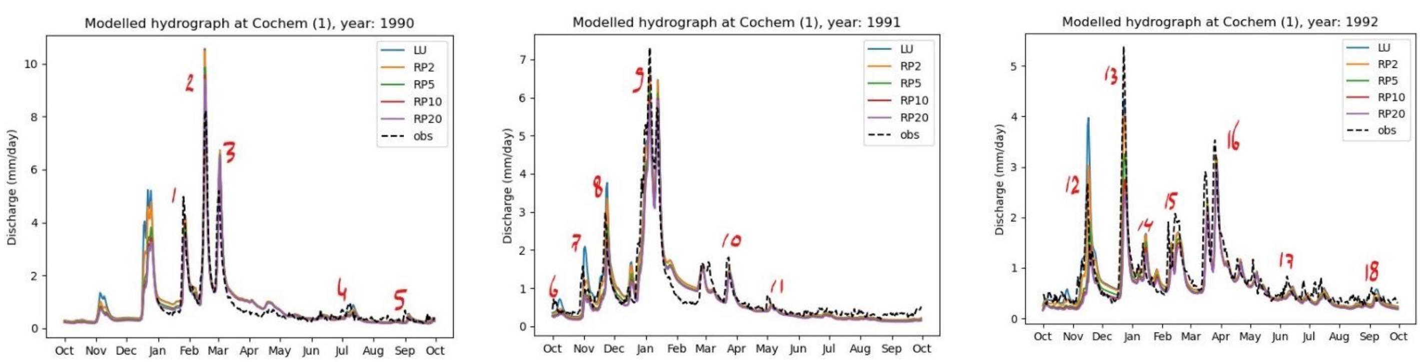

D

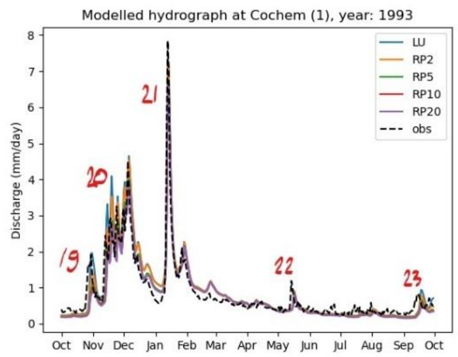

E

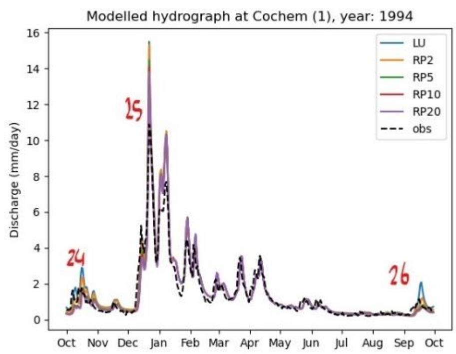

F

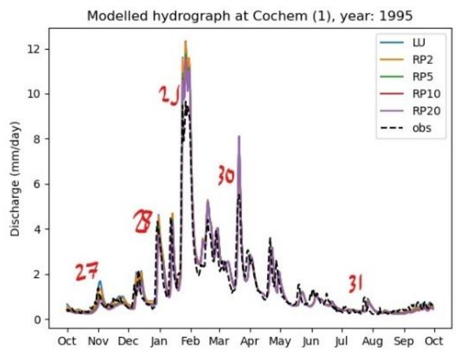

G

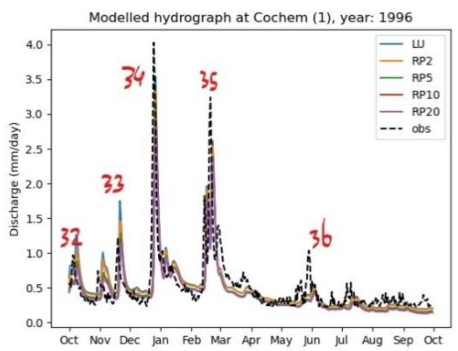

H

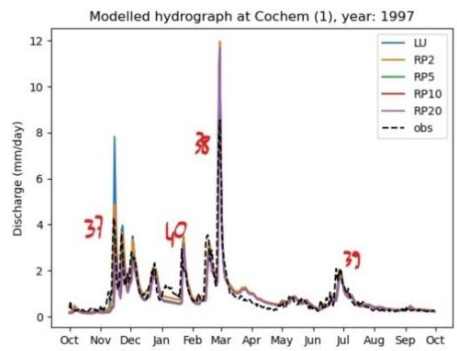

I

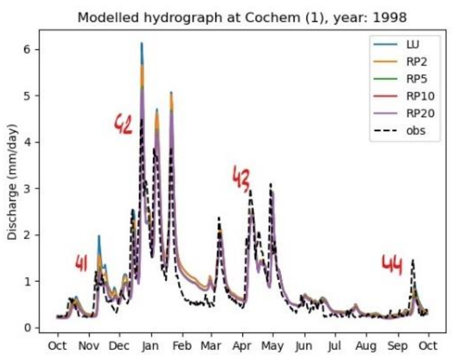

J

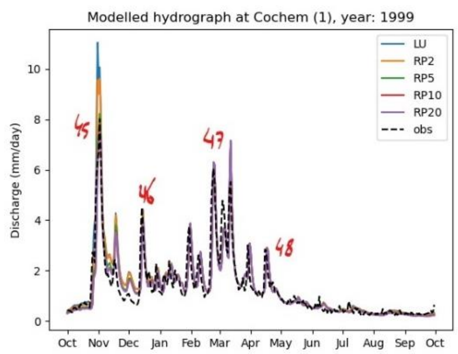

K

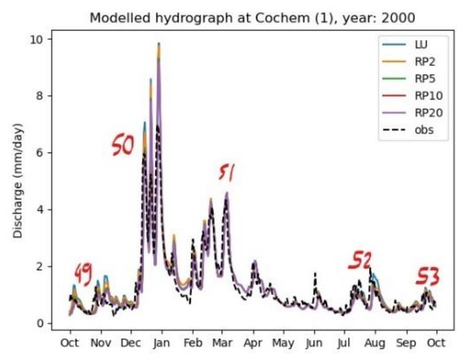

L

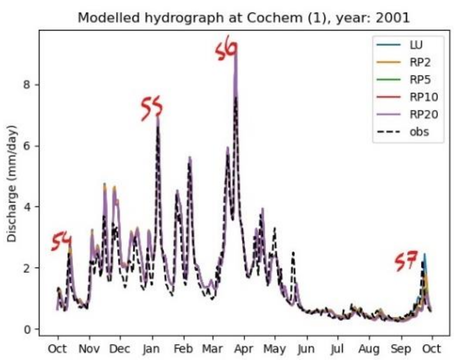

M

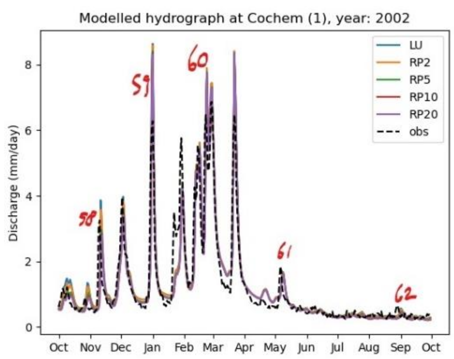

N

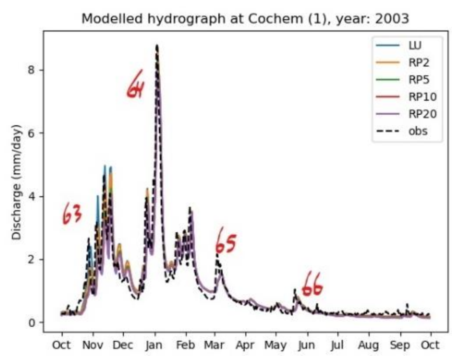

O

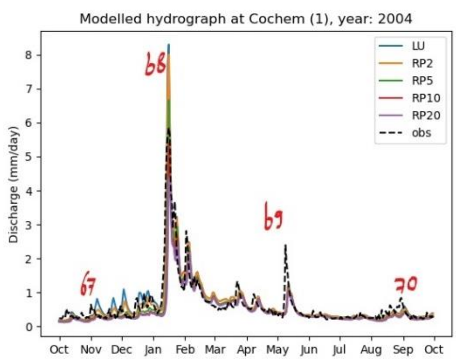

P

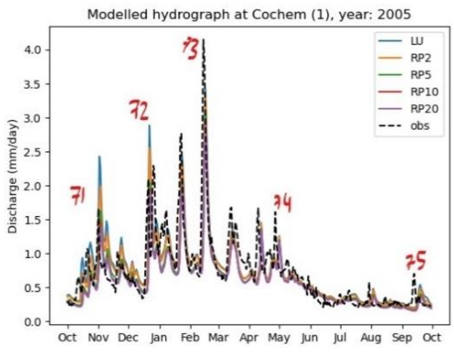

Q

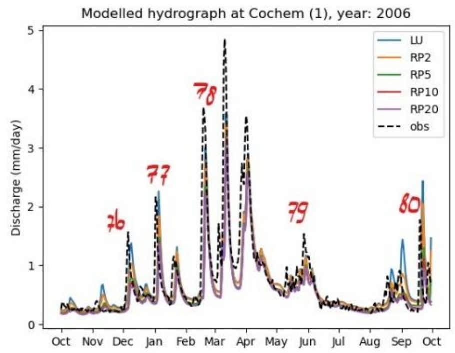

R

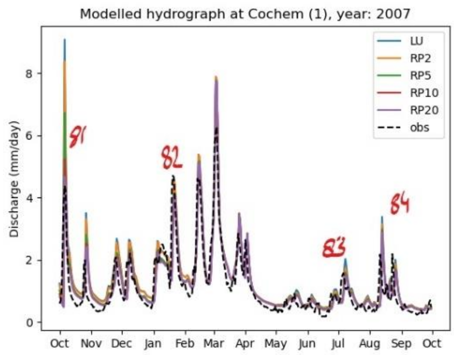

S

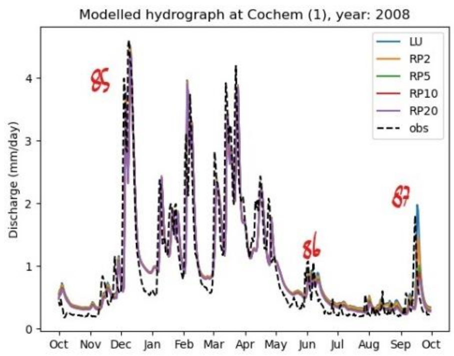

T

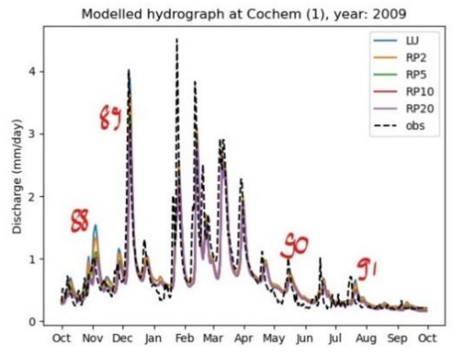

U

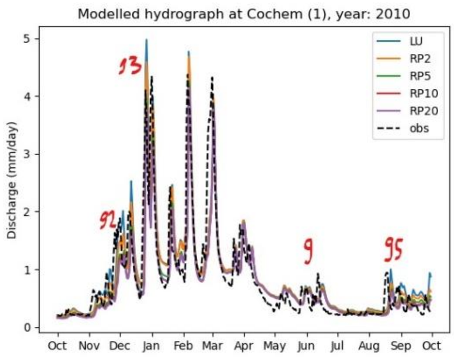

V

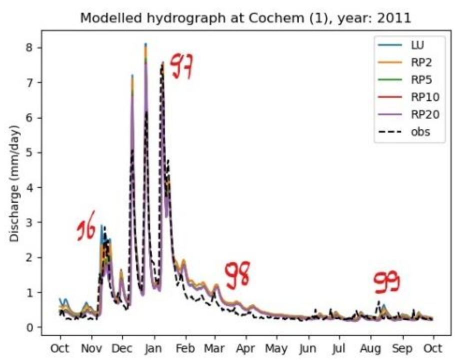

W

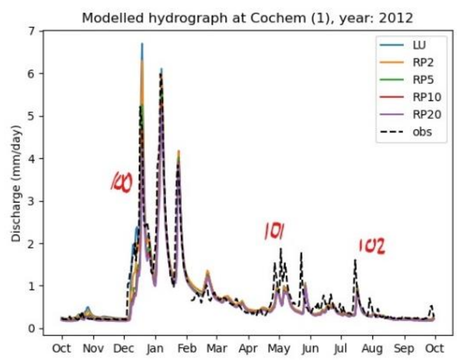

X

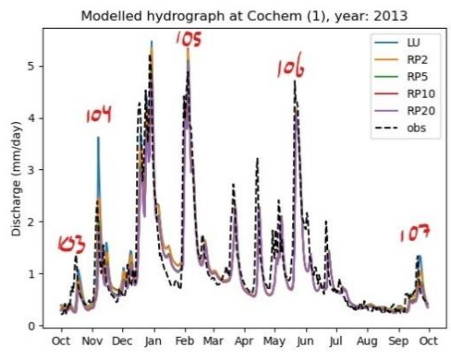

Y

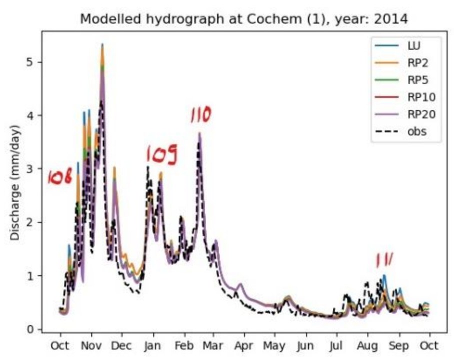

Z

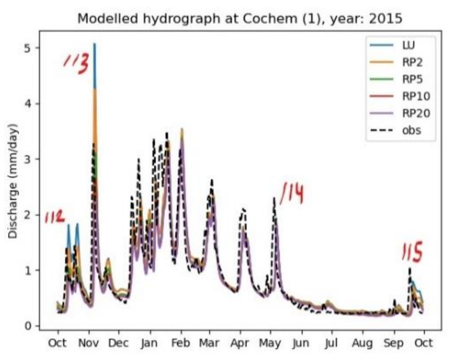

AA

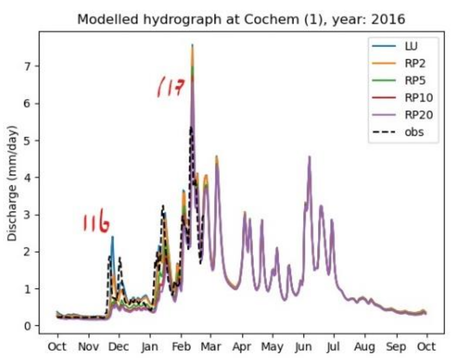

Figure 78: Hydrographs at Cochem (location 1), for each year. Observations are showed with the black dotted line

In Table 9, the results of the analysis of the height of the peaks in the hydrographs can be found. For each number (indicated in the Figures above), in the column 'Height' it is indicated which version of the model performs better.

Table 9: Results of the analysis of the heights of the peaks

#	Year	Season	Year	Height	#	Year	Season	Year	Height	#	Year	Season	Year	Height
1	1990	Wet	-	LU	40	1997	Dry	-	WBA	79	2006	Wet	-	LU
2	1990	Wet	-	WBA	41	1998	Dry	-	WBA	80	2006	Dry	-	WBA
3	1990	Wet	-	WBA	42	1998	Wet	-	WBA	81	2007	Dry	Wet	WBA
4	1990	Dry	-	LU	43	1998	Wet	-	-	82	2007	Wet	Wet	-
5	1990	Dry	-	LU	44	1998	Dry	-	LU	83	2007	Dry	Wet	WBA
6	1991	Dry	Dry	LU	45	1999	Dry	Wet	WBA	84	2007	Dry	Wet	WBA
7	1991	Wet	Dry	WBA	46	1999	Wet	Wet	-	85	2008	Wet	-	LU
8	1991	Wet	Dry	WBA	47	1999	Wet	Wet	-	86	2008	Wet	-	-
9	1991	Wet	Dry	LU	48	1999	Wet	Wet	-	87	2008	Dry	-	-
10	1991	Wet	Dry	-	49	2000	Dry	Wet	WBA	88	2009	Dry	Dry	WBA
11	1991	Dry	Dry	-	50	2000	Wet	Wet	WBA	89	2009	Wet	Dry	LU
12	1992	Wet	-	WBA	51	2000	Wet	Wet	WBA	90	2009	Dry	Dry	LU
13	1992	Wet	-	LU	52	2000	Dry	Wet	-	91	2009	Dry	Dry	-
14	1992	Wet	-	WBA	53	2000	Dry	Wet	WBA	92	2010	Wet	-	WBA
15	1992	Wet	-	LU	54	2001	Dry	Wet	WBA	93	2010	Wet	-	WBA
16	1992	Wet	-	-	55	2001	Wet	Wet	WBA	94	2010	Dry	-	LU
17	1992	Dry	-	LU	56	2001	Wet	Wet	WBA	95	2010	Dry	-	LU
18	1992	Dry	-	-	57	2001	Dry	Wet	-	96	2011	Dry	Dry	LU
19	1993	Dry	-	LU	58	2002	Wet	-	WBA	97	2011	Wet	Dry	WBA
20	1993	Wet	-	WBA	59	2002	Wet	-	WBA	98	2011	Wet	Dry	WBA
21	1993	Wet	-	-	60	2002	Wet	-	WBA	99	2011	Dry	Dry	LU
22	1993	Dry	-	LU	61	2002	Dry	-	-	100	2012	Wet	-	WBA
23	1993	Dry	-	WBA	62	2002	Dry	-	-	101	2012	Wet	-	LU
24	1994	Dry	Wet	WBA	63	2003	Wet	-	LU	102	2012	Dry	-	LU
25	1994	Wet	Wet	WBA	64	2003	Wet	-	LU	103	2013	Dry	-	LU
26	1994	Dry	Wet	WBA	65	2003	Wet	-	LU	104	2013	Wet	-	WBA
27	1995	Dry	Wet	WBA	66	2003	Dry	-	LU	105	2013	Wet	-	WBA
28	1995	Wet	Wet	WBA	67	2004	Dry	-	-	106	2013	Wet	-	LU
29	1995	Wet	Wet	WBA	68	2004	Wet	-	WBA	107	2013	Dry	-	LU
30	1995	Wet	Wet	WBA	69	2004	Wet	-	LU	108	2014	Dry	-	WBA
31	1995	Dry	Wet	LU	70	2004	Dry	-	LU	109	2014	Wet	-	WBA
32	1996	Dry	Dry	WBA	71	2005	Wet	Dry	WBA	110	2014	Wet	-	WBA
33	1996	Wet	Dry	WBA	72	2005	Wet	Dry	WBA	111	2014	Dry	-	-
34	1996	Wet	Dry	LU	73	2005	Wet	Dry	LU	112	2015	Dry	-	WBA
35	1996	Wet	Dry	LU	74	2005	Wet	Dry	LU	113	2015	Wet	-	WBA
36	1996	Dry	Dry	LU	75	2005	Dry	Dry	LU	114	2015	Wet	-	LU
37	1997	Wet	-	WBA	76	2006	Wet	-	LU	115	2015	Dry	-	LU
38	1997	Wet	-	WBA	77	2006	Wet	-	LU	116	2016	Wet	-	-
39	1997	Wet	-	WBA	78	2006	Wet	-	LU	117	2016	Wet	-	WBA

G.5 Possible causes for differences in timing between observed and simulated peaks

As mentioned in section 4.4.4, there is a difference in timing between the simulated discharge peaks and observed discharge peaks: In Cochem, the simulated peaks are on average 3 days later than the observed discharge peaks. In this Appendix, possible causes are discussed.

G.5.1 Observed precipitation peaks in relation with peaks in the hydrograph

As mentioned in section 4.4.4, the difference in timing between simulated discharge peaks and observed discharge peaks could possibly have to do something with measurement errors of precipitation peaks. In case the precipitation peaks were earlier than the observed discharge peaks, this meant something would be wrong with the observations. However, Figure 79, Figure 80 and Figure 81 show this is not the case.

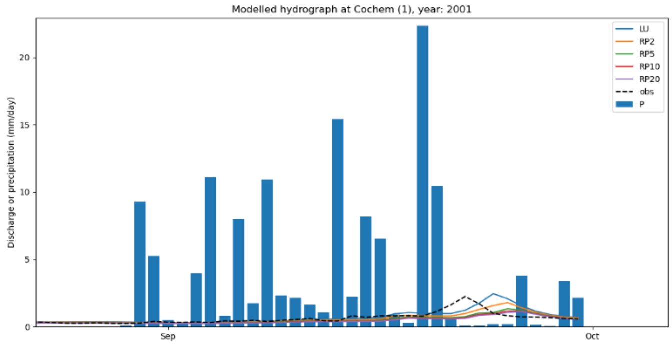

Figure 79: Observed and simulated discharge peaks, as well as daily precipitation values, for the period September 2001 - October 2001 (Cochem)

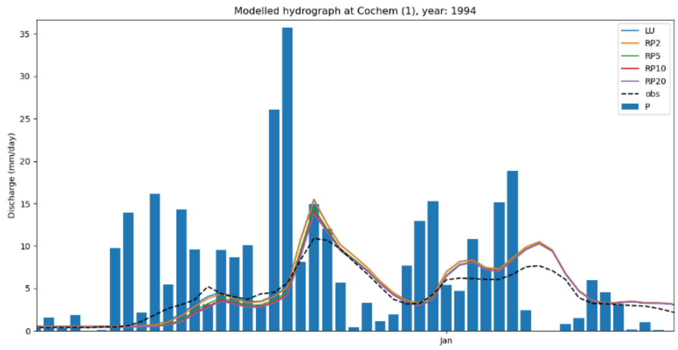

Figure 80:Observed and simulated discharge peaks, as well as daily precipitation values, for the period December 1993 – January 1994 (Cochem)

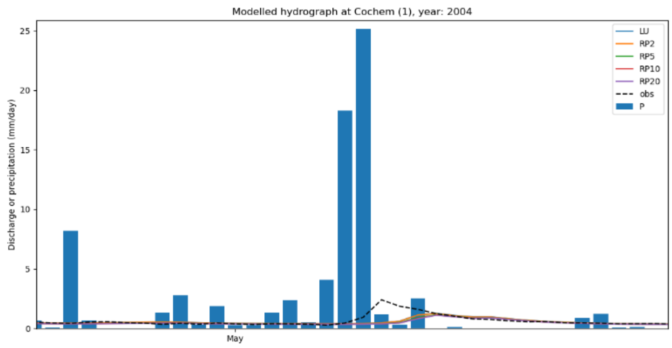

Figure 81: Observed and simulated discharge peaks, as well as daily precipitation values, for the period May 2004 (Cochem)

G.5.2 Uncertainty in the kinematic wave

Another possible cause could be the uncertainty in estimating the kinematic wave, as the approach that is currently used in the wflow_sbm model especially has limitations in non-steep terrain.

In Cochem, the simulated discharge peaks are on average 3 days later than the observed discharge peaks. For La Meurthe à Baccarat (more upstream, Figure 6, page 10), this difference is less extreme. Here, sometimes the simulated discharge peaks are even earlier than observed peaks (Figure 82).

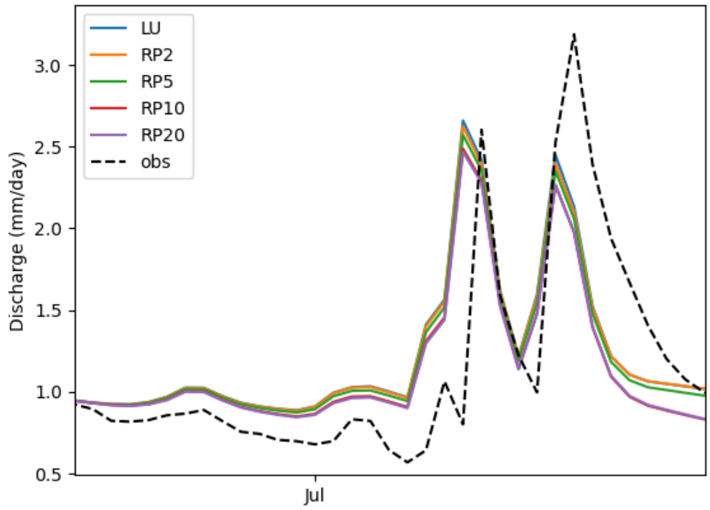

Figure 82: Modelled hydrograph at La Meurthe à Baccarat, located upstream, for July 2000, for different scenarios

Appendix H. Water balance approach using only one gauge for observed data

As stated in Section 6.2.2, it could be useful to assess if the model performance increases when using the water balance approach with only one location for observed discharge data. In Table 10, you can see for each return period in the water balance approach, the average root-zone storage capacity using the approach described in Section 3.2. In the second column, the average root-zone storage capacity is stated when using only the observed discharge data at Cochem. As can be seen, both averages are close to each other. This suggests that when using only observed discharge data at Cochem, the model performance would not deviate substantially from the model performance when using multiple stations for observed discharge data.

Table 10: Average root-zone storage capacity (mm) determined with the water balance approach, and root-zone storage capacity when using only the most downstream gauge (Cochem) for observed discharge data

	Average root-zone storage capacity (mm)	Root-zone storage capacity when using only the most downstream gauge for observed discharge data (mm)
WBA_2	105	101
WBA_5	145	138
WBA_10	171	163
WBA_20	197	187